

AD-A053 237

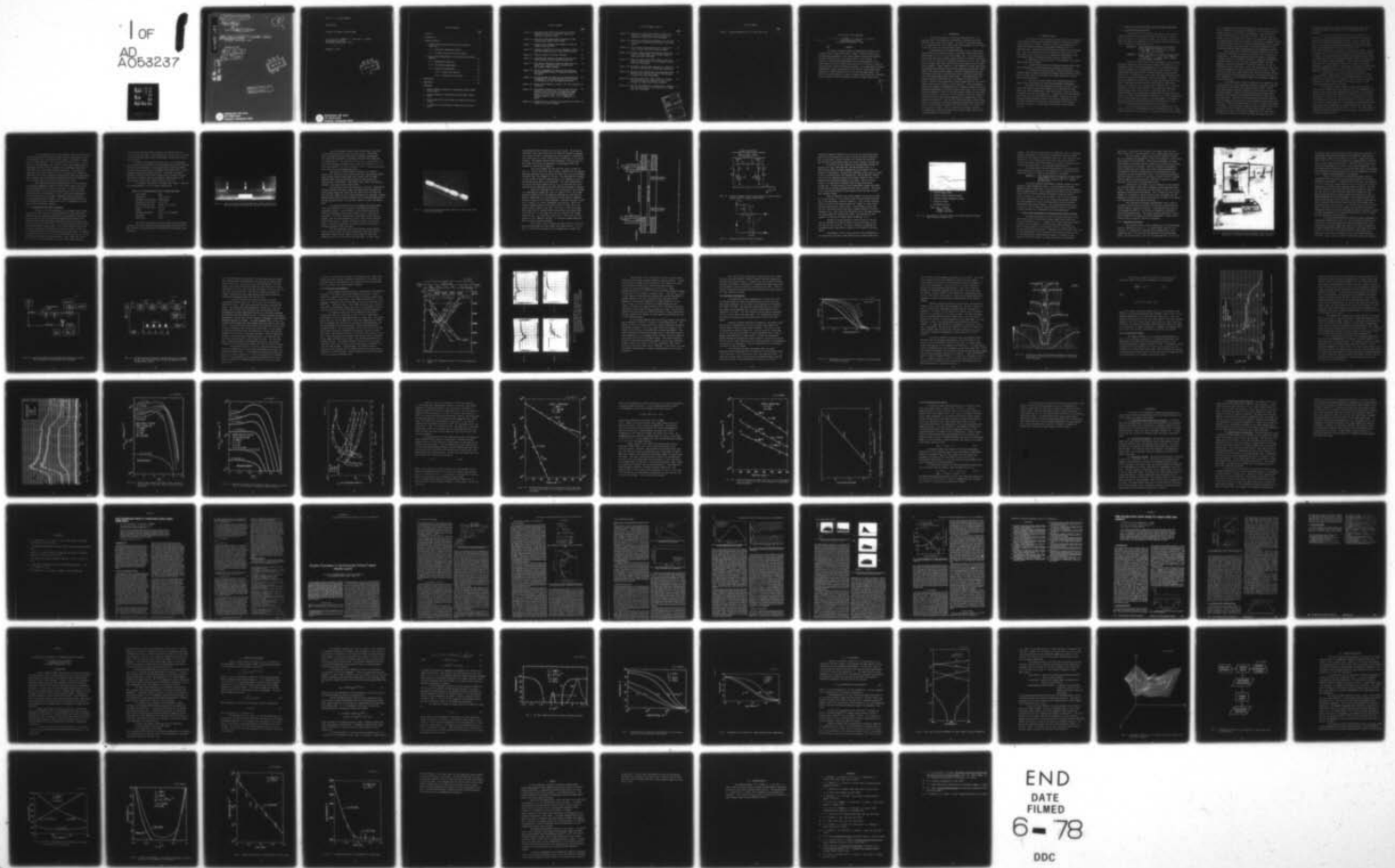
WESTINGHOUSE RESEARCH AND DEVELOPMENT CENTER PITTSBU--ETC F/G 20/5
COPPER HALIDE LASER RESEARCH. (U)
DEC 77 C S LIU, D W FELDMAN, J L PACK

N00014-74-C-0445

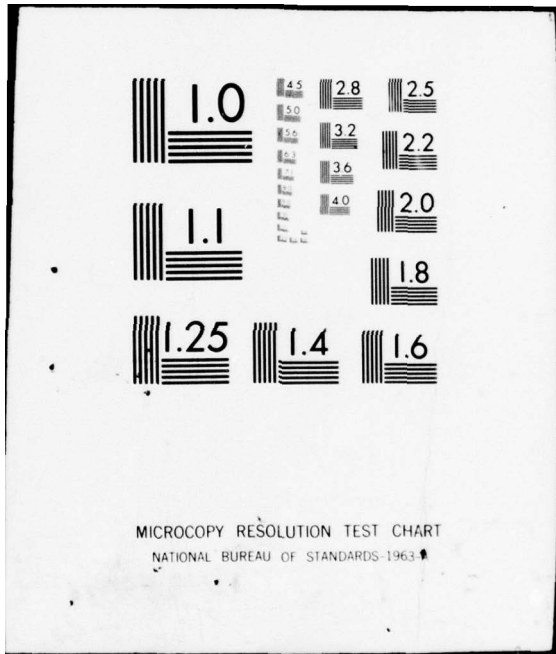
UNCLASSIFIED

NL

1 OF
AD
A063237



END
DATE
FILMED
6-78
DDC



MICROCOPY RESOLUTION TEST CHART
NATIONAL BUREAU OF STANDARDS-1963-A

AD A 053237

AD No. _____
DDC FILE COPY

6 COPPER HALIDE LASER RESEARCH

9 FINAL REPORT

15
Contract No. N00014-74-C-0445 (ONR)

8
5C

10 C. S. / Liu, D. W. / Feldman, J. L. / Pack L. A. / Weaver
Westinghouse R&D Center
Pittsburgh, Pennsylvania 15235


December 31, 1977

11 31 Dec 77

12 94 p.

DDC
APR 27 1978
F

This document has been approved
for public release and sale; its
distribution is unlimited.

 Westinghouse R&D Center
1310 Beulah Road
Pittsburgh, Pennsylvania 15235

COPPER HALIDE LASER RESEARCH

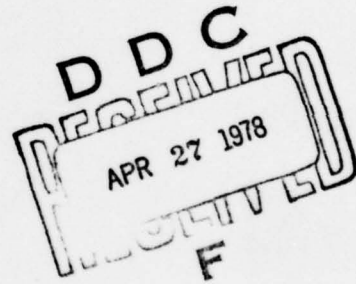
FINAL REPORT

Contract No. N00014-74-C-0445[✓] (ONR)

C. S. Liu, D. W. Feldman, J. L. Pack and L. A. Weaver
Westinghouse, R&D Center
Pittsburgh, Pennsylvania 15235

Steel Corp.

December 31, 1977



Westinghouse R&D Center
1310 Beulah Road
Pittsburgh, Pennsylvania 15235

TABLE OF CONTENTS

	<u>Page</u>
ABSTRACT.	1
1. INTRODUCTION.	2
2. TECHNICAL RESULTS	3
2.1 Double and Continuously-Pulsed Laser Performance Comparisons.	4
2.1.1 Multipulse Degradation Effects.	4
2.1.2 Discharge Tube and Pulser Performance	7
2.2 Spectroscopic Measurements of Multipulse Laser Kinetic Features	17
2.2.1 Experimental Apparatus.	18
2.2.2 Fluorescence Measurements	24
2.2.3 Absorption Measurements	28
2.2.3.1 Ground State Density	32
2.2.3.2 Metastable State Density	44
3. CONCLUSIONS	46
4. REFERENCES.	49
APPENDICES	
A. Axial Cataphoresis Effects in Continuously Pulsed Copper Halide Lasers	
B. Kinetic Processes in Continuously Pulsed Copper Halide Lasers	
C. High Average Power Pulser Design for Copper Halide Laser Systems	
D. A Technique for Determining Gas Temperature and Atomic Density	

LIST OF FIGURES

	<u>Page</u>
Figure 2.1 High power metal halide discharge tube assembly designed for all-hot, sealed-off operation at high pulse repetition rates.	9
Figure 2.2 Electrode feedthrough assembly employed in high average power copper bromide lasers.	11
Figure 2.3 Copper halide discharge tube assembly showing the thermal design features.	13
Figure 2.4 Schematic diagram of the pulser employed to supply high PRF current pulses to copper bromide lasers.	14
Figure 2.5 Temporal sequence of pulser waveforms.	14
Figure 2.6 Experimentally observed voltage and current waveforms obtained from the high PRF pulser unit.	16
Figure 2.7 Experimental absorption apparatus showing the dye laser source, absorption cell container, and multichannel signal averager.	19
Figure 2.8 Optical arrangement for measuring the absorption and fluorescence features of multiply-pulsed CuBr discharges.	21
Figure 2.9 Pulsing sequence and temporal scan synchronization arrangement for dye laser absorption scans through the afterglows of CuBr discharge pulse trains.	22
Figure 2.10 Energy level diagram for copper I (¹ S core configuration only).	25
Figure 2.11 Fluorescence intensities of the (a) 327.8 nm (200 nsec/div) and (b) 510.6 nm (100 nsec/div) copper transitions for the second and eighth discharge pulses in a pulse train. The discharge tube contained CuBr + 10 Torr Ne at a temperature of 500°C.	26
Figure 2.12 Transmission as a function of Cu density for various values of dye laser frequency.	29

LIST OF FIGURES (cont'd.)

	<u>Page</u>
Figure 2.13 Measured Cu ground state absorption shapes as a function of wavelength at various times in the afterglow of pulsed CuBr laser discharges.	31
Figure 2.14 Measured Cu ground state absorption as a function of time for a multipulsed discharge in CuBr laser mixture.	33
Figure 2.15 The Cu ground state absorption as a function of time at various positions along the radius.	35
Figure 2.16 Measured copper ground state density radial profiles at various times in the buildup regime of pulsed CuBr laser discharge.	36
Figure 2.17 Measured copper ground state density radial profiles at various times in the afterglow of pulsed CuBr laser discharges.	37
Figure 2.18 Measured Cu ground state densities as a function of time at various power loading and temperatures.	38
Figure 2.19 Measured copper ground state and metastable state densities as a function of time in the afterglow of pulsed CuBr laser discharges.	40
Figure 2.20 Measured ground state copper density at various wall temperatures as a function of time in the afterglow of pulsed CuBr laser discharge.	42
Figure 2.21 Relative reaction rate vs. square root of temperature for the $\text{Cu}(^2S_{1/2}) + \text{Br}_2$ reaction in a pulsed CuBr laser discharge.	43

ACCESSION for	
NTIS	White Section <input checked="" type="checkbox"/>
DDC	Buff Section <input type="checkbox"/>
UNANNOUNCED	
JUL 1964	
<i>title m/c</i>	
BY	DISTRICT/AVAILABILITY CODES
A	

LIST OF TABLES

	<u>Page</u>
Table 2.1 Design parameters for a 5 W CuBr laser tube.	8



COPPER HALIDE LASER RESEARCH

C. S. Liu, D. W. Feldman, J. L. Pack and L. A. Weaver
Westinghouse R&D Center
Pittsburgh, Pennsylvania 15235

ABSTRACT

This report describes results of experimental studies of continuously-pulsed copper halide laser systems. Optical absorption and fluorescence measurements in the copper bromide discharge have produced detailed information about the laser kinetics in such systems. In particular, the absorption measurements led to determinations of the copper ground state and excited state densities as a function of time and position during a series of electrical pulses. In a longitudinal discharge configuration, radial pumping effects were found to produce appreciable depletion of copper atoms from the core of the discharge region. The effects of this phenomenon on laser performance are discussed and recommendations are made for future development efforts in copper halide lasers.

1. INTRODUCTION

The overall purpose of the program described herein is to determine some of the microscopic properties of multiply-pulsed high repetition rate copper halide lasers. The point of these measurements is to understand those factors which limit the performance of such lasers as they are scaled into the high power regime.

When operated in the double-pulse mode, (i.e., a dissociation pulse followed by an excitation pulse), sealed-off copper halide lasers produce about $50 \mu\text{J cm}^{-3}$ in the 5106 \AA copper line. In the continuously pulsed mode, the specific energy output per pulse is observed to decrease to $\sim 10 \mu\text{J cm}^{-3}$ or less with a conversion efficiency of $\sim 0.3\%$. This reduced specific energy yield limits both the total pulse energy and the average power available. Similar behavior is also observed in copper vapor lasers. To determine those physical factors which influence the volumetric energy yield in the multiply-pulsed regime, a series of measurements has been undertaken to determine fluorescence and optical absorption characteristics of multiply-pulsed copper halide lasers. These measurements have produced detailed information about the temporal evolution during a series of pulses of the populations of those energy levels of the neutral copper atom which are relevant to laser operation. These measurements required the design and implementation of an apparatus capable of optical absorption measurements in operating copper halide lasers with the optical properties measured in both the time and frequency domain, and with good spatial resolution. In addition it was necessary to develop a numerical technique for extracting both gas temperature and number density from optical absorption data. The results of these experimental studies have enabled us to develop a model which explains the power and energy limitations of copper halide and copper lasers and, perhaps, of a number of other gas laser systems. This in turn has led to several important recommendations regarding the directions in which further copper halide system development should proceed.

2. TECHNICAL RESULTS

The technical effort during this contract period was concentrated on measuring and analyzing the operating features of continuously-pulsed copper halide laser systems. Previous work with these lasers had revealed that observed double-pulse performance figures could not be duplicated when multiple electrical pulses were applied to the discharge tube. Thus the potentially attractive features of single-pulse or low prf copper halide lasers could not be extrapolated experimentally into the high prf regime of interest for most practical applications.

To understand the physical nature of this problem, three experimental tasks were performed:

1. Compare double-pulsed and continuously-pulsed copper halide laser performance in suitably fabricated discharge tube apparatus.
2. Determine the physical origin of observed multipulse laser outputs by means of temporally-resolved absorption and fluorescence measurements of ground state and metastable state copper densities in copper halide laser discharges.
3. Describe the copper halide laser operating parameters in terms of both spectroscopic and electrical performance measurements.

These tasks have been performed successfully, and have largely resolved the underlying physical reasons for the reduction of single-pulse laser output energies when a continuous burst of electrical pulses is applied to the laser discharge tube. A high power (~ 5 W) continuously-pulsed CuBr laser has been fabricated and tested. Versatile dye laser absorption measurements and computer data reduction techniques have been developed and applied successfully to copper halide laser discharges. The technical details of these tasks are described in the following sections.

2.1 Double and Continuously-Pulsed Laser Performance Comparisons

2.1.1 Multipulse Degradation Effects

Experiments with continuously-pulsed copper halide laser discharges isolated several important physical effects which influence laser performance in the multipulse regime. The principle results of these experiments are summarized in two scientific journal publications, which are included as Appendices A and B:

Appendix A: "Axial Cataphoresis Effects in Continuously-Pulsed Copper Halide Lasers" by C. S. Liu, D. W. Feldman, J. L. Pack and L. A. Weaver, J. Appl. Phys. 48, 194 (1977).

Appendix B: "Kinetic Processes in Continuously-Pulsed Copper Halide Lasers" by C. S. Liu, D. W. Feldman, J. L. Pack and L. A. Weaver, IEEE J. Quantum Electron. QE-13, 744 (1977).

The first physical effect, axial cataphoresis within the laser discharge, represents a very pronounced spatial redistribution of the discharge species along the discharge axis, with a correspondingly pronounced degradation of the copper halide laser output energy. During single-pulse operation the drift of positive copper ions towards the cathode (i.e., cataphoresis) is very slight, and normal diffusion forces soon equilibrate species densities along the tube length. Thus this particular degradation effect does not operate during single-pulse laser tests. When multiple discharge pulses are applied at high current density and repetition rate, however, these cumulative axial forces are sufficient to drive a large fraction of the copper ions towards the cathode region within a few seconds of multipulse operation. The resulting steady state copper/copper halide density distribution, after electron-ion and/or copper-halogen recombination, is thereby concentrated in the cathode region and depleted in the anode region. This leads to sub-optimum laser excitation throughout the discharge region, and in many cases sub-threshold copper densities near the anode.

Another deleterious effect of this axial segregation is the interruption of the copper-halogen chemical recombination cycle. Copper atoms accumulate near the cathode, and eventually condense on the adjacent

walls. Halogen atoms, which form negative ions through electron attachment, accumulate near the anode and eventually fill the entire tube with halogen molecules after molecular recombination. Thus after several hours of operation, most of the copper is plated on the walls near the cathode, and the discharge tube is filled with unacceptably high levels of halogen molecules which cause arcing. Laser output is degraded initially from single-pulse levels due to rapid axial redistribution of the copper, and over the longer term laser action is terminated completely by the cataphoresis-induced chemical segregation of the decomposition products.

Fortunately, this particular multipulse degradation effect can be remedied quite simply by alternating the polarity of successive discharge pulses. Alternating electrical polarity prevents accumulations of charged species in a preferred direction by essentially averaging the cumulative migration to zero over many discharge pulses. The same engineering solution is applied to fluorescent lamps with the use of alternating current; with direct current, the performance of these lamps would soon degrade due to mercury accumulation at the cathode. Tests performed on high power copper halide laser tubes with advanced polarity-reversing pulser circuitry demonstrated that the deleterious effects of axial cataphoresis in the multipulse regime can be eliminated completely using this technique.

The second general source of multipulse laser degradation discovered during this work is described completely in Appendix B, and has its origins in laser kinetic and radial depletion effects. During normal double-pulse electrical excitation, the first pulse dissociates the copper halide to create free copper atoms, and the second pulse applied several hundred microseconds later excites the copper atom to its lasing state. Typically, the dissociation pulse contains about ten times the energy of the excitation pulse to generate optimum copper atom densities. Under these circumstances $\sim 50 \mu\text{J cm}^{-3}$ of copper laser output is available. In the multipulse regime, however, continuous application of such high current "dissociation" pulses rapidly raises the gas temperature to values which thermally populate the lower laser level, and within a few minutes the quartz discharge tube would melt due to

temperature restrictions, whereas a single high current pulse can be accommodated without difficulty since its total heating effect is negligible.

In practice, we found that pulse energies comparable to the second (i.e., the excitation) pulse could be sustained on a continuous basis without deleterious gas heating effects. Since a single pulse within this train would dissociate only about one tenth of the copper that a full dissociation pulse would generate in a double-pulse experiment, one would expect that as little as one-tenth the laser energy output would be produced in the multipulse regime. However, it happens that for the excited state lifetimes and interpulse spacings of interest, the ground state copper density accumulates to about twice its single-pulse value in the multipulse regime, whereas the copper lower laser level density remains unchanged. Thus the applicable multipulse derating factor is approximately 5 rather than 10 due to beneficial multipulse accumulation effects. This result was confirmed in burst-mode excitation experiments, where $\sim 10 \mu\text{J cm}^{-3}$ was obtained from discharge tubes which produced $\sim 50 \mu\text{J cm}^{-3}$ under double-pulse excitation.

Another degradation effect described in Appendix B is due to a depletion of the copper density on the longitudinal axis of the discharge tube as the pulse train is applied. This is seen as a transient decrease in the laser output energy on a millisecond time scale as successive discharge pulses are applied.

The reduction in laser energy at steady state is typically a factor of two, although near laser threshold reservoir temperatures this depletion effect can actually extinguish laser emission. The depletion can be caused by either gas heating by the discharge, or by the radial cathaphoresis of copper ions. Both effects are cumulative and of sufficient magnitude to cause the observed performance. Neither is important in a double-pulse experiment, but in multipulse operation cumulative gas temperature and/or charged particle radial gradients can force copper atoms radially towards the container walls. Thus in the steady state, an additional multipulse degradation factor as large as ~ 2 can be induced by radial depletion effects.

To a considerable extent, this depletion effect can be minimized or even eliminated by operating at higher reservoir temperatures so that the background axial copper/copper halide density is elevated to compensate for radial depletion. Thus the fractional depletion due to radial forces is correspondingly less. However, in most cases higher operating temperature introduces other problems such as discharge instabilities which render such corrections somewhat ineffective. The deleterious cumulative laser kinetic effects, on the other hand, can be reduced by operating at lower pulse energies and higher pulse repetition frequencies. Thus it appears that the multipulse degradation effects are minimized in the low energy, high prf regime where gas heating is small.

These experiments remove substantially all of the uncertainty of multipulse degradation effects in copper halide lasers, and in some cases recommend specific corrective procedures. An obvious solution to this problem is to provide rapid transverse gas flow which removes deleterious species and gas heat; if this solution were implemented, it is quite certain that the multipulse degradation effects observed in static experiments would disappear. This engineering modification was not attempted during the research effort, but is recommended for future copper halide development programs.

2.1.2 Discharge Tube and Pulser Performance

In order to test the performance of continuously-pulsed copper halide lasers under high prf operating conditions, a high power quartz discharge tube and electrical pulsing unit were designed and fabricated. Both the tube and pulser incorporated advanced design features which permitted total system performance substantially beyond the prior state of the art in copper halide lasers. The discharge tube sustained average power dissipations of approximately 3 kW at pulse repetition rates near 16 kHz for cumulative operating time of 100 hours without failure, and was completely sealed-off and self-heated during these tests. The pulser delivered average powers up to 5 kW at pulse repetition rates up to 20 kHz, with polarity reversal on alternate pulses. Laser output power levels of 3.5 W at 16 kHz were obtained at 0.2% efficiency under continuous

operation, and under burst-mode excitation the average power was 6.5 W at 0.3% efficiency. This apparatus also served as the test stand upon which extensive spectroscopic measurements of multipulse effects were performed.

The laser discharge tube shown in Fig. 2.1 was fabricated from high quality GE-204 quartz with molybdenum:quartz cup seals serving as electrical feedthroughs. Optical grade quartz windows were fused onto the discharge tube ends at a slightly tilted angle ($\sim 10^\circ$) to avoid internal reflections along the tube axis. Electrodes were made of molybdenum cups with heat shields to improve their thermal efficiency. This type of discharge tube was successfully operated for over 100 hours without failure under a power loading of 50 W cm^{-3} .

As a guide to the design of the laser tube, Table 2.1 contains the design parameters for a 5 W copper bromide laser.

Table 2.1. Design Parameters for a 5 W CuBr Laser Tube

Laser Medium:	CuBr
Temperature:	300°C to 600 °C
Discharge Configuration:	Longitudinal
Volumetric Energy Yield:	$2.0 \mu\text{J cm}^{-3}$
Pulse Repetition Rate:	16 kHz (6 to 20 kHz)
Energy Output per Pulse:	313 μJ
Volume:	157 cm^3
Discharge Dimensions:	50 cm x 1.8 cm diameter
Efficiency:	0.2%
Input Power:	2.5 kW

CuBr lasers were excited by current pulses having ultra-fast risetimes, very short durations and high peak amplitudes ($>100 \text{ A cm}^{-2}$). These required low inductance laser tube designs that minimized circuit inductance.

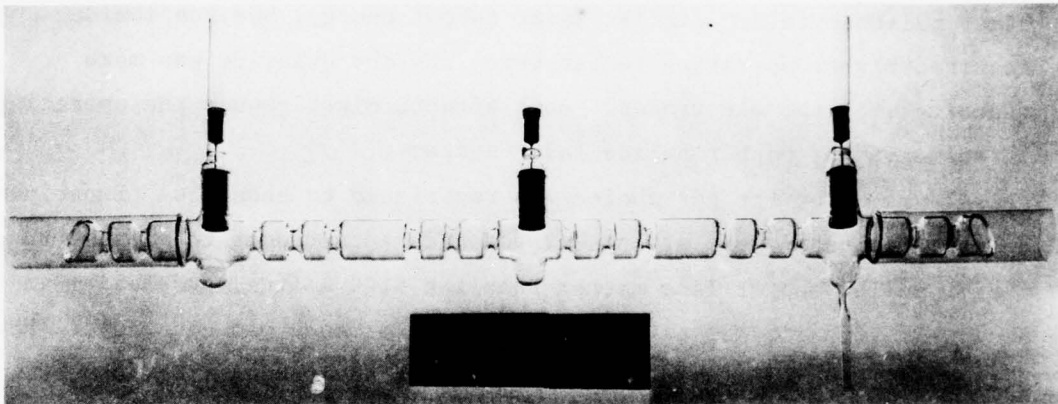


Fig. 2.1. High power metal halide discharge tube assembly designed for all-hot, sealed-off operation at high pulse repetition rates.

We have developed a high-current low-inductance, long-lived hollow cathode electrode for use with these lasers. Conventional quartz:molybdenum cup seals were used for electrical feedthroughs. The current was conducted by a molybdenum tube which was welded onto the molybdenum cup. The electrodes shown in Fig. 2.2 consisted of two concentric molybdenum cylinders with an inner tube diameter of 0.5 cm, outer tube diameter of 1.5 cm and length of 3.0 cm. The electrodes were also welded onto the molybdenum cup seals.

The choice of copper bromide was based on its chemical stability and reactivity, vapor pressure and laser operating performance. Other halides yielded similar laser output energy, but the iodide required higher operating temperatures and the chloride was more reactive with the electrodes. Both effects might reduce the operating lifetime of the copper halide laser system.

The buffer gas choice was restricted to neon gas. Experimental results indicated that argon, krypton and xenon tended to enhance the 5782 Å yellow copper line rather than the 5106 Å line, and helium and neon were very similar as far as laser performance was concerned. However, helium diffused easily through the quartz tube at operating temperatures, and was therefore avoided for long-lived, sealed off laser tube embodiments.

The chemical properties of the molybdenum electrodes appear to be quite satisfactory on the basis of the demonstrated 100 hour operating lifetimes. A small portion of the electrode material was eroded and transported onto the wall during the first 100 hours of operation. If a linear extrapolation of electrode erosion effects is assumed, then these electrodes should last at least several thousand hours without failure. However, diffusion of copper ions into the quartz at elevated temperatures was observed and could constitute a lifetime limitation unless prevented.

The tube dimensions, waste discharge heat, quartz surface emissivities and proper heat shield design were combined to give the appropriate thermal design capable of maintaining the laser tube temperature above 550°C for self-heated operation. An outer jacket

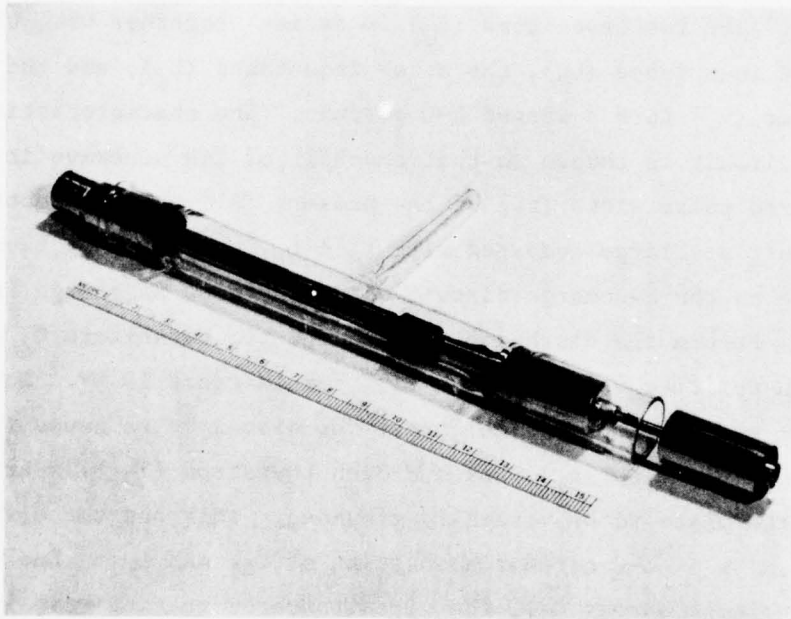


Fig. 2.2. Electrode feedthrough assembly employed in high average power copper bromide lasers.

surrounding the laser tube was used as a heat shield. The jacket was fabricated from a split Pyrex tube, and additional heaters to generate hot N_2 were utilized for maintaining the laser windows at sufficiently high temperatures to prevent copper bromide condensation on the optical surfaces. The complete thermal design embodiment is shown in Fig. 2.3. The steady state operating temperature of approximately $550^\circ C$ was reached in a little over 10 minutes.

The circuit diagram for the high power pulser is shown in Fig. 2.4. The two capacitors (C_d) in series together with the apparent discharge inductance (L_d), the stray inductance (L_s), and the discharge resistance (R_d) form a damped L-C circuit. The characteristic frequency of this circuit is chosen so that one-half of its sinewave is equal to the desired pulse width (t_q) of the pulser. All other inductances in the circuit are large compared with $L_d + L_s$, so that they have little influence on the discharge circuit while the glow discharge is ignited.

Before the discharge occurs, the two capacitors C_d are charged to a high positive voltage ($E_1 = E_2$), for instance 10 kV. No voltage potential exists at this time across the discharge to cause ignition. Then at a given time (t_1), the hydrogen thyratron (Th_1) is triggered, causing its plate to be virtually grounded. This has the effect of suddenly forming a L-C circuit consisting of C_{d1} and L_{r1} . Due to the initial voltage across C_{d1} , the circuit starts to ring with its own characteristic frequency, say 2 MHz. The result is that the voltage (E_1) swings from its original plus 10 kV down past zero toward minus 10 kV (Fig 2.3). If the laser tube were not connected, the voltage difference ($E_2 - E_1$) would reach almost 20 kV. The circuit is often referred to as a "Blumlein Circuit". It provides voltage doubling by what is termed "resonance charging".

If the laser tube is connected as shown in Fig. 2.4 then the glow discharge ignites at some voltage lower than 20 kV (at $t = t_b$ in Fig. 2.5) and the two capacitors (C_d) discharge with a current (i_d)

Dwg. 6401A96

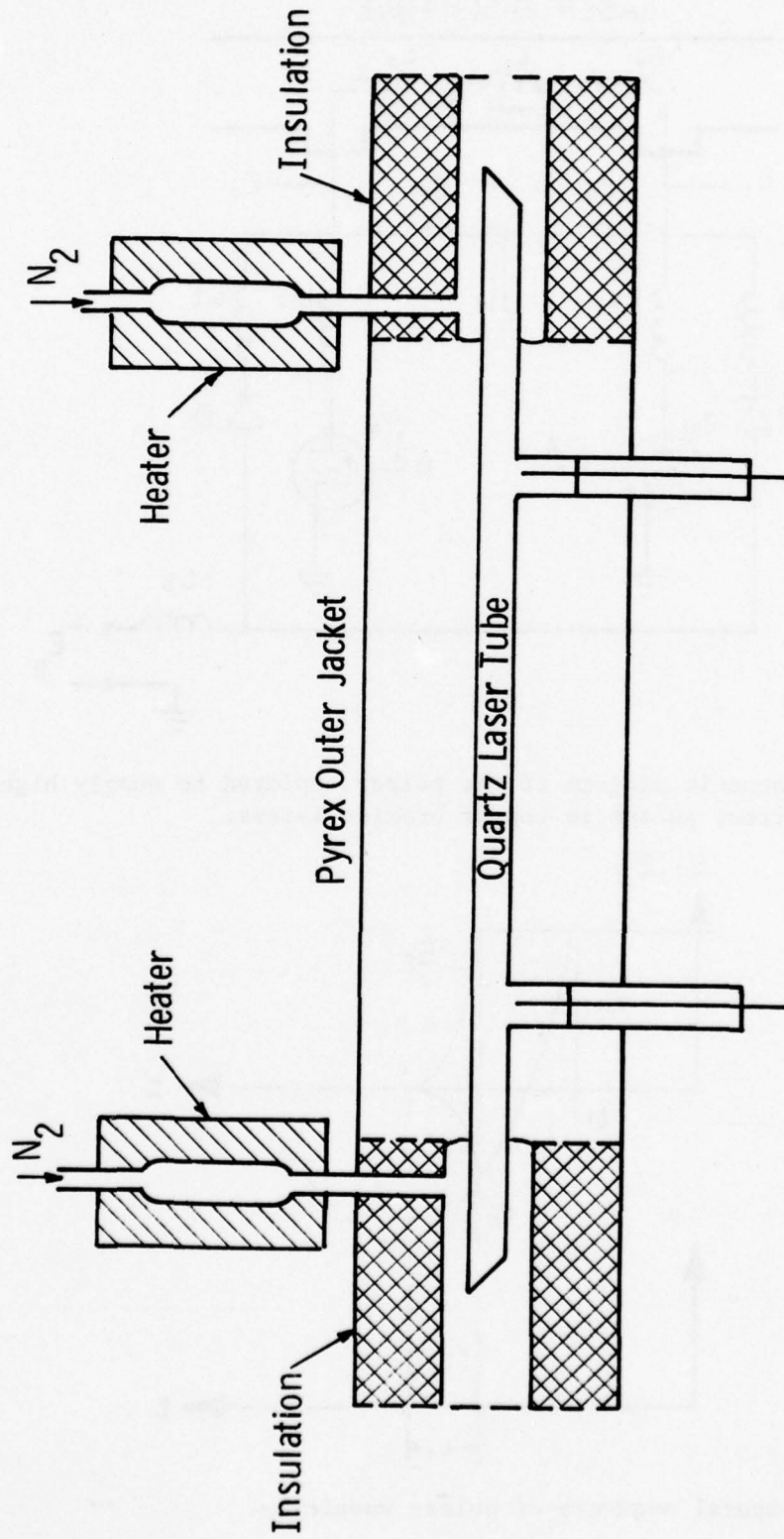


Fig. 2-3. Copper halide discharge tube assembly showing the thermal design features.

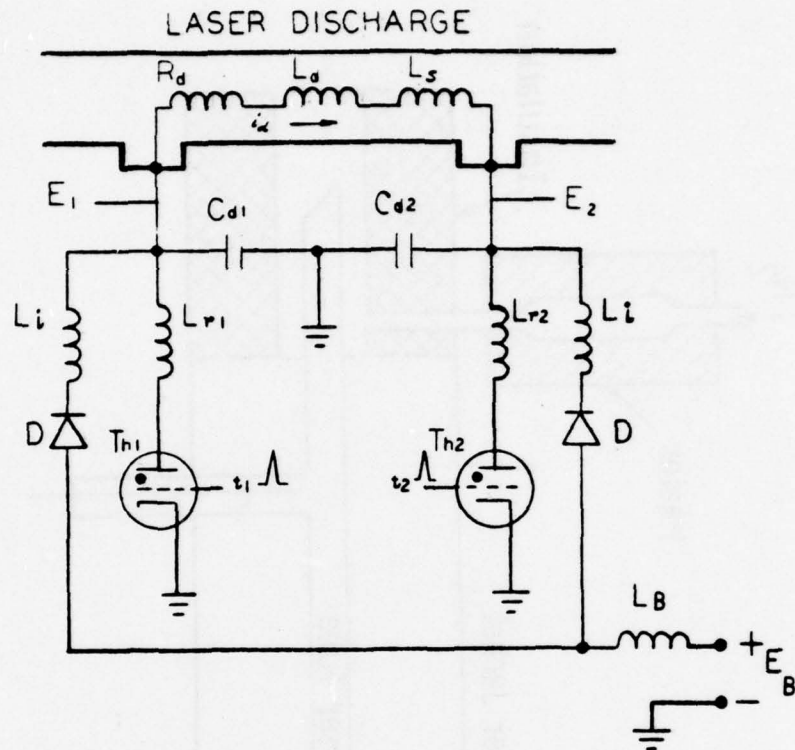


Fig. 2.4. Schematic diagram of the pulser employed to supply high prf current pulses to copper bromide lasers.

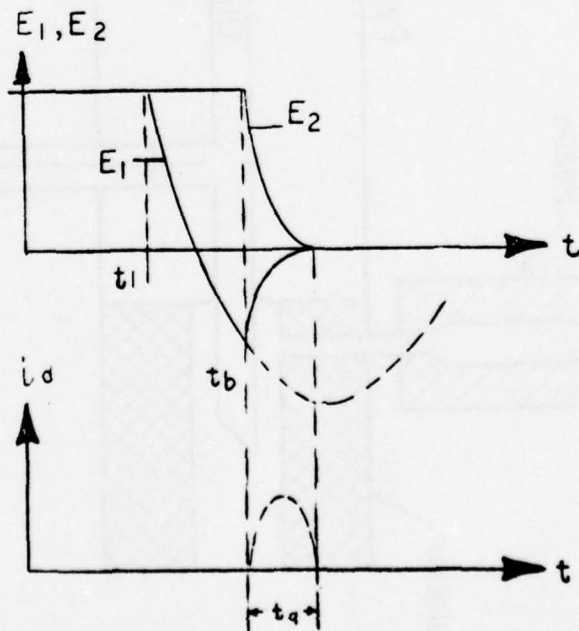


Fig. 2.5. Temporal sequence of pulser waveforms.

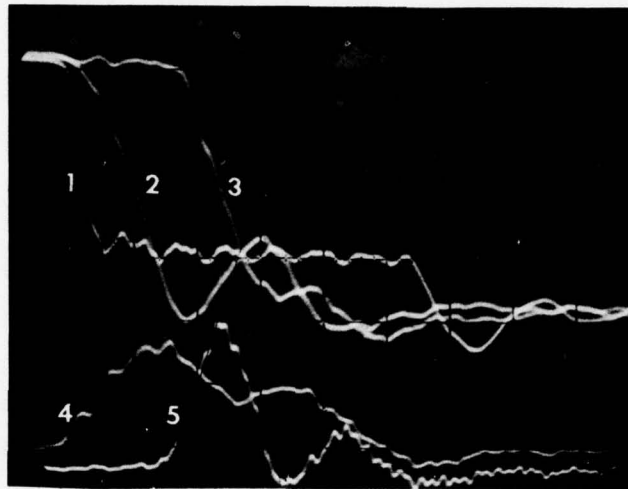
through the impedance formed by L_d , L_g , and R_d with the desired pulse width (t_q) as mentioned before, until the glow discharge extinguishes due to insufficient voltage difference left between the capacitors. The thyatron Th_1 extinguishes when the current through it becomes zero.

After this, the two capacitors C_d recharge again through the charging coil (L_B), the diodes (D), and the isolation coils (L_1). (The isolation coils are small compared with L_B and reduce cross talk between the thyratrons.) As long as the charging current keeps the diodes in their conducting state, the charging coil and the parallel combination of the two capacitors, form an L-C circuit, which is tuned to the maximum pulse repetition frequency of the laser. This L-C circuit rings to a voltage which is ideally twice as high as the supply voltage (E_B). In this way the circuit accomplishes voltage quadrupling by applying the resonant charging principle twice in series. The diodes avoid a premature discharge of the capacitors once they have attained their maximum voltage.

When the capacitors are fully recharged, the circuit is ready for its next pulse at $t = t_2$, which is now initiated through thyatron Th_2 in the same manner as before through Th_1 . This time the discharge current i_d flows in the opposite direction. Figure 2.6 shows traces from our existing laser driver circuit. The discharge current wave (i_d) has a bell-shape rather than half a sinewave because of the non-linearity of R_d . This circuit has delivered 3 kW to the laser discharge at a pulse repetition frequency of 16 kHz. The capacitors C_d were charged to 10 kV with a dc power supply voltage $E_B = 5$ kV.

Perhaps the prime advantage of these circuits is the fact that the thyratrons are almost isolated from the discharge circuit, once ignition has occurred. This makes it possible to maximize the discharge current slope without concern for the thyatron switching speed.

The Blumlein circuit is well suited to the requirements of the long-lived, high power, high repetition rate copper halide laser



1. Thyatron plate voltage.
2. Capacitor voltage (triggered branch).
3. Capacitor voltage (untriggered branch).
4. Thyatron current.
5. Discharge current i_d .

Scale: time - 50 ns/div
voltages - 5 kV/div
currents - 100 A/div

Fig. 2.6. Experimentally observed voltage and current waveforms obtained from the high prf pulser unit.

systems. The current reversing feature is important, since it eliminates problems associated with longitudinal cataphoresis effects and makes possible a truly long-lived, sealed-off laser tube. This pulser has been operated at 2.5 kW average power levels and 15 kHz pulse repetition rates for cumulative times exceeding 300 hours without component failure or observable degradation of the operating characteristics.

The design details and operating features of the Westinghouse high average power pulsing unit were summarized in a scientific journal publication which is attached as an appendix to this report:

Appendix C: "High Average Power Pulser Design for Copper Halide Laser Systems", by J. L. Pack, C. S. Liu, D. W. Feldman and L. A. Weaver, Rev. Sci. Instrum. 48, 1047 (1977).

This paper describes additionally a modular concept for pulser scaling to high average power levels. In this approach, the basic Blumlein circuit configuration is replicated for each additional longitudinal discharge section. This provides all the features of low-inductance drive circuitry while maintaining the applied voltage and polarity reversal features of a single circuit module. This circuit arrangement was tested experimentally, and it was verified that adjacent discharge and pulser segments can operate satisfactorily without deleterious interference from adjacent modules. Thus the engineering practicality of the basic circuit design has been established, and its scalability to higher average power configurations has been demonstrated.

2.2 Spectroscopic Measurements of Multipulse Laser Kinetic Features

The underlying physical reasons for observed decreases in the laser output energy in continuously pulsed copper halide lasers have not been understood clearly. It appears that certain deleterious effects of either a gas discharge or a laser kinetics origin accumulate to inhibit laser processes, but the specific nature of these effects has not been described satisfactorily. Therefore, this Spectroscopic Task area includes measurements of the absorption and fluorescence characteristics of continuously-pulsed copper halide discharges to determine (1) the temporal and spatial behavior of copper ground state and metastable

densities; (2) the effective lifetimes of the copper upper and lower laser levels, and (3) the destruction rate of copper ground state atoms.

For this purpose a general spectroscopic diagnostic facility has been assembled and implemented to probe the afterglows of repetitively-pulsed copper halide discharges. Fluorescence measurements of copper atom emission have yielded valuable information on pulse-to-pulse excited state populations and lifetimes. Similarly, absorption measurements using a tunable dye laser source have yielded detailed information on the temporal evaluation of copper ground state and metastable state populations during discharge pulse trains. The absorption measurements have been taken as a function of tube radius as well, and have confirmed previous empirical observations that a substantial depletion of axial densities occurs during a discharge pulse train.

Absorption at line center is often excessive at high densities and long path lengths, resulting in inadequate transmitted probe signal levels. This effect usually places an upper limit of $\sim 10^{13} \text{ cm}^{-3}$ on the measurable copper ground state density. With a tunable dye laser source, however, it is possible to detune the probe laser wavelength from the absorption line center and obtain useful data in the wings of the absorption feature despite high absorber densities.

This technique was employed experimentally, and in order to deconvolute the absorption and source line profiles a generalized line overlap computer program was developed. Using measured line profiles, this program extracted not only density but temperature information from the experimental data. Thus rather detailed information is available to describe the temporal and radial development of copper species during a burst of high prf electrical discharges.

2.2.1 Experimental Apparatus

The facility used for optical diagnostics of the copper halide laser is illustrated in Fig. 2.7. The copper halide laser test cell consisted of a longitudinal discharge tube contained within a high temperature oven. The laser tube was fabricated from 18 mm diameter quartz, and was 50 cm long. The tube contained CuBr with a few Torr of

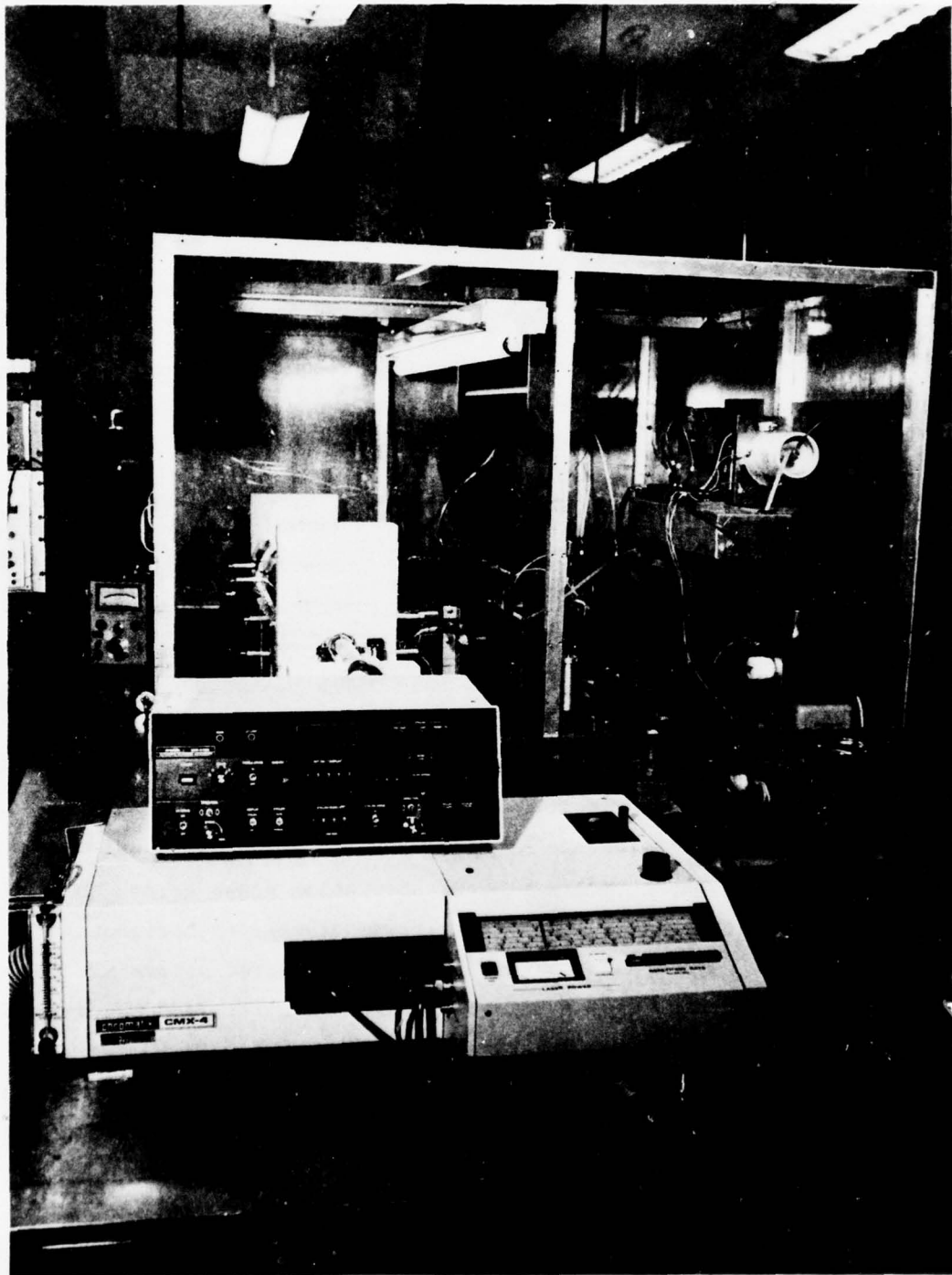


Fig. 2.7. Experimental absorption apparatus showing the dye laser source, absorption cell container, and multichannel signal averager.

Ne, and the entire tube was sealed off under ultra-clean conditions. The experimental measurements were made in the temperature region between 400 and 600°C, where the CuBr density in the cell ranges from about 10^{14} to 10^{17} cm⁻³. The cell was heated in a thermostatically controlled oven to assure temperature uniformity. Additional heat was applied near the optical end-windows of the cell to prevent CuBr condensation. The tube temperature was monitored by calibrated chromel-alumel thermocouples, and the temperature was maintained to the cold spot temperature to within a $\pm 3^\circ\text{C}$ tolerance during spectroscopic measurements.

Figure 2.8 illustrates the absorption experiment optical arrangement and the electronic data processing employed for the burst-mode density measurements. A Chromatix CMX-4 tunable dye laser operating at 10 to 15 pulses per second served as the probe laser source, tuned in wavelength to the desired CuBr discharge absorption feature. This output was divided into two beams, one which passed through the length of the test cell, and a second reference beam which bypassed the cell. Both the absorbed and the reference signals were detected by a pair of matched Hamamatsu HTV R617-2 photodiodes. These detected signals were then directed through a Molectron LP-20 pulse ratiometer to generate the ratio of absorbed and reference signals, and the pulse averaged ratio was displayed on a chart recorder. For absorption scans across the tube radius, the entire oven and tube assembly was translated horizontally. Fluorescence from the end of the discharge was detected separately through a $\frac{1}{4}$ meter monochromator and an EMI 9526 photomultiplier, and the signal was then displayed on an oscilloscope.

The timing synchronization and temporal scanning arrangement is illustrated schematically in Fig. 2.9. The dye laser was pulsed at a 10 to 15 Hz rate in synchronism with the 60Hz line frequency, and at the same time an electronic trigger pulse from the dye laser was applied to a Hewlett-Packard HP214 pulse delay generator. This signal in turn was applied to a Princeton Applied Research CW-1 variable speed boxcar scanning unit to provide a signal whose delay was increasing smoothly with time. After inputs to a HP214 variable-width square wave generator

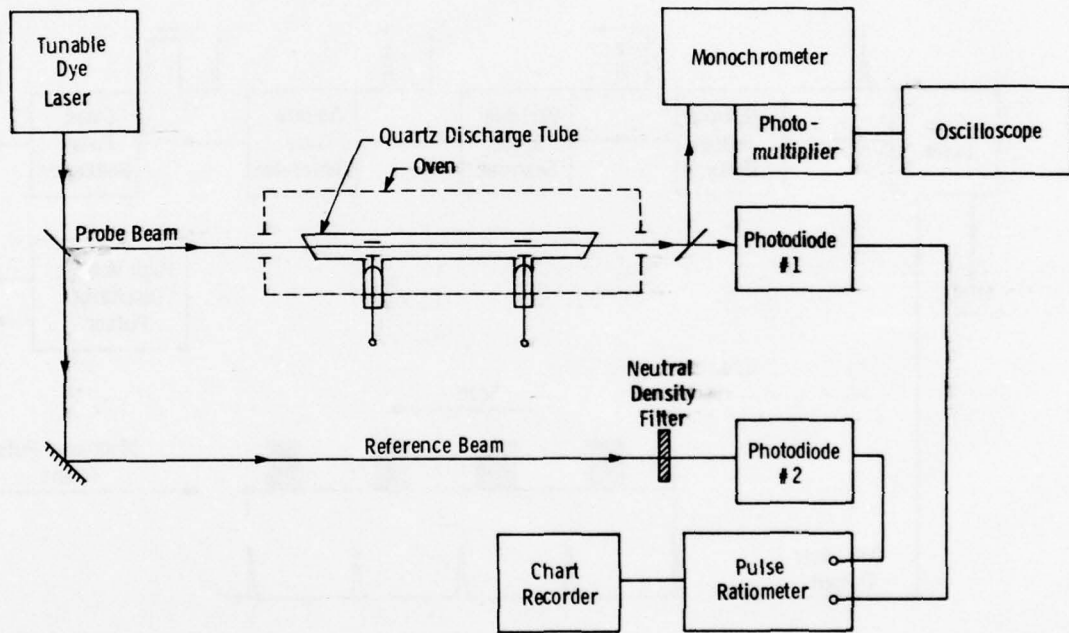


Fig. 2.8. Optical arrangement for measuring the absorption and fluorescence features of multiply-pulsed CuBr discharges.

Dwg. 1693B26

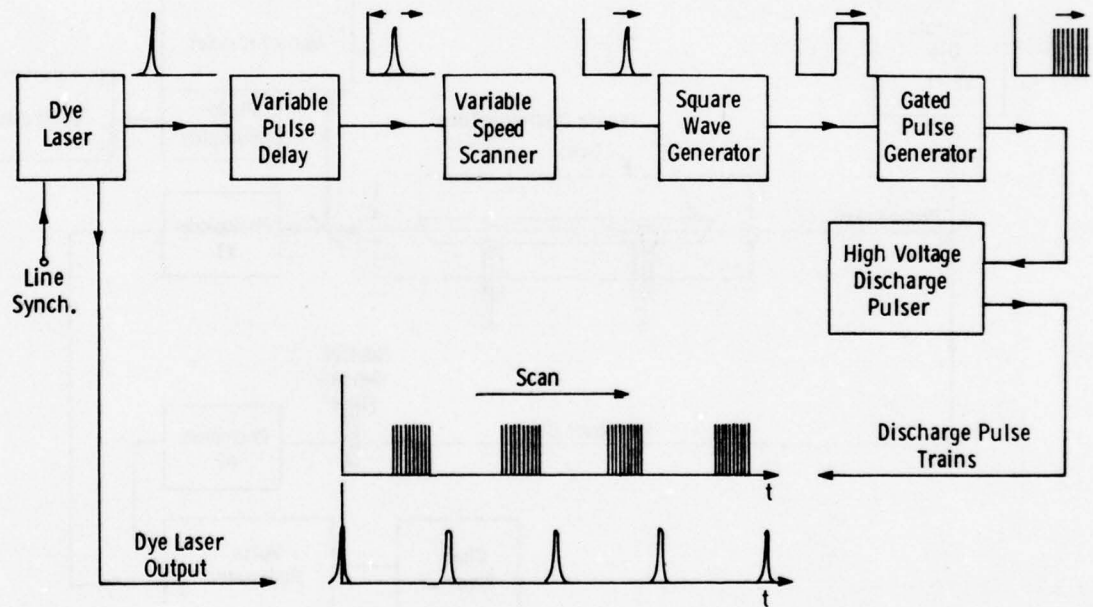


Fig. 2.9. Pulsing sequence and temporal scan synchronization arrangement for dye laser absorption scans through the afterglows of CuBr discharge pulse trains.

and a homemade gated pulse generator, the resulting electronic signal was a high prf burst of pulses whose starting time was being delayed smoothly with time. The initial delay, the scanning rate, the burst duration and the intraburst pulse repetition rate could all be varied independently, and the pulse train was synchronized to the 10 to 15 Hz pulse rate of the dye laser. This burst of pulses was employed to trigger a thyatron-switched, high-voltage pulser which powered the longitudinal discharges within the CuBr test cell.

A typical electrical pulse train consisted of pulses approximately 100 msec apart (ie: 10 kHz prf) with an overall burst duration of 5 msec. Under these conditions each burst contained ~ 50 pulses. The pulse trains were separated by ~ 70 msec for a dye laser pulsing rate of ~ 15 Hz, which maintained the CuBr discharge tube at approximately the same temperature from burst to burst while providing an acceptably high data acquisition rate. To obtain afterglow population measurements, the dye laser was first tuned in wavelength to the discharge absorption feature of interest. As shown diagrammatically in Fig. 2.9, the pulse train sequence was then scanned slowly past the dye laser probe pulses. Thus the dye laser probed conditions successively closer to the electrical discharge pulse with each dye laser pulse. In this fashion the absorption characteristics were measured in reverse time sequence through the entire burst of discharge afterglows. With the appropriate reversal of the boxcar delay scanning direction, the absorption scan could also proceed forward in time through the burst. The resulting chart recording portrayed the discharge absorptance at the probing wavelength as a function of time through the burst of electrical pulses.

The spectral profiles of the copper absorption features were obtained by scanning the dye laser output wavelength slowly across the discharge absorption line. A line-narrowing etalon was employed to reduce the dye laser linewidth to $\sim .4 \text{ cm}^{-1}$ as measured with a scanning Fabry-Perot interferometer, and a frequency-doubling KDP cell was employed to generate the 3248\AA wavelength required to probe the copper ground state.

In practice, the dye laser wavelength was detuned from the 3248Å atomic copper line center because of excessive absorption at line center, and the number density and temperature were deduced from these measurements using a versatile line overlap computer program.

2.2.2 Fluorescence Measurements:

The principal copper fluorescence lines monitored experimentally are shown in the copper energy level diagram of Fig. 2.10. A near-ultraviolet resonance line at 324.8 nm connects the $4p^2P_{3/2}$ upper laser level to the $4s^2S_{1/2}$ ground state. The commonly observed 510.6 nm laser transition originates from the same $4p^2P_{3/2}$ level, and terminates on the $3d^94s^2D_{5/2}$ metastable level. Since these transitions are critically important in understanding copper laser kinetic relationships, these two lines were selected for both fluorescence and absorption measurements.

The temporal features of the 324.8nm and 510.6nm copper fluorescence lines are illustrated in Fig. 2.11 for a continuously-pulsed CuBr + 10 Torr Ar discharge operated in a burst mode. The current pulse width was ~70 nsec FWHM, and the tube wall temperature was 500°C. Each oscillograph was recorded with the same S-13 photomultiplier, and the monochromator slits were adjusted to eliminate photomultiplier saturation effects. At the second pulse in the train, both the 324.8nm and 510.6nm fluorescence intensities increased in ~120 nsec to their peak values, and thereafter decayed to zero with a time constant of ~150 nsec. These risetimes were noticeably less than the current risetimes. By the eighth discharge pulse, however, this fluorescence behavior had changed radically. The 324.8nm intensity rose in ~30 nsec to a peak value about twice that observed on the second pulse, and decayed with a ~150 nsec time constant. Correspondingly, the 510.6nm intensity exhibited a sharp leading spike of doubled intensity and narrow width, followed by a ~150 nsec decay. Similar temporal profiles were observed with all successive discharge pulses.

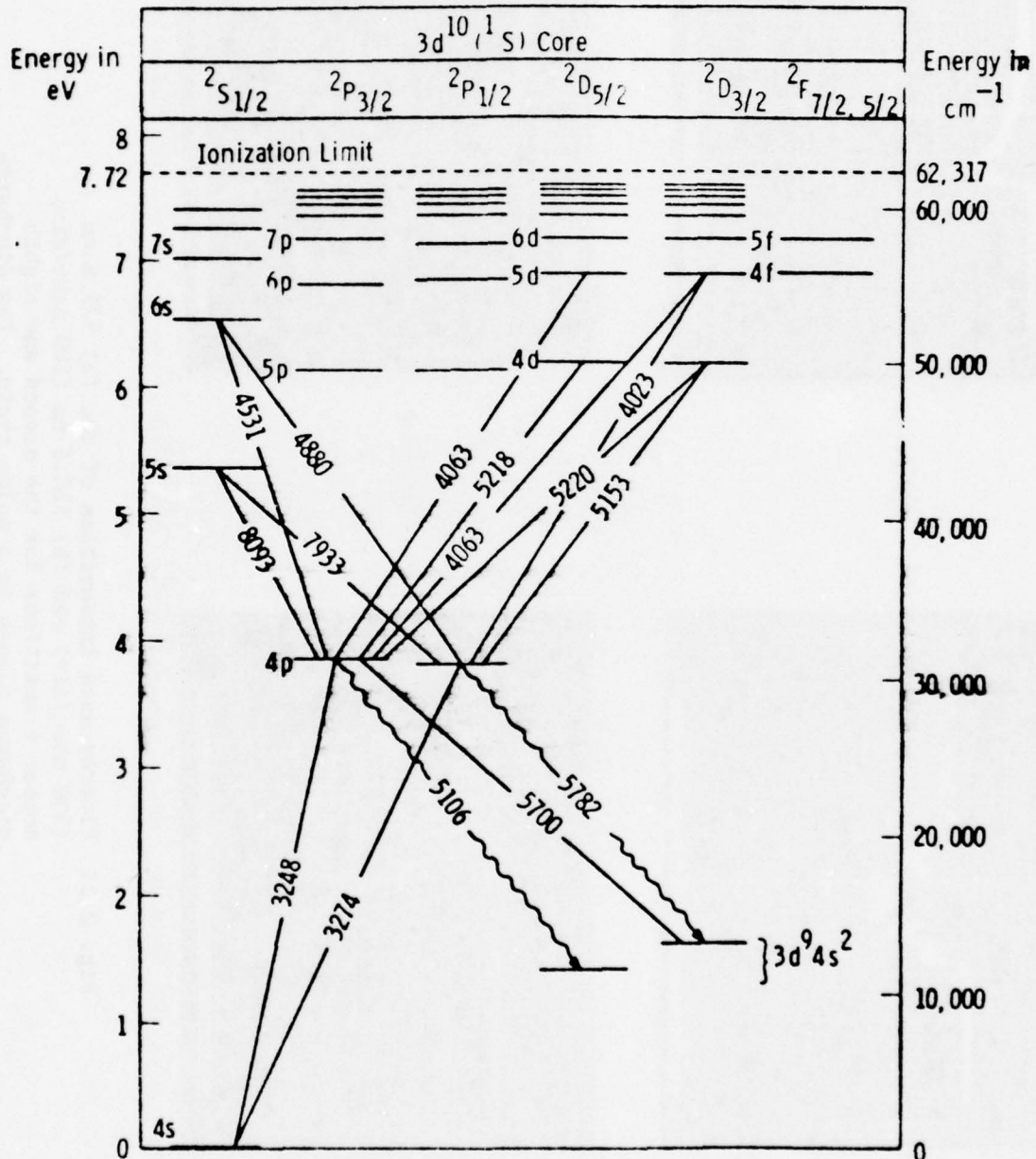
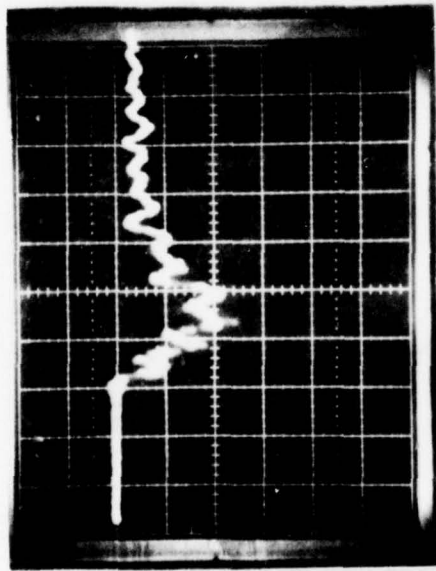
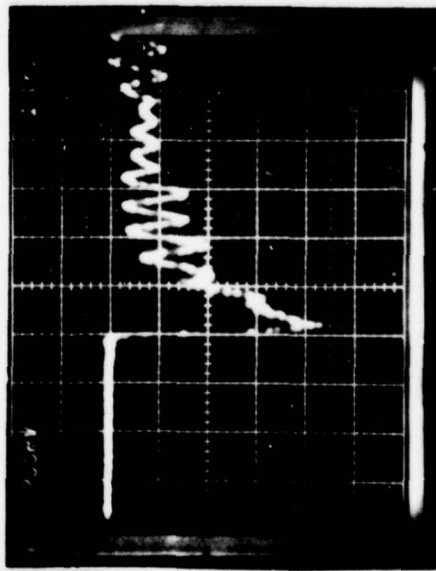


Fig. 2.10. Energy level diagram for copper I ($1S$ core configuration only).

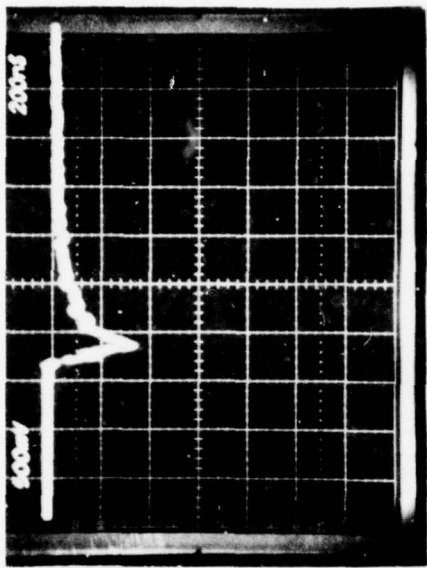


2nd pulse

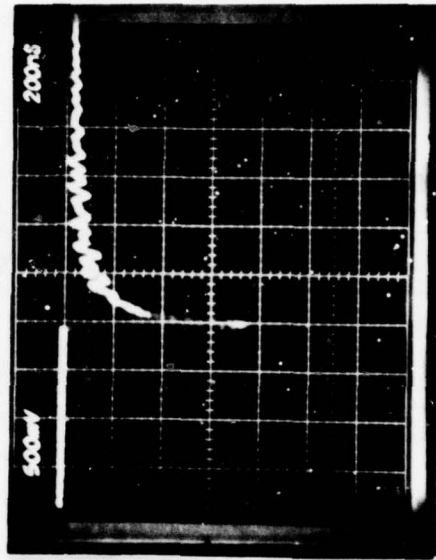


8th pulse

(a) 324.8 nm



2nd pulse



8th pulse

(b) 510.6 nm

Fig. 2.11 Fluorescence intensities of the (a) 327.8 nm (200 nsec/div) and (b) 510.6 nm (100 nsec/div) copper transitions for the second and eighth discharge pulses in a pulse train. The discharge tube contained CuBr + 10 Torr Ar at a temperature of 500°C.

This behavior can be interpreted in terms of copper bromide dissociation and copper resonance radiation trapping dynamics. For the first several discharge pulses insufficient copper ground state atoms are dissociated to imprison the 324.8nm resonance radiation. As shown in the following section, the initial $^2S_{1/2}$ copper ground state density is $\sim 10^{12} \text{ cm}^{-3}$, which is below the radiation trapping threshold for a 0.9cm diameter discharge vessel. Thus the $^2P_{3/2}$ level is only sparsely excited from the ground state, and this excitation is rapidly radiated to the $^2S_{1/2}$ ground and $^2D_{5/2}$ metastable levels. Evidently no dissociative excitation of Cu_3Br_3 produces Cu in the $^2P_{3/2}$ state, so both the 324.8nm and 510.6nm fluorescence rise slowly to relatively low peak intensities due to subsequent electrical excitation of dissociated $\text{Cu}(^2S_{1/2})$ ground state atoms. Thus the first several electrical pulses are invested primarily in Cu_3Br_3 dissociation, and only relatively low amounts of copper ground state excitation occur in this untrapped regime.

By the eighth discharge pulse the $\text{Cu}(^2S_{1/2})$ ground state density has accumulated to $\sim 10^{14} \text{ cm}^{-3}$, as shown in the following section. This density is above the resonance radiation trapping threshold, and permits substantial excitation to the $^2P_{3/2}$ upper laser level because of the larger initial $\text{Cu}(^2S_{1/2})$ density and the radiation imprisonment. Thus both the 324.8nm and 510.6nm fluorescence rises to their peak values in times comparable to the discharge current risetime, and these peaks are twice those attained in the untrapped regime. The 510.6nm transition develops a large stimulated emission component as the $^2P_{3/2}$ population becomes inverted with respect to the $^2D_{5/2}$ population, and a rapid depletion of the upper laser level is observed. At this point, a strong longitudinal superradiance is observed experimentally at the 510.6nm wavelength.

The ~ 150 nsec $^2P_{3/2}$ fluorescence lifetime varies only slightly with the buffer gas pressure, whereas increased reservoir temperatures decrease the lifetime slightly. It appears that the 324.8nm and 510.6nm afterglow fluorescence is dominated by cascading from higher-lying copper levels formed by slower electron-ion recombination processes. Thus the 150 nsec fluorescence lifetime should be interpreted as an upper limit to the $^2P_{3/2}$ radiative lifetime.

2.2.3 Absorption Measurements

For ground state density measurements as a function of time the Chromatix CMX-4 dye laser was employed without etalon narrowing. Under these conditions, the full width at half maximum for UV operation was 5.6cm^{-1} or 0.59\AA . This width was large enough that the dye laser line shape could be measured with a one meter monochromator having a resolution of $\sim 0.3\text{cm}^{-1}$. The line intensity profile measured experimentally to a value $\sim 10\%$ of the peak height. For computational purposes, this shape was extended with Lorentzian tails to $\sim 0.5\%$ of the peak height.

Using the technique described in appendix D, the optical transmission can be calculated as a function of copper vapor density for various values of the dye laser center frequency. The results of such a calculation are shown in Figure 2.12. It was necessary in some cases to use the dye laser offset from the copper absorption line in order to measure vapor densities at higher values. Although the transmission depends somewhat on temperature as well as density, calculations indicate that for the dye laser operating without etalon narrowing, the transmission is insensitive to temperature. Thus the transmission can be considered a function of only the density.

For obtaining line shape information about the copper absorption and for measuring these low densities of the metastable level, it was necessary to use the dye laser with a line narrowing etalon. In this case the line shape of the dye laser was measured using a scanning Fabry-Perot etalon. These measurements were made in the visible.

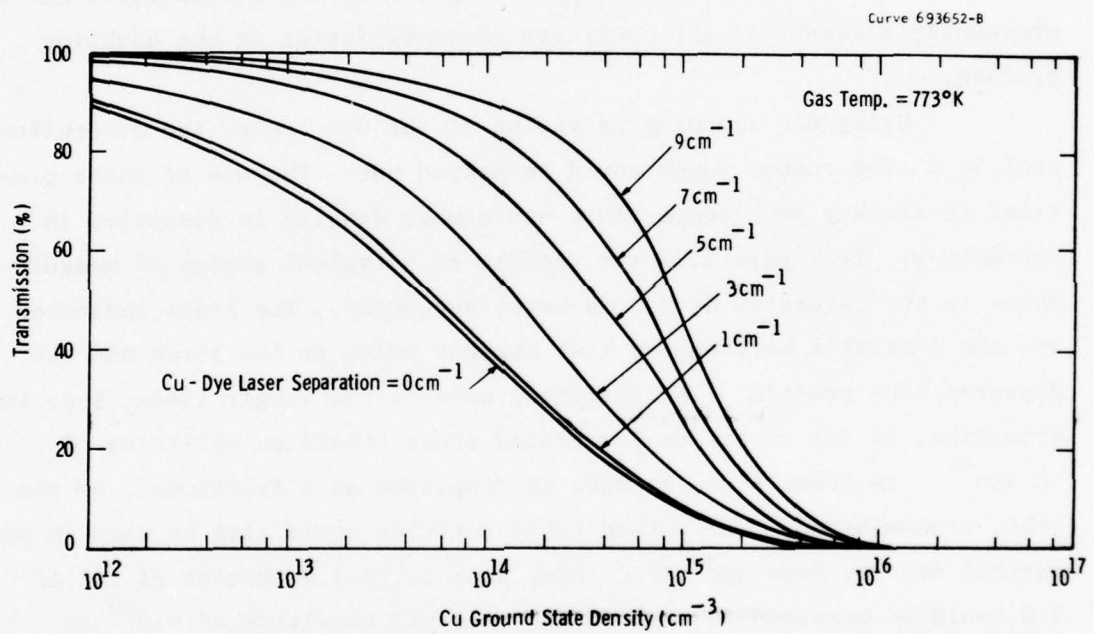


Fig. 2.12. Transmission as a function of Cu density for various values of dye laser frequency.

The full width at half maximum was measured to be 0.18 cm^{-1} . The height of the intensity profile was measured to $\sim 10\%$ of the peak height; Lorentzian tails were fitted to the experimental values and extended to $\sim 0.5\%$ of the peak height. For use in the UV it was not possible to measure the etalon-narrowed width directly. Since the UV output is produced by intracavity doubling from the visible, the UV line shape was taken to be that measured in the visible with a multiplying factor of 1.8. This factor, rather than 2, is given by the manufacturer and is presumably a result of the nonlinear characteristics of the doubling process.

Using the scanning provision of the dye laser, the absorption profile of the copper vapor could be mapped out. The use of these profiles to extract both temperature and number density is discussed in Appendix D. In Figure 2.13 the results of a typical series of measurements in the afterglow of a 2 ms burst are shown. The times indicated are the intervals between the last current pulse in the burst and the measured line profile. The splitting seen at the longer times, i.e. lower densities, is due to the copper ground state hyperfine splitting of $\sim 0.4 \text{ cm}^{-1}$. In these runs the data is displayed as a fractional, or per cent, transmission. The pulsed ratio detector could also be used in an optical density mode and using this, peak optical densities of .01 to 4.0 could be measured corresponding to copper densities of $\sim 10^{10}$ to 10^{16} cm^{-3} .

In order to determine the ground state and metastable copper densities from the absorption measurements, the line profiles of the probing source and absorbing medium must be known. The pulsed copper bromide discharge has a time dependent gas temperature. The copper ground state and metastable state have broadening and splitting terms some of which are temperature dependent, such as Doppler and Van Der Waal and some of which are not, such as natural, resonance and hyperfine. Thus, the absorption profiles cannot be expressed simply as a single time independent Voigt profile. A computer program for the data reduction has been developed to calculate the Cu densities and gas temperatures simultaneously and the detail description is included in Appendix D.

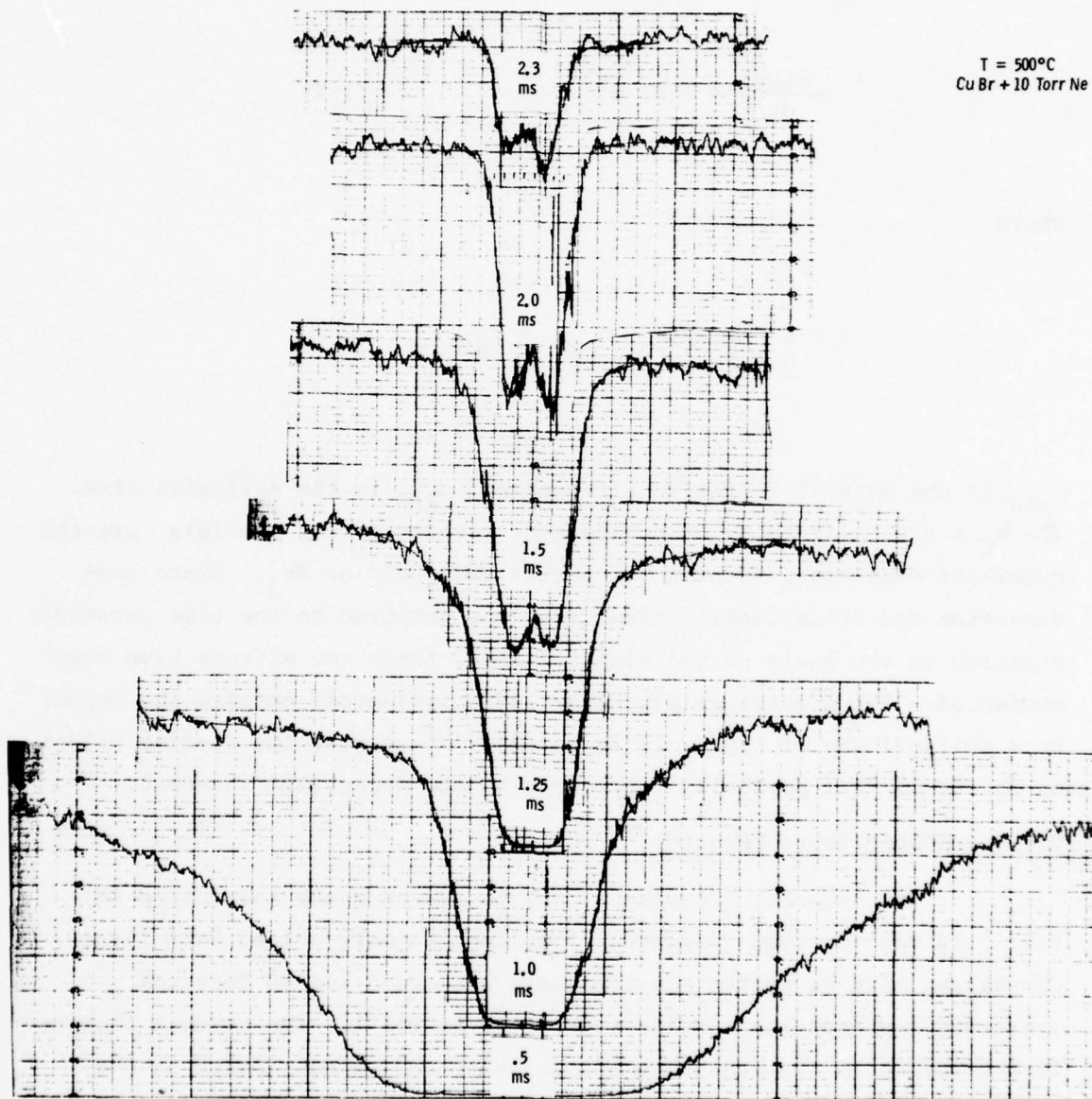


Fig. 2.13. Measured Cu ground state absorption shapes as a function of wavelength at various times in the afterglow of pulsed CuBr laser discharges.

The absorption signal decay after the current pulse of a particular copper atomic state is governed by the relationship

$$-\frac{d(\text{Cu})}{dt} = (\text{Cu}) \gamma^{-1} \quad (2-1)$$

where

$$\gamma = \sum_Q k_Q (Q) + \tau_{\text{rad}} + \tau_{\text{dif}}$$

τ_{rad} is the natural radiative lifetime and τ_{dif} is the diffusion time. The k_Q s are collisional quenching rate constants, and the (Q) s are the quenchant densities, such as the buffer gas, CuBr or Br₂. Since condensation and trimerization times are long compared to the time constants measured on the basis of gas kinetic rates, these two effects have been neglected. The electrical discharge indiscriminately excites the copper to a multiplicity of higher lying levels. Therefore, the feeding effect in Eq. (2-1) will partially contribute to the decay time constant.

2.2.3.1 Ground State Density

The temporal behavior of the Cu ground state absorption in Fig. 2.14 was observed consistently in continuously-pulsed CuBr laser discharges with Ne buffer gas pressures between 5 and 50 Torr and operating temperatures ranging from 400°C to 550°C. The gradual increase in absorption in the beginning of the burst can be attributed to the build-up of the ground state copper atoms. Since the decay time constant of the ground state copper atoms is longer than the pulse separation time, the copper density can accumulate from pulse to pulse.

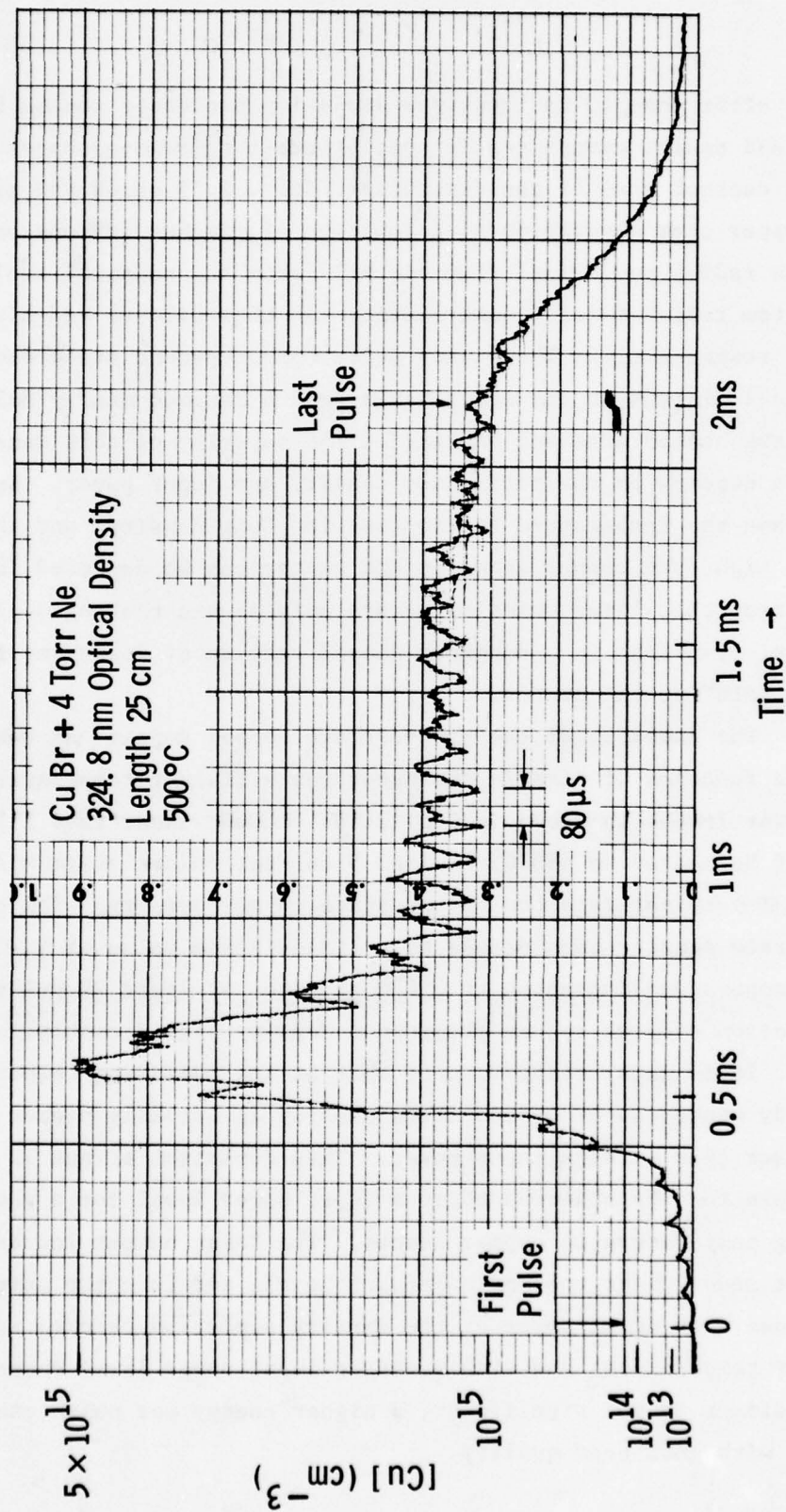


Fig. 2.14. Measured Cu ground state absorption as a function of time for a multipulsed discharge in CuBr laser mixture.

However, after some 10 to 15 pulses depletion processes caused by gas heating and radial cataphoretic pumping start to remove copper atoms from the central core of the discharges. Fig. 2.15 shows the ground state copper atom absorption as a function of time at various positions along the radius and, Figs. 2.16 and 2.17 show the temporal evolution of copper atom radial density distributions in the build-up and afterglow regimes, respectively. The steady state copper ground state density has a local minimum at the center axis, and a maximum nearly halfway between the center axis and the wall. The severity of this density depletion depends on the total CuBr density and input power. In some cases, when the temperature is low (ie: low CuBr density) and the input power is high, the copper atoms at the center can be depleted to such a large extent that laser emission occurs only around the edges of the discharge, resulting in a doughnut-shaped pattern of laser emission with a "black hole" at the center.

The envelope of the ground state copper density at the central axis as a function of time in the burst for different temperatures and input power levels is shown in Fig. 2.18. A CuBr laser tube filled with 4 Torr of Ne heated to 450°C requires 5 current pulses at 100 mj/pulse (1nF at 14kv) to saturate the ground state copper density. The copper ground state density then decays to a steady state value of $\sim 4 \times 10^{14} \text{ cm}^{-3}$. As the temperature increases to 550°C it takes at least 20 pulse before the depletion effects reduce the copper density significantly.

It is interesting to note that at low operating temperatures, the steady state copper ground state density is actually higher at low input power than at high input power. This depletion effect is evidently responsible for the observed optimum input power level for a given operating temperature in copper lasers. The laser output increases with the input power up to the optimal input level, and then the output starts to decrease with input power as the density depletion becomes substantial. At higher temperatures and with moderate input power level where the depletion effect is not significant, a higher energy per pulse can be obtained with good beam quality.

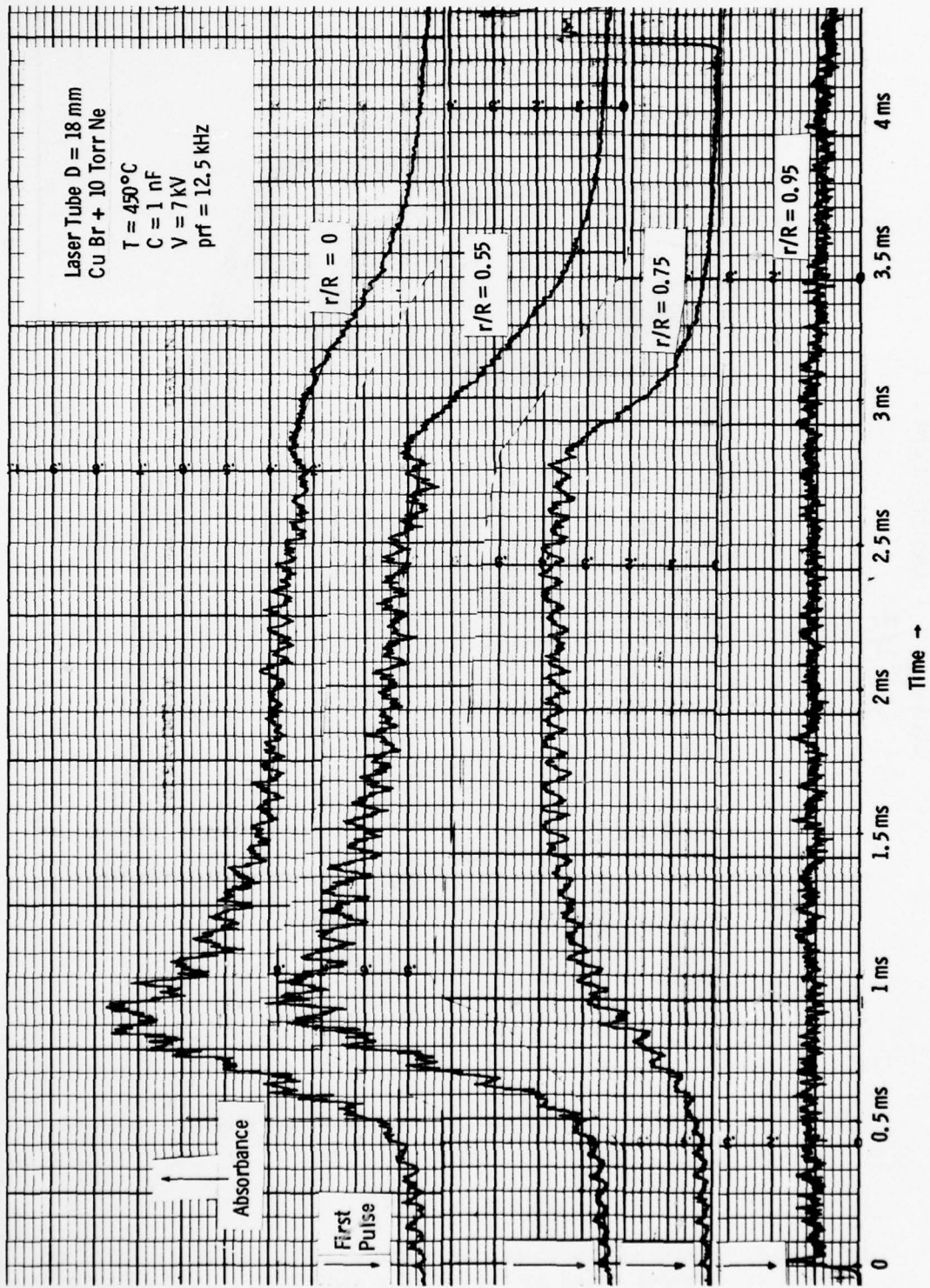


Fig. 2.15. The Cu ground state absorption as a function of time at various positions along the radius.

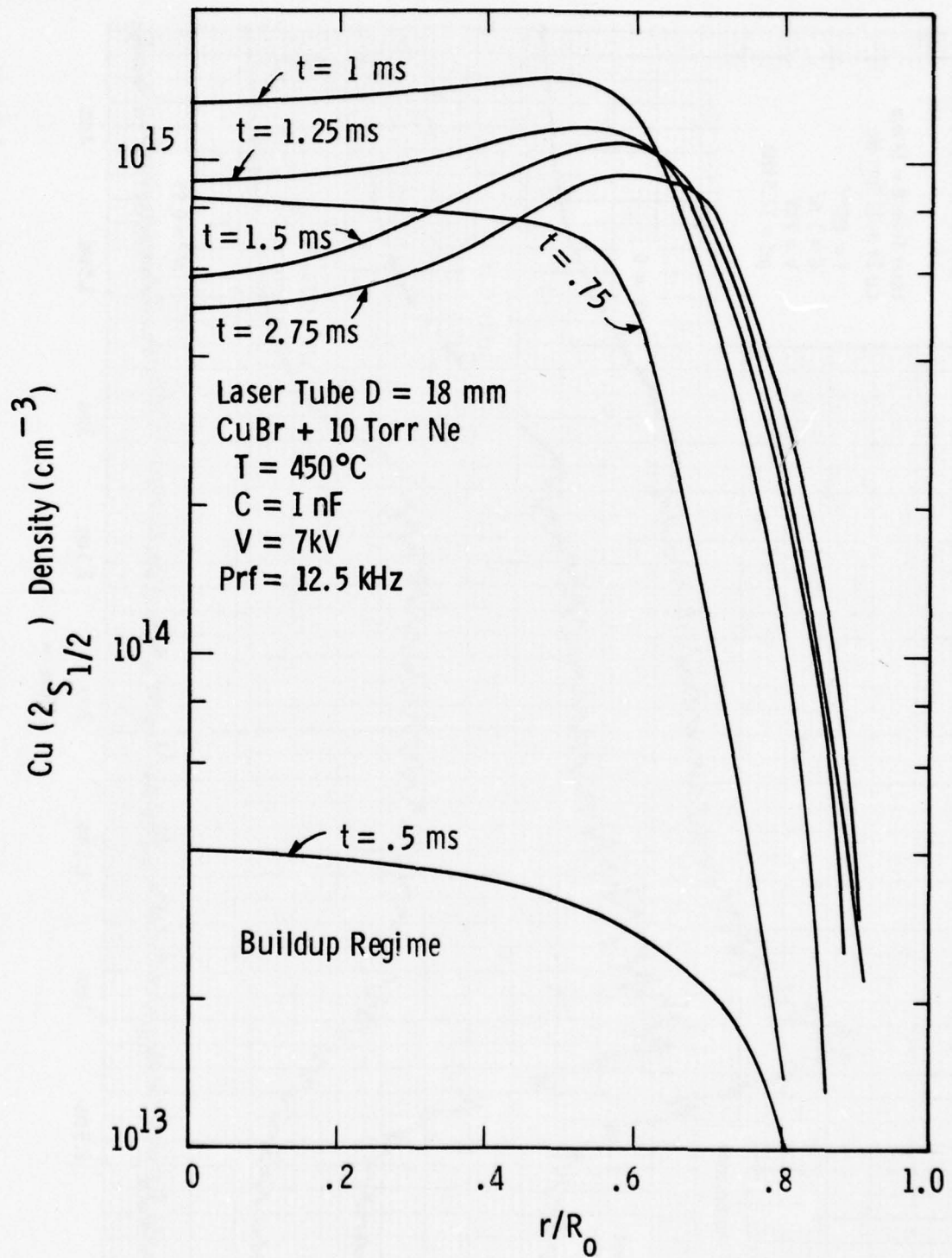


Fig. 2.16. Measured copper ground state density radial profiles at various times in the buildup regime of pulsed CuBr laser discharges.

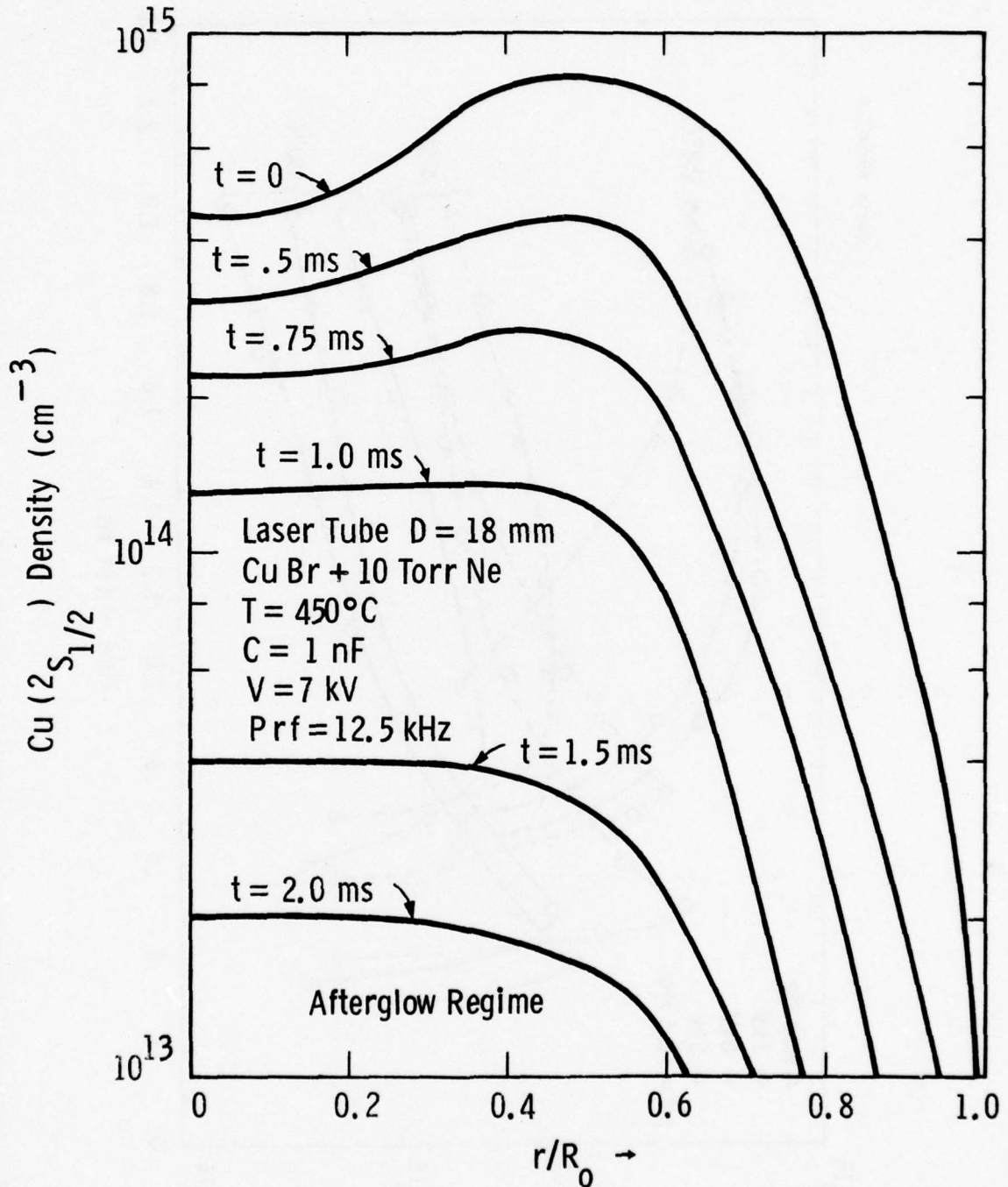


Fig. 2.17. Measured copper ground state density radial profiles at various times in the afterglow of pulsed CuBr laser discharges.

Curve 692007-A

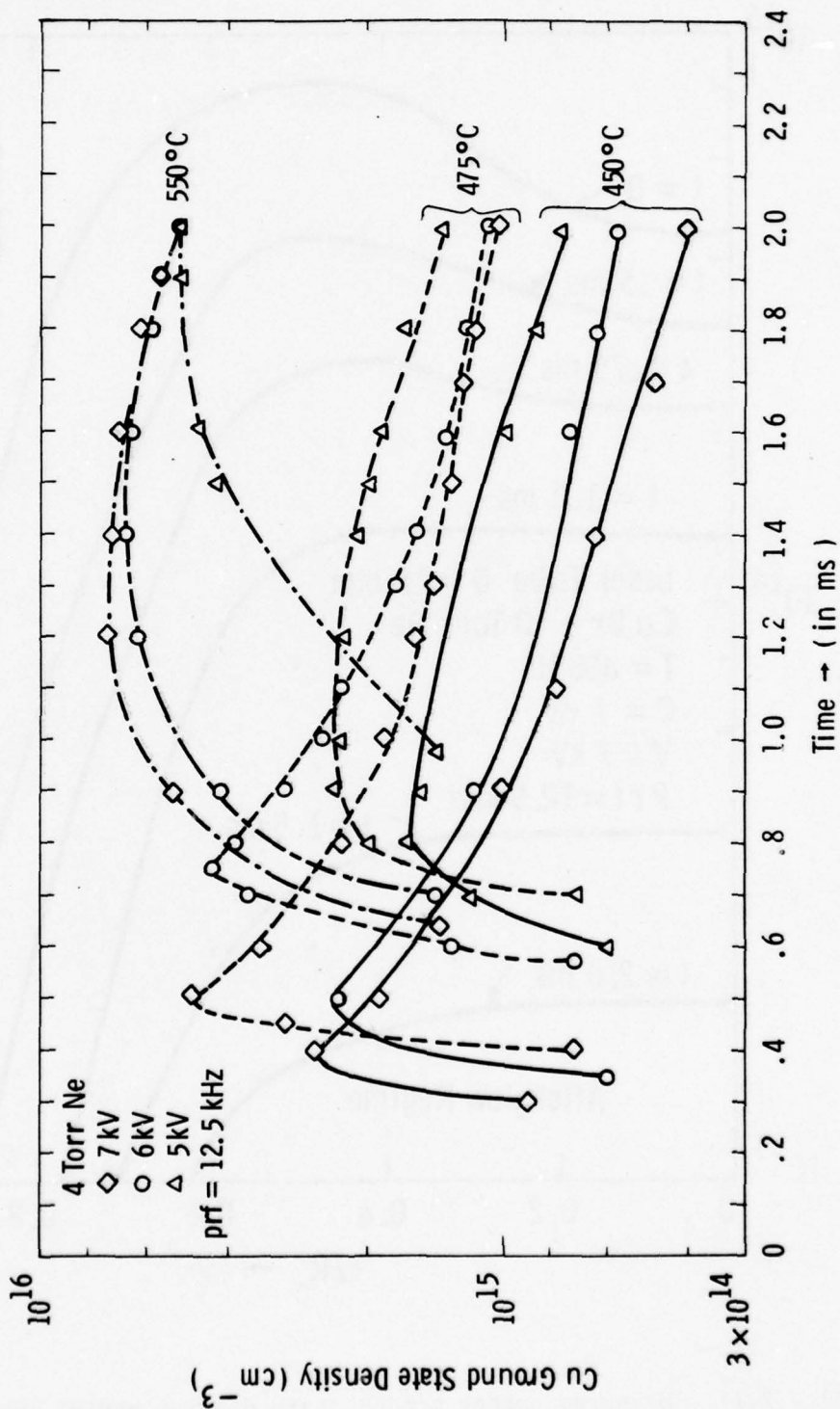


Fig. 2.18. Measured Cu ground state densities as a function of time at various power loading and temperatures.

From Fig. 2.14, one can observe two decay time constants for the ground state copper density, namely, a very fast time constant immediately following cessation of the current pulse, followed by a gradual transition into a slower (~ 200 usec) decay. Fig. 2.19 shows the measured ground state density of a CuBr + 10 Torr Ne laser mixture at 550°C with a quasi-continuous pulsed electrical input of ~ 100 mJ per pulse. For discharge dimension of 25 cm long and 1.8 cm diameter, this corresponds to an input pulse energy density of 1.6 mJ cm^{-3} . The initial copper ground state density reaches $6 \times 10^{16} \text{ cm}^{-3}$ and decays with a time constant of $T \sim 55 \mu\text{s}$. In the first 60 μsec , the decay rate of the copper ground state atoms fits a straight line on a semilogarithmic plot, but after ~ 60 μsec , the decay rate decreases and can be fitted with a ~ 160 μsec time constant.

The destruction rate of the copper ground state is governed by either diffusion and/or chemical recombination. Varying the Ne gas pressure from 5 to 50 Torr has only a slight effect on the decay rate of copper ground state atoms. Since the measured decay time constants are too fast for atoms diffusing through a 10 Torr Ne buffer gas ($T_D \sim 1$ msec), one can infer that the diffusion process plays only a minor role in the Copper ground state removal process. On the other hand, atoms react with Br_2 molecules with a reaction rate given by

$$\gamma = n \bar{v} \sigma, \quad (2-2)$$

where n is the density of the Br_2 molecules, \bar{v} is the average velocity between colliding particles, and σ is the total reaction cross section. Thus, the recombination rate γ is proportional to the product of the Br_2 density and the square root of temperature, since $\bar{v} \propto \sqrt{T}$. The two different decay rates for the Cu ground state density can be correlated with the time dependent changes in the Br_2 density and the gas temperature.

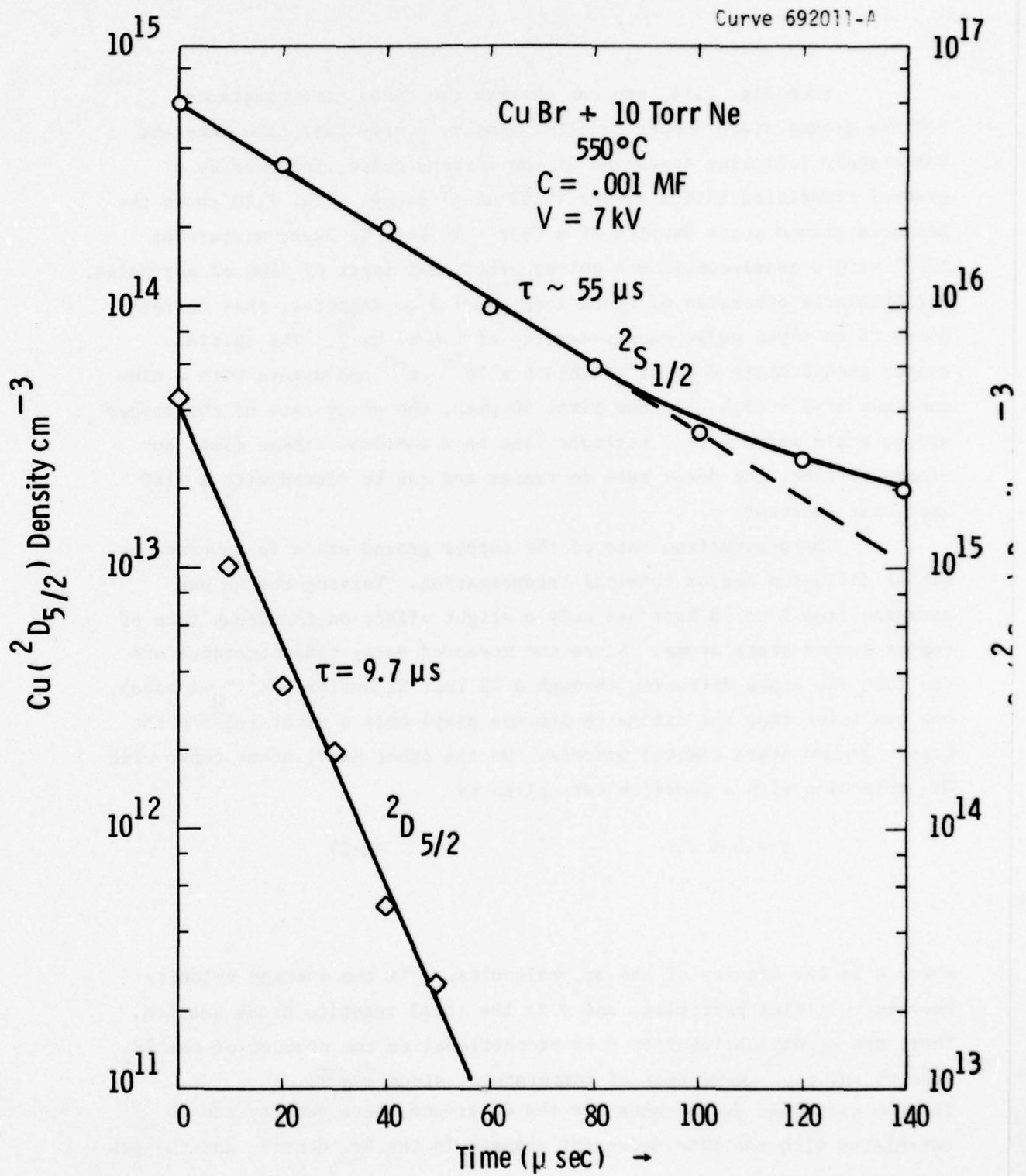
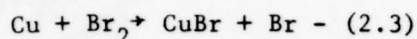


Fig. 2.19. Measured copper ground state and metastable state densities as a function of time in the afterglow of pulsed CuBr laser discharges.

After the gas temperature reaches equilibrium, the Br_2 density approaches a constant steady state value. If the recombination cross section σ is independent of the collision energy, the reaction rate for



should vary linearly with the square root of temperature. Figure 2.20 shows the ground state copper density decay as a function of time for various reservoir temperatures. The measured decay time constants decrease gradually with increasing temperature, and the reaction rate γ plotted against the square root of this temperature in ($^{\circ}\text{K}$) forms the straight line shown in Fig. 2-21. The recombination rate coefficient estimated from this plot is in the range of $10^{-13} \text{ cm}^3 \text{ sec}^{-1}$, if one assumes a Br_2 vapor equilibrium vapor pressure of ~ 1 Torr in the discharge afterglow.

Copper, similar to the alkali and thallium atoms, has one relatively loosely bound outer electron which participates in the collision process. Therefore, some properties derived from these atoms for collisions with halogen molecules may also be applicable to copper. There are, however, some significant differences between the alkali atoms and copper. The alkali halide molecules are known to be predominately ionically bound, and indeed copper can participate in ionic interactions with halogen atoms and molecules. But the ground state of copper bromide is predominantly covalent² like the thallium halides.³ Thus copper and thallium might be expected to display reaction similarities. The estimated value of the reaction rate coefficient for the $(\text{Cu} + \text{Br}_2 \rightarrow \text{CuBr} + \text{Br})$ reaction is not unreasonable in comparison with the reaction rates of alkali and halogen⁴ and of thallium and halogen.⁵

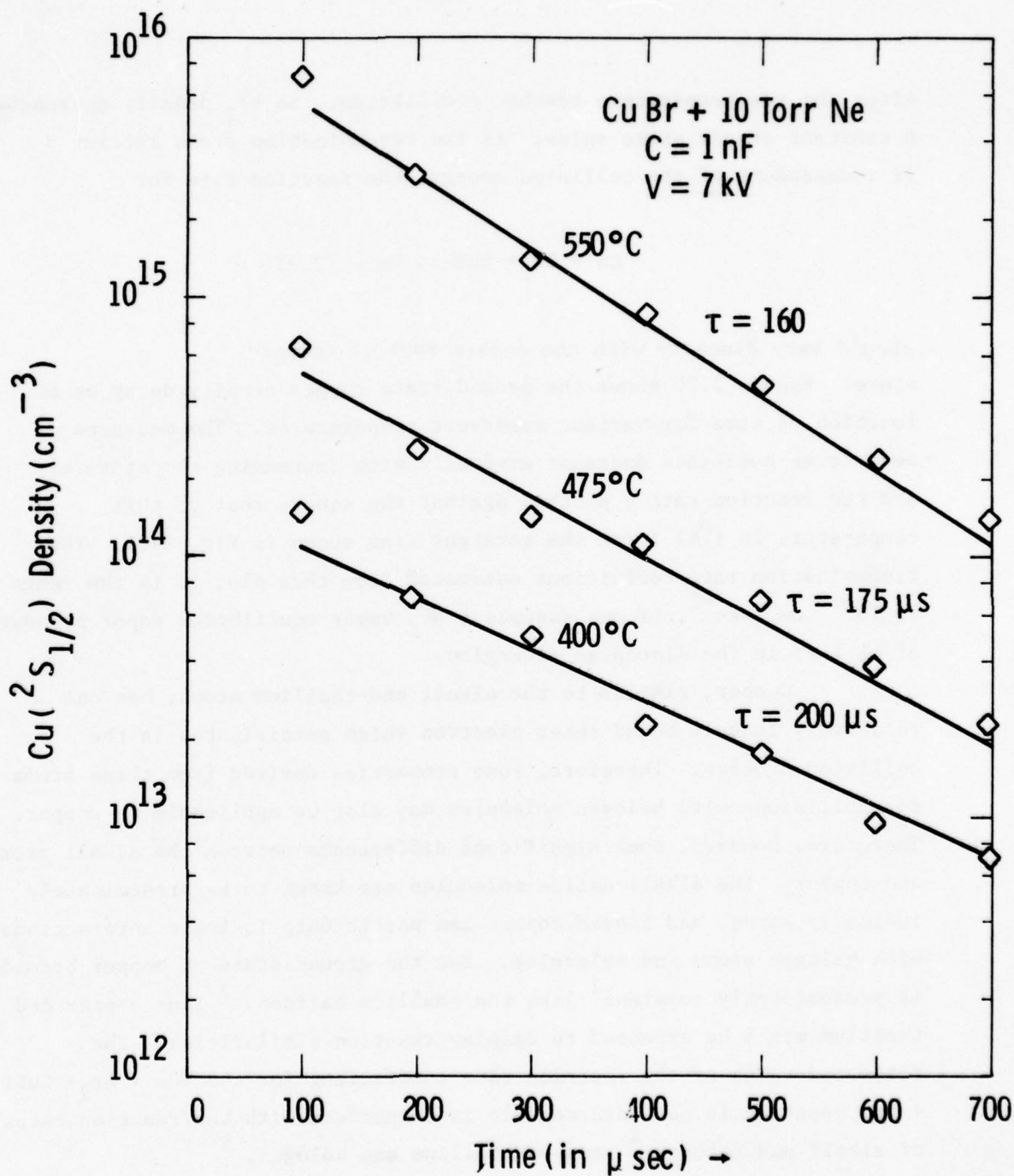


Fig. 2.20. Measured ground state copper density at various wall temperatures as a function of time in the afterglow of pulsed CuBr laser discharges.

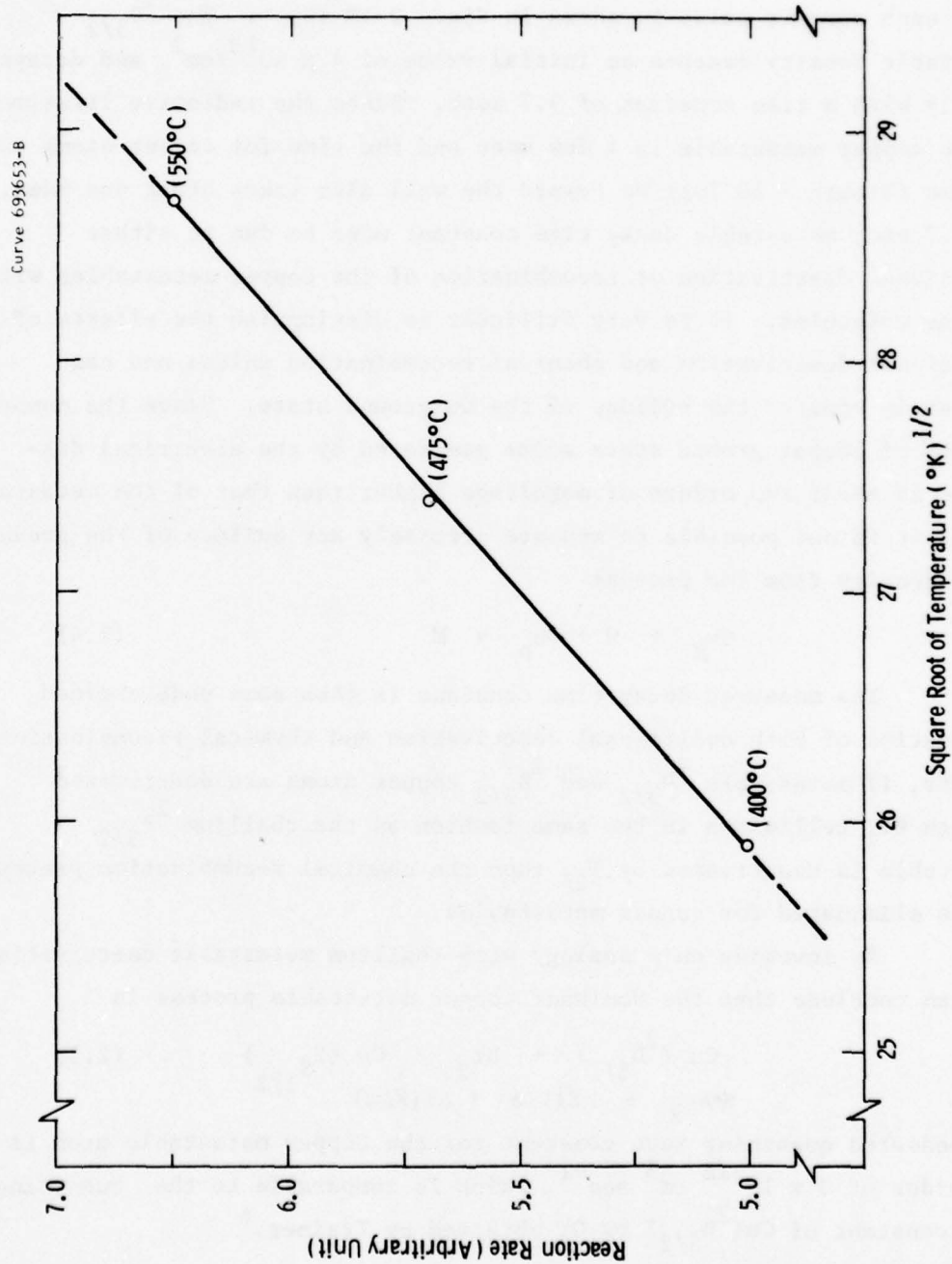


Fig. 2.21. Relative reaction rate vs. square root of temperature for the $\text{Cu}(\text{S}_{1/2}) + \text{Br}_2$ Reaction in a pulsed CuBr laser discharge.

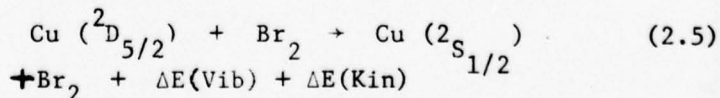
2.2.3.2 Metastable State Density

The measured copper metastable density as a function of time after each current pulse is shown in Fig. 2-19 (b). The ${}^2D_{5/2}$ metastable density reaches an initial value of $4 \times 10^{13}/\text{cm}^3$, and decays rapidly with a time constant of 9.7 μsec . Since the radiative lifetime of the copper metastable is a few msec and the time for copper atoms to diffuse through a 10 Torr Ne toward the wall also takes about one msec, the 9.7 μsec metastable decay time constant must be due to either collisional deactivation or recombination of the copper metastables with bromine molecules. It is very difficult to distinguish the effects of collisional deactivation and chemical recombination unless one can accurately monitor the buildup of the Cu ground state. Since the number density of copper ground state atoms generated by the electrical discharge is about two orders of magnitude higher than that of the metastable atoms, it is not possible to measure precisely any buildup of the ground state density from the process



The measured decay time constant is thus some undetermined combination of both collisional deactivation and chemical recombination. However, if metastable ${}^2D_{3/2}$ and ${}^2D_{5/2}$ copper atoms are deactivated through Br_2 collisions in the same fashion as the thallium ${}^2P_{3/2}$ metastable is deactivated by I_2 , then the chemical recombination process can be eliminated for copper metastables.

By invoking this analogy with thallium metastable deactivation, one can conclude that the dominant copper metastable process is



The measured quenching rate constant for the copper metastable atom is on the order of $3 \times 10^{-12} \text{ cm}^3 \text{ sec}^{-1}$, which is comparable to the quenching rate constant of $\text{Cu} ({}^2D_{5/2})$ by O_2 obtained by Trainer.⁶

Since the decay time constant for the copper metastable is much shorter than the time between pulses, there is no accumulation of $\text{Cu}(^2\text{D}_{5/2})$ atoms when the CuBr laser is operated at repetition rates as high as 20KHz. Thus, the cumulative buildup of copper metastables contributes very little to the observed deterioration in the continuously pulsed CuBr lasers. The deactivation of the copper laser level is sufficiently rapid to prevent bottlenecking effects even at rather high pulse repetition rates, and the observed degradation of laser performance can be attributed almost entirely to thermal or cataphoretic effects which deplete the copper density on the tube axis.

3. CONCLUSIONS

The results of the experimental studies performed under this contract have clarified the underlying physical processes involved in the cyclic operation of copper halide lasers:

(1) Dissociation and Excited State Production: The buildup over many discharge pulses of the fluorescence intensity and the gradual change of the excited state lifetime due to trapping, indicate that the discharge does not produce excited state copper directly from the copper halide molecule. Rather the copper is produced initially as ground state atoms with excitation to excited states occurring by successive pulses.

(2) Excited State Lifetime: The lifetime of the copper upper laser level after lasing is observed to be very long compared to known radiative lifetimes, even with trapping effects included. This time is the same as that observed in fluorescence from states above the laser excited state. Thus the upper laser level appears to be generated, at least in part, by a complicated series of cascading steps from still higher-lying levels.

(3) Metastable Lifetime: The metastable population is observed to decay with a lifetime of $\sim 10 \mu\text{s}$. The decay of the metastable level appears to be controlled by collisions with halogen molecules rather than by diffusion to the walls, since the optimum frequency as determined in our experiments and in other laboratories is independent of tube diameter. This has important consequences for the copper halide system vis a vis the copper vapor laser. The copper vapor laser evidently cannot be scaled beneficially to larger diameters since the metastable level is quenched by diffusion to the walls. This tendency results in lower operating frequencies for larger diameter tubes, and thus lower average specific power. The copper halide laser does not suffer from this limitation, and therefore appears to offer substantial promise in applications where high frequencies (10-25 KHz) are permitted or required.

(4) Copper Ground State Lifetime: The temporal decay of the copper ground state density has at least two time constants. A rather rapid rate with a time constant of $\sim 35 \mu\text{s}$ is most evident during the burst, with a longer time constant of $\sim 120 \mu\text{s}$ most evident in the after-glow. The decay rates seem to be only weakly dependent on buffer gas pressure, and are too rapid for diffusion. The ground state lifetime appears to be controlled by chemical recombination with the halogen, and the two or more time constants are reasonably consistent with measured gas temperatures as discussed in Appendix D. Because of the cylindrical geometry of the longitudinal discharge and the radial pumping effects, the description of the decay rates of both copper density and temperature is very complicated and at this point must remain qualitative.

(5) Copper Ground State Densities: The most significant result to emerge from these studies is the evidence for the depletion of copper ground state atoms from the core of the discharge. The evolution of the copper density with respect to both time and radial position clearly indicates that after an initial buildup, a redistribution of the copper atoms occurs which produces a core density significantly lower than the maximum value. This diminution, which would not have time to occur in the double-pulsed mode, is apparently the source of the limitation of specific output pulse energy in the multiply-pulsed mode. Circumventing this effect by raising the temperature and, hence, the density is not entirely effective. In the copper halide laser, the increase in halide and halogen density results in discharge instabilities. In the copper vapor laser, the temperatures required would be incompatible with the laser tube's materials properties.

At this point we are not able to determine the relative roles of ambipolar diffusion and the radial temperature gradient in establishing the axial depletion of copper atoms. Because the effect increases with input power, the axial depletion is also probably responsible for the observed fact that the output energy tends to saturate with input power, so that the efficiency of copper and copper halide lasers decreases at higher energy loadings. In the longitudinal discharge configuration, the copper or copper halide laser appears to be limited to specific pulse

energies of $5-10 \mu\text{J cm}^{-3}$ if conversion efficiencies of $\sim 1\%$ are required. In a transverse discharge configuration, cathoretic and thermal gradient effects would be greatly reduced and significantly higher energies may be obtained. Operation of a transverse discharge with high energy loading at $500-700^\circ\text{C}$ and low pressures presents formidable technological problems, but we feel that given sufficient resources it is technically feasible. The studies carried out under this contract have significantly increased the understanding of the laser kinetics of the copper halide laser. As a result of this increased understanding, it is recommended that in its longitudinal discharge configuration, the copper halide laser should be developed as a moderate to high power, high PRF, high efficiency laser in a long-lived, sealed-off system, where mission requirements are compatible with such a system. If high energy, compact systems are of sufficient importance, the development of a transverse discharge embodiment should be pursued.

REFERENCES

1. L. A. Weaver, C. S. Liu, and E. W. Sucof, IEEE Journal of Quantum Electronics, QE-10, 140, 1974.
2. L. Pauling, The Nature of the Chemical Bond, Cornell University Press, 1960.
3. Gedeon, S. A. Edelstein and P. Davidovits, the Journal of Chemical Physics, V. 55, No. 11, Dec. 1, 1971.
4. L. E. Brus, the Journal of Chemical Physics, V. 52, No. 4, Feb. 15, 1970.
5. J. Maya and P. Davidovits, the Journal of Chemical Physics, V. 59, No. 6, Sept. 15, 1973.
6. D. Trainer et al, U. S. Dept. of Commerce, NIIS AD/A-022 596.

Axial cataphoresis effects in continuously pulsed copper halide lasers*

C. S. Liu, D. W. Feldman, J. L. Pack, and L. A. Weaver

Westinghouse Research Laboratories, Pittsburgh, Pennsylvania 15235
(Received 28 June 1976; in final form 30 August 1976)

It has been observed in a continuously pulsed copper halide laser that laser performance deteriorates rapidly due to axial cataphoresis effects. Dissociated copper ions are pumped cataphoretically toward the cathode by the applied electric field, causing nonuniform laser discharges and preferential copper condensation near the cathode. These effects can be eliminated experimentally by alternating the polarity of the applied voltage either mechanically or electronically. This improvement permits long-lived copper halide laser operating at average power levels in the 1-10-W range.

PACS numbers: 42.55.Hq, 51.50.+v, 82.45.+z

I. INTRODUCTION

Copper laser emission at 510.6 and 578.2 nm has been reported from copper halide noble gas discharges in all-hot sealed-off quartz discharge tubes for both double-pulsed^{1,2} and multiply pulsed³ electrical excitation. Recently we have observed the development of severe axial density gradients in similar longitudinal laser tubes when 10-kHz pulsed excitation was applied continuously for extended periods of time. This effect is attributed to axial cataphoresis forces^{4,5} within the copper halide discharge, and results in degraded laser performance and the eventual cessation of laser emission after only a few hours of operation. This paper describes the observed laser system behavior and its physical origins, and suggests a simple method for nullifying these potentially deleterious discharge effects.

II. AXIAL CATAPHORESIS EFFECTS

Axial cataphoresis occurs in multicomponent gas discharges when the most easily ionized species drifts as a positive ion towards the cathode due to the applied axial electrical field. In both copper halide and pure copper lasers with noble gas buffers the copper atom has the lowest ionization potential (7.72 eV), and consequently copper atoms accumulate in the cathode region after ion drift and subsequent electron-ion recombination. The resultant cathode-directed copper density gradient is likely accompanied by a similar axial gradient in the electron density, as has been measured in longitudinal He-Xe laser discharges.⁶ Since current density is conserved along the tube, this implies an oppositely directed gradient in the electron drift velocity and mean electron energy. Thus excitation efficiencies and laser inversion densities can vary significantly from anode to cathode in laser discharges dominated by cataphoretic pumping of the laser species. In addition, nonvolatile species such as copper atoms condense on the cold walls near the cathode, constituting a possibly irreversible loss of laser material from the discharge region.

Axial nonuniformities and preferential copper deposition near the cathode were observed under continuously pulsed 10-kHz electrical excitation of copper halide lasers. After only a few seconds of operation, the cathode region of 25 cm × 1.8 cm diameter discharges in

CuBr + 10 Torr He at 525 °C displayed the intense greenish emission characteristic of atomic copper, whereas the anode region emitted primarily the pinkish-blue radiation of a bromine-helium discharge. Furthermore, the maximum laser output pulse energy obtained under continuous 10-kHz pulsed operation was initially only one-third that obtained from double-pulse excitation, indicating that nonoptimum laser inversion conditions existed along the tube length. Laser output and discharge stability degraded further as pulsing continued, and emission finally ceased after several hours of operation. Upon examination after cooling, the cathode region was found to be coated with a dark metallic material identified as copper by chemical analysis, whereas the remainder of the tube interior was clear. This film was dissolved by treatment with full-strength sulphuric acid, but the quartz wall near the cathode retained a reddish tint due to diffusion of copper ions into the quartz lattice, replacing alkali ions such as Na⁺ within the quartz. Reconstitution of the copper bromide was obtained by heating the unopened tube for several days without a discharge, although the quartz reddening near the cathode appeared to be irreversible.

Since the laser tubes were entirely sealed and operated with both windows and electrical feedthroughs at temperatures of ~525 °C, the copper bromide vapor pressure and condensation zone in the absence of discharges were controlled by the <525 °C "cold spot" located midway between the anode and cathode. Thus the copper deposition near the cathode can be attributed to discharge-induced cataphoretic forces which pump the copper in directions opposing normal thermal diffusion forces. Although these forces exist in all copper and copper halide discharge lasers, their effects are typically masked by other processes. For example, double-pulse excitation of copper halide discharges⁷⁻⁹ at low repetition rates introduces cataphoretic forces lasting only a few hundred nanoseconds per pulse, which is typically insufficient to establish observable axial density gradients. Under multiply and continuously pulsed conditions the cumulative effects of axial cataphoresis are usually obscured in nonisothermal copper halide¹⁰⁻¹² and pure copper¹³⁻¹⁶ lasers by massive thermal diffusion of the laser material to room temperature feedthrough and window regions. However, substantial degradation of the copper population inversion density in the anode region and preferential copper condensation in the cath-

ode region very likely occur in such multiply pulsed lasers, contributing to decreased energy output, efficiency, and tube lifetime.

These axial cataphoresis effects in longitudinal discharges can be estimated by considering a quasi neutral weakly ionized plasma within a low-pressure laser mixture whose majority species is a noble gas, and whose ionization occurs predominantly from the minority copper species. By ignoring transverse density gradients and axial gradients in the applied electric field E_z , it can be shown that the steady-state axial distribution of the copper ion plus neutral density $n(z)$ is^{17,18}

$$n(z) = n(0) \exp(-\phi z), \quad (1)$$

where

$$\phi = 11.605 \gamma E_z / T_e \quad (2)$$

and $n(0)$ is the steady-state density at the cathode, z is the axial distance from the cathode, γ is the degree of ionization, and T_e is the gas temperature. Here it is assumed that both temperatures and diffusion coefficients are equal in neutral and ionic copper, and the Einstein relationship¹⁹ has been employed to express Eq. (2) in terms of the particle temperature. For the conditions of this experiment, the discharge length is $z = L = 20$ cm, $\gamma = 5 \times 10^{-3}$, $E_z = 100$ V cm⁻¹, and $T_e = 800$ °K,²⁰ giving a ratio of cathode-to-anode copper densities of 145. Thus substantial separation of the copper species can occur, especially in long discharge tubes. This separation can be sufficiently large to reduce the anode density to below laser threshold levels and concentrate the laser population inversion near the cathode.

The characteristic time τ' for the establishment of cathoretic density gradients is given by^{17,18}

$$\tau' = T_e / 2.901 \gamma^2 \mu_i E_z^2, \quad (3)$$

where μ_i is the copper ion mobility, and a negligible additive term has been deleted. For a copper ion mobility²¹ μ_i of 4.3×10^3 cm² V⁻¹ sec⁻¹ in 10 Torr of He at 800 °K, the quantity τ' is 0.26 msec. Thus a continuously applied sequence of ~100 nsec current pulses at a 10 kHz repetition rate would produce significant axial density gradients in about 0.26 sec for this 0.1% duty cycle, neglecting back-diffusion effects between pulses. On this basis the steady-state anode-to-cathode copper density ratio of ~145 will occur after less than 1 sec of continuous pulsing under typical copper halide laser operating conditions.

A simple solution to the problem of axial cataphoresis density gradients is to reverse the discharge current polarity periodically on a time scale comparable to or faster than the characteristic cataphoresis time. This was accomplished initially with a solenoid-actuated DPDT reversing switch and timer connected between the pulsing unit and the laser tube. Polarity reversal times of about 1 sec were short enough to prevent copper deposition near the electrode end bulbs. With this technique laser operating lifetimes were extended to beyond 5 h with 10-kHz continuously pulsed excitation. The laser volumetric energy yield, however, re-

mained at the reduced value observed previously for continuously pulsed copper halide lasers.

A more advanced electrical pulsing unit which provides polarity reversal automatically on alternate electrical pulses has also been designed and tested. This pulser operates at repetition rates up to 20 kHz on a continuous basis, and for the nominal 10-kHz pulsing rates employed during laser discharge tests the corresponding polarity reversal time of 100 μ sec is significantly shorter than the typical cathoretic separation time $\tau' = 260$ μ sec. Thus for the 0.1% duty cycle corresponding to 100-nsec current pulses, the harmful effects of axial cataphoresis should be nullified completely. This has been confirmed in recent tests with continuously pulsed alternating polarity discharges in CuBr + 10 Torr Ne at operating temperatures of 525 °C. An all-hot 25-cm-long laser discharge tube has been operated for cumulative times of 50 h without any observable copper deposition near the electrode end bulbs. It is suggested on the basis of these experiments that practical long-lived high-average-power copper halide and pure copper laser systems must incorporate design features such as electrical polarity reversal in order to eliminate the otherwise deleterious effects of axial cataphoresis upon laser performance and operating lifetime.

ACKNOWLEDGMENTS

The authors gratefully acknowledge helpful technical discussions with Dr. G. L. Rogoff and the expert technical assistance of R. K. Williams and J. S. Nee.

*Work supported by the Office of Naval Research under Contract No. N00014-74-C-0445.

¹L. A. Weaver, C. S. Liu, and E. W. Sucov, IEEE J. Quantum Electron. QE-9, 645 (1973); QE-10, 140 (1974).

²C. S. Liu, E. W. Sucov, and L. A. Weaver, Appl. Phys. Lett. 23, 92 (1973).

³I. Liberman, R. V. Babcock, C. S. Liu, T. V. George, and L. A. Weaver, Appl. Phys. Lett. 25, 334 (1974).

⁴I. Langmuir, J. Franklin Inst. 196, 751 (1923).

⁵M. J. Druyvesteyn, Physica (Utr.) 2, 255 (1935).

⁶R. J. Freiberg and L. A. Weaver, J. Appl. Phys. 38, 250 (1967).

⁷C. J. Chen, N. M. Nerheim, and G. R. Russell, Appl. Phys. Lett. 23, 514 (1973).

⁸J. A. Piper, Opt. Commun. 14, 296 (1975).

⁹I. Smilanski, L. A. Levin, and G. Erez, IEEE J. Quantum Electron. QE-11, 919 (1975).

¹⁰C. J. Chen and G. R. Russell, Appl. Phys. Lett. 26, 504 (1975).

¹¹O. S. Akirtava, V. L. Dzhikiya, and Yu. M. Oleinik, Sov. J. Quantum Electron. 5, 1001 (1975).

¹²N. V. Subotinov, S. D. Kalchev, and P. K. Telbizov, Sov. J. Quantum Electron. 5, 1003 (1975).

¹³W. T. Walter, IEEE J. Quantum Electron. QE-4, 355 (1968).

¹⁴A. A. Isaev, M. A. Kazaryan, and G. G. Petrash, Opt. Spectrosc. 35, 307 (1973).

¹⁵R. S. Anderson, L. Springer, B. G. Bricks and T. W. Karras, IEEE J. Quantum Electron. QE-11, 172 (1975).

¹⁶P. A. Bokham, V. N. Nikolaev, and V. I. Solomonov, Sov. J. Quantum Electron. 5, 96 (1975).

¹⁷J. Freudenthal, J. Appl. Phys. 38, 4818 (1967).

¹⁸F. H. Shair and D. S. Remer, J. Appl. Phys. 39, 5762 (1968).

¹⁹E. W. McDaniel, Collision Phenomena in Ionized Gases (Wiley, New York, 1964), p. 491.

²⁰The discharge voltage is approximately 2 kV with a peak current density of 300 A cm⁻².

²¹L. M. Chanin and M. A. Biondi, Phys. Rev. 107, 1219 (1957).

Kinetic Processes in Continuously Pulsed Copper Halide Lasers

C. S. LIU, D. W. FELDMAN, JOHN L. PACK, SENIOR MEMBER, IEEE,
AND LELLAND A. WEAVER, SENIOR MEMBER, IEEE

Abstract—Absorption measurements in the afterglow of electrically excited copper halide laser mixtures are described. Ground state and metastable copper density decay rates determine the optimum delay for application of a second electrical pulse. Output energy densities of $45 \mu\text{J} \cdot \text{cm}^{-3}$ have been observed for single-pulse conditions. Gas temperature increases limit the electrical pulse energy which can be applied on a continuous basis, and in this regime the output energy density is reduced to $\sim 11 \mu\text{J} \cdot \text{cm}^{-3}$ due to the decreased pulse energy and cumulative population effects. Thermal gradients and radial cataphoresis are suggested as explanations for observed transient effects in the multipulse output envelope. Average 5106 Å power levels of 1.34 W at 0.3 percent efficiency were observed within 18 kHz burst-mode pulses applied at low duty cycle.

I. INTRODUCTION

THE use of copper halides to obtain pulsed 5106 Å and 5782 Å laser emission from atomic copper has received

considerable attention in recent years [1]–[10], primarily due to the substantially lower operating temperatures associated with the more volatile halide species. This approach permits the use of standard quartz discharge tube technology rather than the ceramic envelopes required with metallic copper [11]–[14], and laser performance characteristics have been found to be generally equivalent to the higher temperature pure copper systems. In particular, both approaches have demonstrated laser volumetric energy yields exceeding $35 \mu\text{J} \cdot \text{cm}^{-3}$ in a single laser output pulse [3], [5], [14], and in recent experiments we have observed outputs as high as $70 \mu\text{J} \cdot \text{cm}^{-3}$ from a double-pulsed copper iodide laser tube. While these results are very encouraging for high average power applications, considerable caution must be exercised in extrapolating these single laser pulse experiments into the multipulse regime. We have found that certain cumulative effects in copper halide laser discharges render the burst-mode and continuously pulsed systems significantly different from the double-pulsed systems. Moreover, the substantially higher average power dissipations and axial gas temperatures of multiply-pulsed discharges alter both the spatial and temporal distribution of laser species in

Manuscript received October 27, 1976; revised April 25, 1977. This work was supported in part by the Office of Naval Research under Contract N00014-74-C-0445.

The authors are with Westinghouse Research Laboratories, Pittsburgh, PA 15235.

copper halide laser discharges. These effects vary with reservoir temperature and the electrical pulse spacing, and generally reduce the single-pulse volumetric energy yield by factors as high as 5 in the multipulse regime. Thus, the use of single-pulse laser energies and optimum pulse separations to predict the average output levels available from continuously pulsed copper halide lasers is invalid, and typically overestimates observed multipulse performance by a factor of 5.

The explanation for this observed behavior resides in the production and destruction rates of the copper laser species and their accumulation throughout the temporal evolution of a series of electrical pulses. In addition, radial temperature and charged particle gradients can result in depletion of the axial copper density due to thermal diffusion and radial cathoporesis forces. Copper ground state and metastable density measurements in the afterglow of pulsed copper halide laser discharges reveal that for pulse repetition rates of about 16 kHz, the metastable density decays to negligible levels between pulses, whereas copper ground state densities accumulate to about twice their initial value throughout the course of a pulse train. However, it is shown that the application of equivalent single-pulse electrical energies on a continuous basis results in excessive gas heating which degrades the laser output. This necessitates a reduction of the applied electrical pulse energies by a factor of typically 10 in the multipulse case to maintain the gas temperature within tolerable limits. It is the combination of the copper multipulse accumulation factor and the required reduction in electrical pulse energy which yields the observed factor of 5 reduction in the volumetric energy yield for these systems. The laser efficiency remains unchanged by these effects. The explanation of this multipulse behavior indicates that significant improvements in continuously operating copper halide lasers can be effected by more advanced system designs which minimize atomic copper losses and gas temperature increases.

II. EXPERIMENTAL APPARATUS

The laser discharge tubes employed in these experiments are similar to those described previously [1]-[3]. The tube envelopes and windows are formed from fused silica, with molybdenum used for electrodes and feedthroughs. These fabrication techniques permit all-hot operation of the copper halide laser mixtures within a completely sealed-off enclosure. Thus, the temperature distribution and vapor pressure can be controlled quite precisely. In order to maintain external control of the tube temperature, the entire assembly is placed within a three-zone thermostatically controlled oven, and the thermal contribution from the laser discharge is minimized by restricting the electrical pulse input to double-pulse or burst-mode excitation at low overall duty cycle.

The experimental apparatus is shown schematically in Fig. 1. Copper ground state and metastable state densities were measured as a function of time after the first discharge pulse using either a xenon short arc lamp, a Westinghouse copper hollow cathode discharge lamp, or a second copper halide laser as the spectroscopic source. The selection of the spectroscopic source was based on the wavelength studied and the number density measured. In the high density region ($n \approx 10^{13} \text{ cm}^{-3}$), the

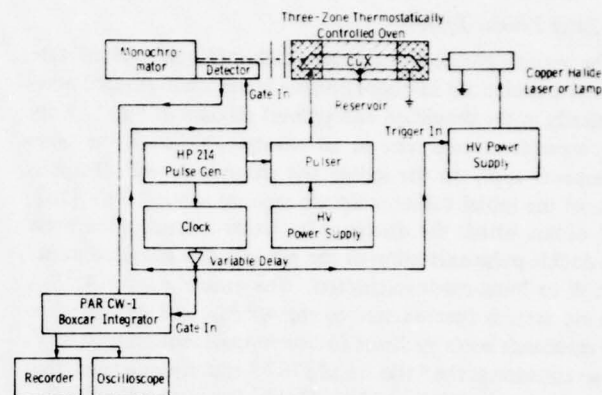


Fig. 1. Schematic diagram of the experimental apparatus used to measure absorption in pulsed copper halide laser afterglows.

absorption of the copper ground state is so high that any narrow line at the center of the copper line will be totally absorbed. Greater accuracy can be obtained under these circumstances with the broad spectroscopic source from the xenon short arc. In the low density region ($n \leq 10^{12} \text{ cm}^{-3}$), the very narrow line from copper hollow cathode lamp can significantly improve the sensitivity of ground state density measurements. The second copper halide laser was employed to measure the absorption from the copper metastable state. The transmitted signals were detected by a gated S-5 response photomultiplier and a 0.5 Jarrell-Ash Ebert monochromator. The absorption measurements could not be performed immediately after the discharge pulse because the spontaneous emission from the copper halide discharge at both 3247 Å and 5106 Å was much more intense than that from the source in most cases. The afterglow radiation decayed rapidly in a few tens of microseconds, and the electronic circuitry used in the gated photomultiplier tube extended the signal decay to several tens of microseconds. These effects prevented accurate measurement of the afterglow absorption characteristics during the first 50 μs ; consequently, absorption measurements are reported only for periods beyond this 50 μs region.

Ground state and metastable copper densities were computed from the measured absorption by employing the methods described by Mitchell and Zemansky [15]. The absorption coefficient of the copper ground state or metastable state is given by the Voigt profile which includes the effects of Doppler, natural resonance, and Van der Waal broadening. The radial variation of the gas temperature within the discharge cell was assumed to be parabolic in accordance with classical heat flow relations. In addition, the temporal variation of the temperature in the afterglow region was computed from classical thermodynamic relationships and included in the Doppler broadening portion of line profile formulation. For the sake of simplicity, the hyperfine structure and isotope shift were not considered in the calculation.

A calibrated ITT FW114A photodiode was employed to measure the laser output energy and multiple pulse outputs of the copper halide laser discharges. Gas filling and electrical pulsing techniques were identical to those described previously [1]-[3].

III. EXPERIMENTAL RESULTS AND DISCUSSION

A. Laser Kinetic Effects

The various physical processes which influence excited state species populations in copper halide lasers are illustrated schematically in the simplified energy level diagram of Fig. 2. Copper bromide is used here as an example, although the same comments apply to the iodide and chloride as well. Dissociation of the initial halide molecule requires about 2.5 eV [16], and occurs within the discharge by either a dissociation pulse for double-pulse excitation or the previous few electrical pulses in CW or burst-mode excitation. The atomic copper $4s^2S_{1/2}$ ground state is then excited to the $4p^2P_{3/2}$ and $4p^2P_{1/2}$ copper resonance levels by direct electron impact requiring ~ 3.8 eV. Laser emission at the 5106 Å and 5782 Å transitions occurs from these resonance levels to the $3d^94s^2^2D_{5/2}$ and $3d^94s^2^2D_{3/2}$ copper metastable levels, respectively. Since the copper metastables are destroyed only by wall or gas collisions, their rapid accumulation due to the stimulated emission process terminates laser emission within approximately 10–50 ns. Subsequent laser output pulses must await removal of the metastable "bottleneck," which occurs in typically 10–100 μ s by wall or gas collisions. The ground state copper atoms are then available for subsequent reexcitation, or alternatively, they suffer recombination with halogen particles to reconstitute the original copper halide starting species.

The recombination process is usually quite long, requiring from 0.1 to 1 ms to remove the ground state copper species. Thus, copper atoms are recycled through the excitation, lasing, and deactivation sequence many times before the initial 2.5 eV dissociation energy investment is lost due to recombination. When this recycling occurs, the system inefficiency due to the dissociation requirement is diminished substantially, and the principle sources of the laser cycle inefficiency are those experienced in pure copper systems, namely, the electrical excitation efficiency factor, the fraction of excited copper atoms available for lasing before metastable bottlenecking, and the ~ 1.4 eV lost due to metastable deactivation [11]. Thus, the conversion efficiency in copper halide systems is expected to be comparable to that obtained in pure copper lasers, as observed in practice [8], [17].

However, the decay rates of copper ground state and metastable atoms greatly influence the observed laser behavior, especially in the multipulse regime. Fig. 3 shows the measured ground state and metastable densities in the afterglow of a CuI + 10 torr Ar laser mixture subjected to a single electrical pulse of 2.7 J. For discharge dimensions of 30 cm length and 1.1 cm diameter, this corresponds to a dissociation pulse energy density of $95 \text{ mJ} \cdot \text{cm}^{-3}$. The $3d^94s^2^2D_{5/2}$ metastable density decays rapidly with a time constant of about 15 μ s for these conditions, and starting at $\sim 80 \mu$ s into the afterglow copper laser emission at 5106 Å can be observed upon application of a second electrical excitation pulse. This is interpreted as specifying a maximum tolerable metastable density of $\sim 10^{13} \text{ cm}^{-3}$ for threshold laser conditions. Beyond this time, laser emission is available until the ground state $4s^2S_{1/2}$ copper density becomes insufficient to sustain threshold population inversion densities. Laser output ceases at about 230 μ s into the afterglow, which is interpreted as specifying a mini-

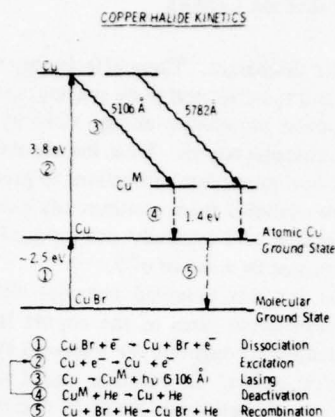


Fig. 2. Simplified energy level diagram for the copper bromide laser system.

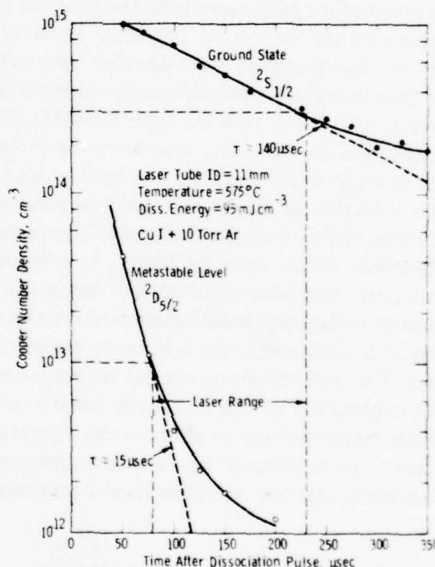


Fig. 3. Measured ground state and metastable copper densities as a function of time in the afterglow of pulsed copper iodide discharges.

imum tolerable ground state density of $\sim 3 \times 10^{14} \text{ cm}^{-3}$ for the laser threshold. Thus, the afterglow kinetics of the copper system can be visualized as opening a temporal window which permits laser inversions when metastable densities fall below $\sim 10^{13} \text{ cm}^{-3}$, and closing this window to extinguish laser emission when ground state densities fall below $\sim 3 \times 10^{14} \text{ cm}^{-3}$. The delay in opening the window is determined primarily by the 15 μ s metastable decay rate, and the window closing is determined primarily by the 140 μ s ground state decay rate. Since the population density excited to copper upper laser level by the succession of electrical pulses depends upon the ground state density left over from previous pulses, the ground state copper density can be interpreted as a measure of the available upper laser level density. In this example, the maximum laser output energy is obtained at $\sim 120 \mu$ s after the dissociation pulse, which corresponds to conditions of maximum difference between ground state (and presumably the upper laser

level population) and metastable densities while the window is open.

The threshold for resonance radiation trapping has been established [2] as a ground state copper density of $\sim 10^{13} \text{ cm}^{-3}$ for a tube diameter of 1.1 cm. Thus, the observed laser threshold of $\sim 3 \times 10^{14} \text{ cm}^{-3}$ is a factor of 30 higher than the minimum feasible copper density required to imprison the 3248 Å resonance radiation, indicating that the laser threshold is determined principally by metastable absorption and optical cavity losses. In addition, the maximum available copper atom density at the 575°C operating temperature is [2] $\sim 10^{17} \text{ cm}^{-3}$, whereas the measured ground state copper density extrapolated to zero delay time is $\sim 3 \times 10^{15} \text{ cm}^{-3}$. Thus, the initial dissociation fraction is deduced to be ~ 3 percent, and this fraction falls to ~ 1 percent at the onset of laser threshold. Since the population densities of the upper and lower laser levels are equal at threshold if degeneracy factors are neglected, the excitation fraction can also be inferred by noting that for threshold conditions, the ground state density is ~ 100 times the metastable density. This implies that the upper laser level population is about 1 percent of the ground state density at threshold. Clearly, improvements in both the dissociation and excitation fractions can effect substantial increases in the laser output energy and efficiency.

The afterglow measurements further reveal that for the optimum 120 μs delay, a second laser pulse could be extracted before the temporal window closed, and if the minimum delay of $\sim 80 \mu\text{s}$ were employed, about four laser pulses could be generated. Thus, ingoring the cumulative population effects of multiple pulsing, it is evident that an average copper atom can be recycled up to four times through the laser sequence before recombination occurs, and pulse repetition rates as high as $\sim 12 \text{ kHz}$ should be available. As shown in the following discussion, the cumulative effects of multiple pulsing serve to increase these estimates by producing a higher level of copper ground state atoms in the steady state.

B. Multipulse Cumulative Effects

The actual single-pulse laser output energy density as a function of delay time in the afterglow of a 1.17 J dissociation pulse is shown in Fig. 4. In this case, the laser medium is CuBr + 10 torr He at a cold spot temperature of 530°C, and the discharge dimensions are 25 cm length and 0.6 cm diameter. This corresponds to a dissociation energy density of $165 \text{ mJ} \cdot \text{cm}^{-3}$, for which the optimum excitation energy density is found to be about one-tenth of this value or $16.5 \text{ mJ} \cdot \text{cm}^{-3}$. The metastable and ground state density decay rates are 20 and 90 μs respectively, for this mixture, and as shown in Fig. 4, the maximum energy output density of $\sim 45 \mu\text{J} \cdot \text{cm}^{-3}$ is obtained for an optimum delay time of $\sim 60 \mu\text{s}$. Thus, the conversion efficiency of the excitation pulse alone is ~ 0.27 percent, although inclusion of the dissociation pulse energy reduces this efficiency by more than a factor of 10.

The variation of laser output energy with excitation pulse energy is shown in Fig. 5 for the same discharge tube and a slightly higher dissociation energy density of $187 \text{ mJ} \cdot \text{cm}^{-3}$ with the optimum delay time of 60 μs . The excitation energy was changed by varying the voltage across the storage capaci-

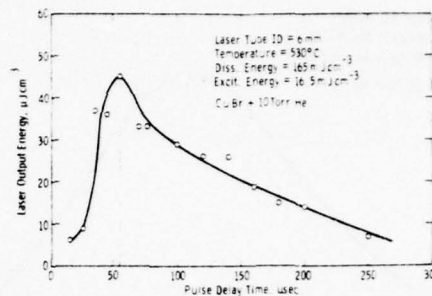


Fig. 4. Laser output energy density as a function of pulse delay in double-pulsed copper bromide discharges.

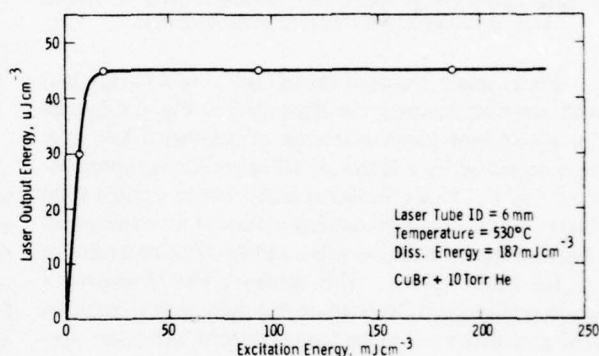


Fig. 5. Laser output energy density as a function of excitation pulse energy in double-pulsed copper bromide discharges.

tor. The laser output energy density rises to its maximum value of $\sim 45 \mu\text{J} \cdot \text{cm}^{-3}$ for an excitation pulse energy density of $\sim 20 \text{ mJ} \cdot \text{cm}^{-3}$ (0.001 μF capacitor charged to 6.3 kV), and remains constant at this value for pulse energies up to $\sim 200 \text{ mJ} \cdot \text{cm}^{-3}$ (0.001 μF capacitor charged to 20 kV). Thus, for a given dissociation pulse energy density of $187 \text{ mJ} \cdot \text{cm}^{-3}$, no further improvement in laser performance is obtained by increasing the excitation pulse energy density beyond about one-tenth of the dissociation pulse energy density. Evidently, the ground state copper density available for this level of dissociation provides a finite maximum population inversion for excitation pulse energy densities of $\sim 20 \text{ mJ} \cdot \text{cm}^{-3}$, and beyond this the output saturates because no further copper atoms are available for excitation regardless of pulse energy. Obviously, the most efficient operating point is just at the knee of the curve in Fig. 5 where the ratio of excitation to dissociation energy densities is about one-tenth. Under these circumstances, it is possible to obtain single-pulse laser energy densities as high as $70 \mu\text{J} \cdot \text{cm}^{-3}$ from small-bore laser tubes; typical conversion efficiencies are near 0.3 percent ignoring the dissociation pulse energy investment.

It is tempting to infer from these data that with continuously pulsed excitation, the $45 \mu\text{J} \cdot \text{cm}^{-3}$ output energy at an optimum pulse spacing of 60 μs will yield an average power of $45 \mu\text{J} \cdot \text{cm}^{-3} / 60 \mu\text{s} = 0.75 \text{ W} \cdot \text{cm}^{-3}$ or 5.3 W for this laser tube. However, this is not observed in practice and is erroneous because this extrapolation ignores multipulse cumulative effects, such as gas temperature increases and axial density de-

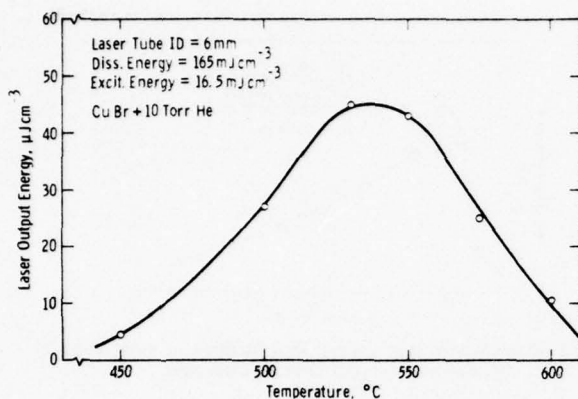


Fig. 6. Laser output energy density as a function of reservoir temperature in double-pulsed copper bromide discharges.

pletion. For example, the variation of laser output energy density with reservoir temperature illustrated in Fig. 6 indicates that for a cold-spot temperature rise of less than 100°C , the output is decreased by a factor of 10 below the optimum observed at 530°C . This behavior is likely due to excited state laser kinetic or gas discharge stability effects at the correspondingly higher copper halide densities, and has been observed for each of the halide species. This tendency clearly obviates a multipulse replication of isolated double-pulse laser conditions, since the cumulative rise in gas temperature at high pulse repetition rates would drive the system beyond the optimum reservoir temperature regime defined by Fig. 6. For example, a continuous succession of 1.17 J dissociation pulses at $60\text{ }\mu\text{s}$ intervals would generate an average power dissipation of 19.5 kW over the 25 cm long tube or $780\text{ W}\cdot\text{cm}^{-1}$. This excessive heat loading would raise the axial gas temperature by $\sim 13\text{ }000^{\circ}\text{C}$ and would quickly melt the quartz envelope [18]. Clearly, the continuously pulsed copper halide laser system requires a more modest and efficient succession of 0.117 J excitation pulses, which at $60\text{ }\mu\text{s}$ intervals would dissipate 1.95 kW at $78\text{ W}\cdot\text{cm}^{-1}$ and raise the axial gas temperature by a tolerable 1300°C . This thermal loading is easily accommodated by quartz, and permits maintenance of the cold-spot temperature at 530°C .

Since continuously pulsed copper halide lasers must operate with lower energy electrical pulses to satisfy temperature restrictions, it follows that the dissociated copper ground state densities measured for the single-pulse conditions of Fig. 3 will not be achieved. If the dissociated copper density is assumed to be proportional to the dissociation pulse energy, then 0.117 J electrical pulse would be expected to produce one-tenth the copper density of the 1.17 J pulse employed in single-pulse experiments. This, in turn, would result in one-tenth the output energy density available upon application of a second excitation pulse, or 4.5 rather than $45\text{ }\mu\text{J}\cdot\text{cm}^{-3}$. But a continuous succession of such lower energy pulses might conceivably build up the dissociated copper density over many pulses and thereby achieve the same dissociation levels as those obtained with a single 1.17 J pulse. In that case, the laser output energy density might approach the original $45\text{ }\mu\text{J}\cdot\text{cm}^{-3}$ in the steady state, other conditions being equal.

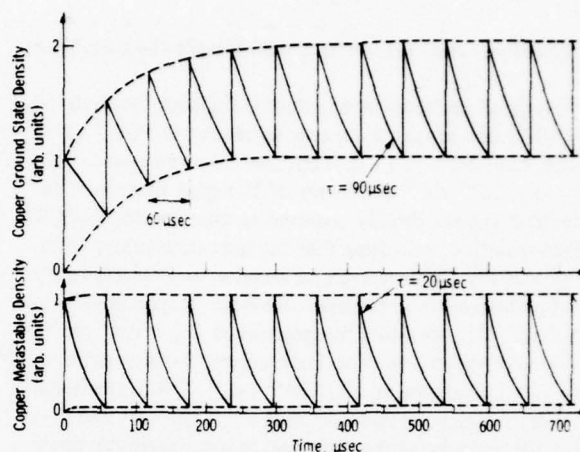


Fig. 7. Computed copper ground state and metastable densities as a function of time for continuously pulsed discharges in copper bromide laser mixtures.

This cumulative effect has been investigated by computing the relative populations of both ground state and metastable copper species subjected to a constant creation rate applied at $60\text{ }\mu\text{s}$ intervals to simulate repetitive pulsing conditions. The temporal evolution of these populations is reproduced in Fig. 7 for the 20 and $90\text{ }\mu\text{s}$ decay rates corresponding to metastable and ground state densities in $\text{CuBr} + 10\text{ torr He}$, respectively. It is seen that copper metastable densities decay almost completely between pulses and accumulate to levels only slightly in excess of the initial value. On the other hand, the longer-lived copper ground state species accumulates to a steady-state value of about twice the initial dissociation level [19]. Thus, for these conditions the cumulative effects of metastable buildup can be ignored, and the cumulative effects of copper ground state density buildup contribute a factor of 2 to the available steady-state laser output. It is concluded that a continuous succession of 0.117 J pulses (one-tenth the single-pulse dissociation energy) will approach a steady-state laser output reduced by a net factor of 5 from the equivalent single-pulse output or $45/5 = 9\text{ }\mu\text{J}\cdot\text{cm}^{-3}$. Thus, the single-pulse performance must be degraded for cumulative temperature effects and simultaneously adjusted for cumulative population effects in predicting the expected performance in the multipulse regime. In this case, the cumulative population adjustment is upwards, but it is important to note that other combinations of decay rates and pulse separations can enhance metastable populations and thereby degrade multipulse performance. This procedure more accurately predicts the performance of copper halide lasers in the multipulse regime, but as demonstrated in the following section, even further physical effects which cause axial depletion of the laser species must also be considered for a completely accurate extrapolation.

C. Multipulse Depletion Effects

The copper bromide laser tubes described in the previous section were supplied with multipulse electrical excitation of approximately 0.1 J/pulse . In order to maintain the reservoir temperature near the optimum 530°C value shown in Fig. 6,

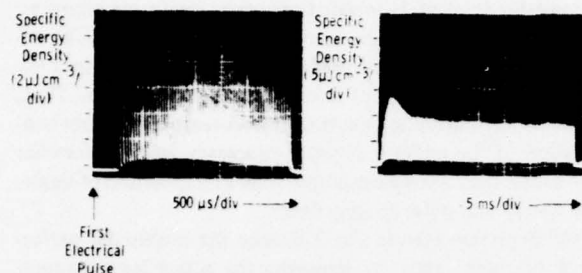


Fig. 8. Temporal behavior of pulsed copper bromide laser output with 10 torr He at 525°C. (a) 500 μ s/div. (b) 5 ms/div.

the electrical pulser was operated in a burst mode with low duty cycle to minimize the average power dissipation of the discharge. The burst durations ranged between 5 and 50 ms to assure that steady-state conditions had been reached, and the pulse repetition rate within the burst was typically 15–20 kHz. The observed laser output pulse train is illustrated in Fig. 8 (a) and (b) for both 5 and 50 ms burst durations at the optimum pulse repetition frequency of 18 kHz. Laser output is not obtained until about the tenth electrical pulse has been applied; this indicates that approximately 1 J of input energy is required to accumulate threshold copper ground state densities, and is in good qualitative agreement with the equivalent single pulse dissociation energy requirement and the accumulation times depicted in Fig. 7. Beyond threshold, the laser output rises to a maximum of $\sim 11 \mu\text{J} \cdot \text{cm}^{-3}$ in about 1 ms, and then falls to a steady-state level of $\sim 6 \mu\text{J} \cdot \text{cm}^{-3}$ with a time constant of about 1.3 ms. This output level persists for burst durations up to 50 ms as shown in Fig. 8(b), demonstrating that thermal steady-state conditions have been achieved for this power loading. The peak value of $11 \mu\text{J} \cdot \text{cm}^{-3}$ was obtained with a 0.3 percent conversion efficiency, and corresponds to a peak intraburst average power level of 1.34 W for these conditions. These performance figures are in good agreement with observed single-pulse efficiencies and the factor of 5 reduction to $9 \mu\text{J} \cdot \text{cm}^{-3}$ predicted in Section III-B, but apparently some additional transient effects are occurring which retard the atomic copper accumulation and decrease the steady-state laser output on a millisecond time scale.

The variation of the laser output pulse envelope with reservoir temperature shown in Fig. 9 reveals that a principle contributor to this transient effect is the copper bromide vapor pressure. At 400°C the molecular vapor density [20] is near threshold at $1.6 \times 10^{15} \text{ cm}^{-3}$, and approximately 18 electrical pulses are required to obtain the threshold copper densities capable of sustaining laser output. Peak pulse energy is attained in about 0.5 ms, and then the laser output falls steadily towards 0 in about 2 ms. At the single-pulse temperature optimum of 525°C where the CuBr vapor density is $7.9 \times 10^{16} \text{ cm}^{-3}$, less pronounced effects are observed: about ten electrical pulses are required to reach threshold, and the steady-state output declines to ~ 0.6 of the peak value rather than vanishing completely. With the CuBr vapor density increased to $2.4 \times 10^{17} \text{ cm}^{-3}$ at 575°C, this transient decline in the steady-state output is virtually eliminated. Thus, the continued application of electrical pulses can actually deplete the ground state copper

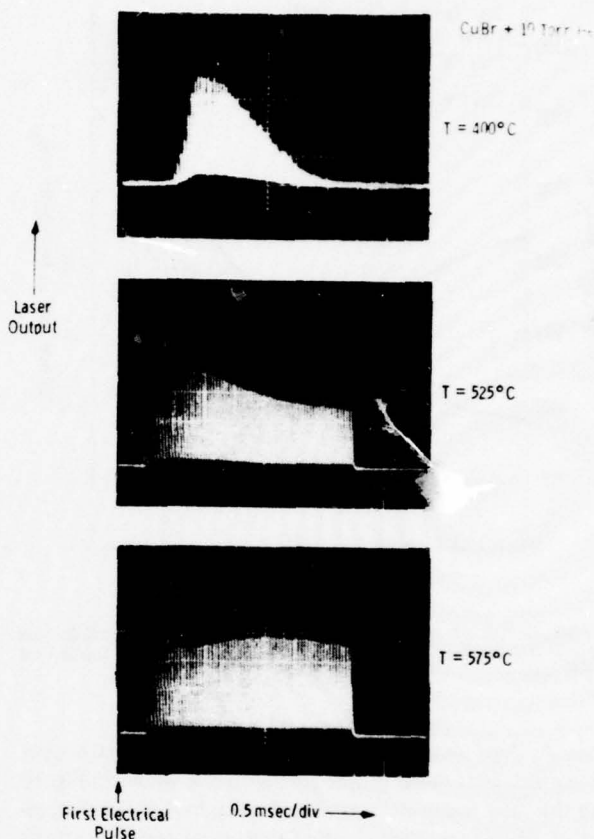


Fig. 9. Temporal behavior of multipulsed copper bromide laser output for reservoir temperatures of 400, 525, and 575°C.

population at the low densities corresponding to a 400°C reservoir temperature, but increasing the CuBr vapor pressure to $\sim 2.4 \times 10^{17} \text{ cm}^{-3}$ provides sufficient material to prevent significant deterioration of the laser output for these pulsing conditions. This behavior suggests depletion of the copper density within the axial region of highest current density, and possibly a radial transport of copper atoms to the walls as the pulse train develops. These axial depletion effects can degrade the laser output energy and beam profile, and generally tend to raise the optimum reservoir temperature in the multipulse regime.

Both radial temperature and charged particle gradients can deplete axial densities by transporting discharge species to the walls. As noted in Section III-B, an average power dissipation of $78 \text{ W} \cdot \text{cm}^{-1}$ would raise the axial gas temperature by about 1300°C; with a wall temperature $T_w = 527^\circ\text{C} = 800 \text{ K}$, the parabolic radial temperature profile shown in Fig. 10 is established in the steady state. The hot axial core becomes a region of reduced gas density as the gas expands radially, and for these conditions the radial density profile of Fig. 10 yields an axial gas density ~ 0.4 times the density at the wall. An axial depletion of this magnitude could account for the reduced laser output observed in the oscillographs of Fig. 8. Similarly, radial cataphoresis during the current pulse can extract positive copper ions from the central portion of the discharge by ambipolar diffusion in the radial space charge field of the tube

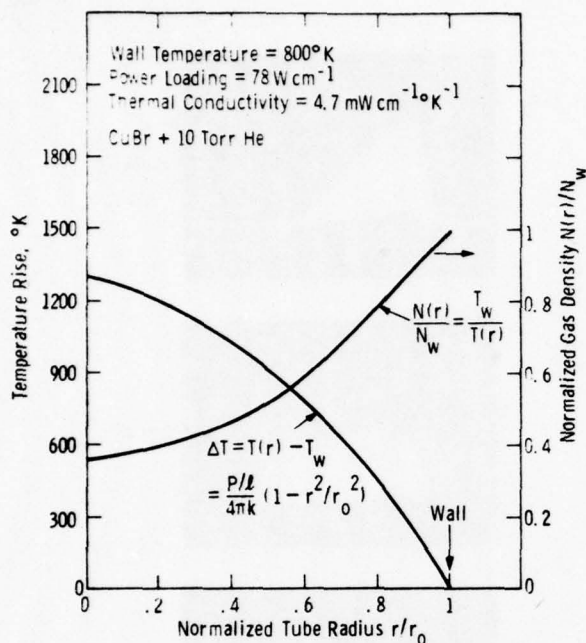


Fig. 10. Computed temperature and gas density radial profiles for copper halide laser discharges with an average power loading of $78 \text{ W} \cdot \text{cm}^{-1}$.

[21]. As these ions recombine at the walls, the neutral copper density assumes a radial profile similar to that shown in Fig. 10 with the axial region decreased in density by the radial transport of charged particles. Both of these axial depletion effects occur cyclically during the pulsed discharge sequence, but are counteracted by thermalization and diffusion processes which occur between pulses. The actual steady-state radial distribution produced by the cyclical occurrence of these various radial processes is beyond the scope of this present analysis. However, these spatial redistributions of copper atoms undoubtedly occur under certain circumstances, and are the most likely explanation for frequently observed annular output beam patterns and transient variations in laser output energy on a millisecond time scale.

IV. CONCLUSIONS

Laser output energy densities as high as $70 \mu\text{J} \cdot \text{cm}^{-3}$ have been measured with optimized double-pulse excitation of copper halide laser mixtures. Typical performance figures in CuBr + 10 torr He are $45 \mu\text{J} \cdot \text{cm}^{-3}$ at a 0.3 percent single-pulse conversion efficiency with a $60 \mu\text{s}$ optimum pulse delay. Without careful consideration of laser kinetic effects, it might be inferred that on a continuously pulsed basis, approximately $45 \mu\text{J} \cdot \text{cm}^{-3} / 60 \mu\text{s} = 0.75 \text{ W} \cdot \text{cm}^{-3}$ of average power should be obtained from these systems. However, this is not observed in practice, and the copper halide afterglow absorption measurements supply a plausible explanation for the observed average power levels in the multipulse regime. Because of thermal dissipation and temperature rise constraints, the multipulse electrical pulse energy must be reduced by a factor of about 10 from the corresponding dissociation pulse energies em-

ployed in producing single laser output pulses. This reduces the available level of dissociated copper ground state atoms by this same factor, but when combined with the multipulse accumulation factor of 2, the net reduction in a laser output energy is typically a factor of 5 for multipulse excitation. Thus, the observed multipulse behavior follows reasonably from consideration of the relevant physical processes, and is somewhat more subtle than a simple multiplicative extrapolation of single-pulse energy and pulse spacing data.

Axial depletion effects also influence the multipulse performance of these lasers by removing the active laser medium from the central portion of the laser discharge. Radial temperature gradients established at high average power loadings can reduce axial gas densities by factors of about two, and radial cataphoresis forces can provide a similar axial depletion of copper atoms by ambipolar diffusion of copper ions to the tube walls. These effects are especially pronounced at lower reservoir temperatures where radial transport forces or the electrical excitation process itself can reduce copper ground state densities below laser threshold levels and actually extinguish laser emission as the pulse train continues. To a considerable extent, these depletion effects can be counteracted by increasing the reservoir temperature to provide higher copper halide background densities. This generally leads to higher optimum temperatures for continuously pulsed copper halide lasers.

The absorption measurements reveal that copper halide dissociation levels are in the range of 1 to 3 percent for typical double-pulse excitation, and upper laser level populations are about 1 percent of the copper ground state density. Furthermore, the average dissociated copper atom can be recycled two to four times through the laser sequence before recombination occurs. However, due to cumulative effects, these densities build up to levels of about a factor of 2 higher than this with multipulse excitation. This implies that the average copper atom can be recycled more frequently through the laser sequence, and this generally leads to higher optimum pulse repetition rates for continuously pulsed systems. The laser efficiency remains substantially unchanged in extrapolating to the multipulse regime, although the more effective use of dissociated copper at high pulse-repetition frequencies (PRF'S) certainly contributes to a higher level of efficiency.

These experiments indicate that significant improvements in laser operation can be realized by understanding and controlling laser kinetic variables. For example, any increases in the effective lifetime of the dissociated copper ground state will permit higher energy density operation, and decreases in the copper metastable life-time will permit higher PRF operation. Techniques which limit temperature rise in the gas will also improve performance by permitting higher excitation pulse energies. These studies emphasize the importance of laser kinetic effects in the operation of copper halide lasers and indicate several promising approaches to the improvement of existing systems.

ACKNOWLEDGMENT

The authors wish to thank R. K. Williams, J. S. Nee, and W. Mamrose for their excellent technical assistance.

REFERENCES

- [1] C. S. Liu, E. W. Sucov, and L. A. Weaver, "Copper superradiant emission from pulsed discharges in copper iodide vapor," *Appl. Phys. Lett.*, vol. 26, pp. 92-93, 1973.
- [2] L. A. Weaver, C. S. Liu, and E. W. Sucov, "Superradiant emission at 5106, 5700 and 5782 Å in pulsed copper iodide discharges," *IEEE J. Quantum Electron.*, vol. QE-10, pp. 140-147, Feb. 1974.
- [3] I. Liberman, R. V. Babcock, C. S. Liu, T. V. George, and L. A. Weaver, "High-repetition-rate copper iodide laser," *Appl. Phys. Lett.*, vol. 25, pp. 334-335, 1974.
- [4] C. J. Chen, N. M. Nerheim, and G. R. Russell, "Double-discharge copper vapor laser with copper chloride as a lasant," *Appl. Phys. Lett.*, vol. 23, pp. 514-515, 1973.
- [5] C. J. Chen and G. R. Russell, "High-efficiency multiply pulsed copper vapor laser utilizing copper chloride as a lasant," *Appl. Phys. Lett.*, vol. 26, pp. 504-505, 1975.
- [6] J. A. Piper, "A copper iodide laser excited by transverse discharge," *Opt. Commun.*, vol. 14, pp. 296-300, 1975.
- [7] I. Smilanski, L. A. Levin, and G. Erez, "A copper laser using CuI vapor," *IEEE J. Quantum Electron.*, vol. QE-11, pp. 919-920, Nov. 1975.
- [8] O. S. Arkitava, V. L. Dzhikiya, and Yu. M. Oleinik, "Laser utilizing CuI transitions in copper halide vapors," *Sov. J. Quantum Electron.*, vol. 5, pp. 1001-1002, Aug. 1975.
- [9] N. V. Subotinov, S. D. Kalchev, and P. K. Telbizov, "Copper vapor laser operating at a high pulse repetition frequency," *Sov. J. Quantum Electron.*, vol. 5, pp. 1003-1004, Aug. 1975.
- [10] A. M. Shukhtin, G. A. Fedotov, and V. G. Mishakov, "Lasing with CuI lines using copper bromide vapor," *Opt. Spectros C.*, vol. 39, p. 681, Dec. 1975.
- [11] W. T. Walter, N. Solimene, M. Piltch, and G. Gould, "Efficient pulsed gas discharge lasers," *IEEE J. Quantum Electron.*, vol. QE-2, pp. 474-479, Sept. 1966.
- [12] A. A. Isaev, M. A. Kazaryan, and G. G. Petrash, "Copper vapor pulsed laser with a repetition frequency of 10 kHz," *Opt. Spectrosc.*, vol. 35, pp. 307-308, Sept. 1973.
- [13] P. A. Bokhan, V. N. Nikolaev, and V. I. Solomonov, "Sealed copper vapor laser," *Sov. J. Quantum Electron.*, vol. 5, pp. 96-97, July 1975.
- [14] R. S. Anderson, L. Springer, B. G. Bricks, and T. W. Karras, "A discharge heated copper vapor laser," *IEEE J. Quantum Electron.*, vol. QE-11, pp. 172-174, Apr. 1975.
- [15] A. C. G. Mitchell and M. W. Zemansky, *Resonance Radiation and Excited Atoms*. Cambridge, MA: Cambridge Univ. Press, 1961.
- [16] A. G. Gaydon, *Dissociation Energies and Spectra of Diatomic Molecules*, 2nd ed. London, England: Chapman and Hall, 1953, p. 224.
- [17] A. A. Isaev, M. A. Kazaryan, and G. G. Petrash, "Effective pulsed copper-vapor laser with high average generation power," *JETP Lett.*, vol. 16, pp. 27-29, 1972.
- [18] This computation of temperature rise assumes a thermal conductivity for the predominant 10 torr He component of $4.7 \text{ mW} \cdot \text{cm}^{-1} \cdot \text{K}^{-1}$.
- [19] The asymptotic value approached by the maximum values of repetitively decaying exponentials is given by $(1 - \exp(-t'/\tau))^{-1}$ where t' is the repetition period and τ is the decay time constant. For the values of this example, the metastables approach 1.05 and the ground states approach 2.05.
- [20] R. A. J. Shelton, "Vapor pressures of solid copper (I) halides," *Trans. Faraday Soc.*, vol. 57, pp. 2113-2118, 1961.
- [21] J. F. Waymouth, *Electric Discharge Lamps*. Cambridge, MA: MIT Press, 1971.

High average power pulser design for copper halide laser systems*

J. L. Pack, C. S. Liu, D. W. Feldman, and L. A. Weaver

Westinghouse Research Laboratories, Pittsburgh, Pennsylvania 15235

(Received 6 April 1977; in final form, 6 May 1977)

A circuit using two thyratrons is described which provides alternating polarity, high-current pulses at pulse repetition rates up to 20 kHz, suitable for operating copper halide lasers. The circuit is a modification of a Blumlein configuration in which two networks are charged in parallel and discharged in series, providing a voltage quadrupling effect when used with resonant charging. By triggering the thyratrons sequentially the current is reversed on alternate pulses, which greatly reduces axial cathaphoretic effects and extends the laser tube operating lifetime. The circuit can deliver up to 5 kW average power at 15 kHz.

I. INTRODUCTION

Recent experiments involving both copper halide¹⁻⁶ and pure copper⁷⁻¹⁰ lasers require electrical pulsing units capable of delivering high-current pulses at repetition rates up to 20 kHz and average power levels up to 2 kW. Pulses of several hundred amperes in amplitude and 50–200 nsec in width are required. In experiments utilizing longitudinal discharges^{1,4-9} the voltages applied across the tube range from a few to about 50 kV, being limited by the capability of the switching tube. To provide the maximum voltage across the discharge tube either a transformer or a Blumlein circuit is typically used to couple the thyatron to the discharge. A transformer has been employed successfully to power a 30-cm copper halide discharge tube,⁴ but the inductance associated with this circuit arrangement can limit the current rise time to unacceptably large values. An attractive circuit which provides voltage doubling and minimizes circuit inductance is the Blumlein configuration described by Bokhan *et al.*⁹ and others.^{3,11} This circuit, as well as those using secondary capacitors connected in parallel with the laser discharge,^{2,12-14} minimizes the discharge circuit inductance by placing the switching tube outside the discharge circuit. In addition, it has been shown in both copper halide lasers¹⁵ and many types of discharge lamps¹⁶ that axial cathaphoretic effects greatly diminish the tube operating lifetime unless a periodic current reversal is introduced. Thus present copper halide and metallic copper lasers not only require high pulse repetition rates and average power levels, but also circuit configurations which incorporate voltage multiplication, minimum circuit inductance, and current reversal capabilities. The operating characteristics of such a pulsing unit are described in the following sections.

II. PULSING CIRCUITRY

A circuit which provides current reversal, minimum inductance, and voltage doubling properties is shown in Fig. 1. The operation of this circuit for each switching

tube is similar to that described by Bokhan *et al.*⁹ Some rearrangement of components has been introduced to reduce the electrical stress on the hold-off diode D , and one diode was replaced by a coupling choke L_3 . C_1 and C_2 are resonantly charged from the power supply by means of the charging choke L_c and the holdoff diode D . The value of L_c is chosen so that the recharge time is slightly less than the time between pulses at the highest frequency of operation, typically 20 kHz. The coupling choke L_3 has a value about 1% of L_c so that C_2 is fully charged only a few microseconds after C_1 . Using inductors as charging⁴ and coupling¹¹ elements minimizes circuit losses.

Current flows in one direction through the laser tube when T_1 is triggered, and in the opposite direction when T_2 is triggered; thus by triggering T_1 and T_2 alternately current reversal is achieved. Since two thyratrons are used, twice the power can be delivered to the laser tube compared with circuits using only one thyatron. Values of C_1 and C_2 range from 0.5 to 5 nF, with $L_c \approx 0.1$ H and $L_3 \approx 1$ mH. The ring-up chokes L_1 and L_2 have values around 3 μ H and are chosen such that the capacitors C_1 or C_2 are reversed in about 200 nsec.

EGG No. 1802 thyratrons have performed in this circuit at frequencies up to 20 kHz, delivering in excess of

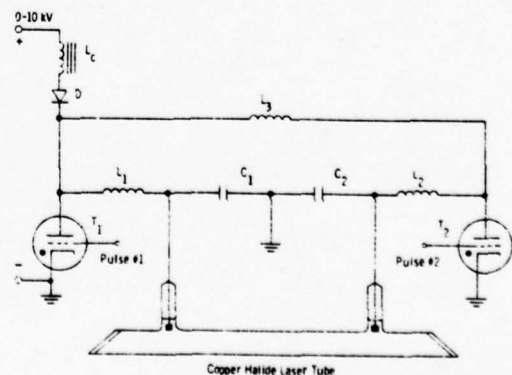


FIG. 1. Alternating polarity pulse generator suitable for high-power copper halide laser applications.

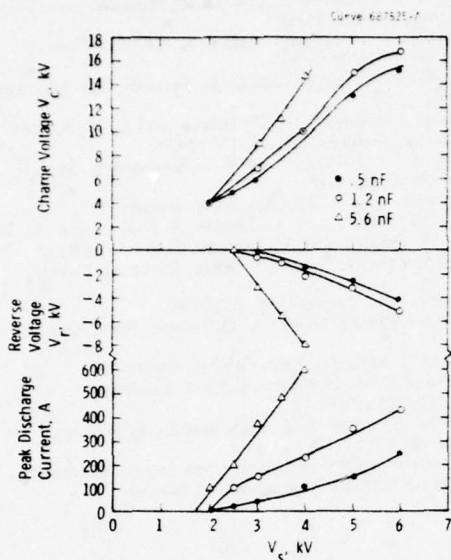


FIG. 2. Charge voltage, reverse voltage, and peak discharge current as a function of power supply voltage for various values of capacitance.

2-kW average power to a discharge tube 20 cm long and 1.2 cm in diameter filled with 10 Torr He. The voltage developed across the capacitors was expected to be twice the power supply voltage due to resonant charging; however, in practice the voltage always exceeded this value due to reverse voltage left on the capacitors from the preceding discharge pulse. This effect is illustrated in Fig. 2 where peak current, charging voltage, and reverse voltage are presented as a function of power supply voltage for storage capacitors of 0.5, 1.2, and 5.6 nF with ring-up chokes L_1 and L_2 equal to $4.6 \mu\text{H}$. The operating frequency was 2 kHz for the 0.5- and 1.2-nF cases, and was reduced to 1 kHz for storage capacitors of 5.6 nF. With ring-up coils of $2.6 \mu\text{H}$, the 5.6-nF capacitors delivered peak currents of more than 900 A for a power supply voltage of 4.5 kV with a reverse voltage of 6 kV. The rate of rise of current was a function of only the voltage on the storage capacitors. For pumping metal halide lasers the rate of rise of the current in the discharge is just as important as the current amplitude, so the choice of storage capacitance again is determined by characteristics of the laser medium. That is, the current pulse width should be matched to the width of the laser pulse to obtain maximum laser efficiency, which for copper halide lasers is typically less than 50 nsec.¹⁻⁶ The current pulse width is given by $\pi(2L_d C_1)^{1/2}$, where L_d is the inductance in the discharge circuit which for these tests was approximately $0.75 \mu\text{H}$.

III. PULSER SCALING CONFIGURATIONS

Effective pulser and discharge scaling to higher average power levels can be achieved by operating a segmented discharge tube with the sections electrically parallel but optically in series. Such longitudinal discharge scaling permits higher average power levels

while maintaining the same current pulse width and power supply voltage. A simplified schematic of a four-section copper halide laser tube pulsing circuit is shown in Fig. 3. In order to operate the multiple section tube it is only necessary to increase the number of storage capacitors and ring-up coils as shown. The component values are modeled after those determined from the single section discharge circuit of Fig. 1. The storage capacitors are all equal to one another at 0.5 nF. The ring-up inductors are equal for the electrodes in the central portions of the tube, whereas the inductors at each end are twice this value to render the same ring-up times for the commonly driven electrodes. A value of L equal to $4.5 \mu\text{H}$ gives a ring-up time of about 150 nsec for 0.5-nF storage capacitors. Since the pulse widths in the discharge tube are nearly independent of the value of ring-up inductance, this inductance value is not critical. However, the common ring-up coils should be matched to assure that the sections will break down synchronously.

At an operating frequency of 15 kHz the four-section circuit shown in Fig. 3 delivers about 5-kW average power to the discharge for a charging voltage on the storage capacitors of less than 15 kV and a power supply voltage of less than 7 kV. The same power can be delivered at less voltage by using larger storage capacitors if longer pulse widths can be tolerated. By triggering the thyratrons sequentially the current is alternately reversed in each section of the discharge tube, thereby counteracting discharge cathaphoretic effects and equalizing the electrode temperature. Although only four sections are shown, more sections could be driven using this scheme to achieve effective modular scaling of the discharge length and pulsing unit.

Several copper halide laser tubes were constructed and operated using the circuit shown in Fig. 1. Outputs up to 3.5-W average power were obtained from quartz laser tubes ranging from 1.2×50 cm up to 3×100 cm with a fill of CuBr and about 10-Torr Ne at an operating efficiency of about 0.2% at 16 kHz.

It is proposed that scaling to many sections is possible and a four-segment 100-cm tube was operated. Further scaling in length would eventually exceed the power handling capability of two No. 1802 thyratrons used in the circuit of Fig. 3. This problem can be circumvented by either using a multiplicity of thyratrons, each of which operates its own subsections of the entire sys-

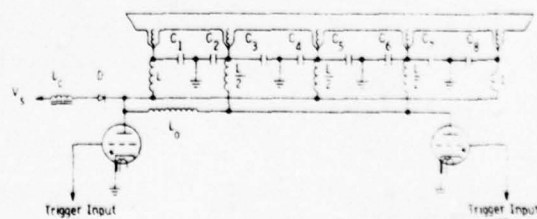


FIG. 3. Pulsing circuitry for a four-section copper halide tube.

tem. and/or using a number of thyratrons in parallel and sequentially switching the thyratrons in order to share the current. It is believed by the authors that scaling up to over 50-kW average input power should be possible using a number of No. 1802 type thyratrons.

V. ACKNOWLEDGMENT

The authors gratefully acknowledge helpful discussions with R. Spreadbury and the expert technical assistance of J. S. Nee, R. K. Williams, and W. Mamrose.

* This work was partially supported by the Office of Naval Research under Contract no. N00014-74-C-0445.

¹ I. Liberman, R. V. Babcock, C. S. Liu, T. V. George, and L. A. Weaver, *Appl. Phys. Lett.* **25**, 334 (1974).

² J. A. Piper, *Opt. Commun.* **14**, 296 (1975).

³ I. Smilanski, L. A. Levin, and G. Erez, *IEEE J. Quantum Electron.* **QE-11**, 919 (1975).

⁴ C. J. Chen and G. R. Russell, *Appl. Phys. Lett.* **26**, 504 (1975).

⁵ O. S. Akirtava, V. L. Dzhikiya, and Yu. M. Oleinik, *Sov. J. Quant. Electron.* **5**, 1001 (1976).

⁶ N. V. Subotinov, S. D. Kalchev, and P. K. Telbizov, *Sov. J. Quant. Electron.* **5**, 1003 (1976).

⁷ A. A. Isaev, M. A. Kazaryan, and G. G. Petrash, *Opt. Spectrosc.* **35**, 307 (1973).

⁸ R. S. Anderson, L. Springer, B. G. Bricks, and T. W. Karras, *IEEE J. Quantum Electron.* **QE-11**, 172 (1975).

⁹ P. A. Bokhan, V. N. Nikolaev, and V. I. Solomonov, *Sov. J. Quant. Electron.* **5**, 96 (1975).

¹⁰ I. S. Aleksandrov, Yu. A. Babeiko, A. A. Babaev, O. I. Buzhinskii, L. A. Vasil'ev, A. V. Efimov, S. I. Krysanov, G. N. Nikolaev, A. A. Slivitskii, A. V. Sokolov, L. V. Tatarintsev, and V. S. Tereschchenkov, *Sov. J. Quant. Electron.* **5**, 1132 (1976).

¹¹ C. P. Wang, *Rev. Sci. Instrum.* **47**, 92 (1976).

¹² M. Geller, D. E. Altman, and T. A. DeTemple, *Appl. Opt.* **7**, 2232 (1968).

¹³ P. Schenck and H. Metcalf, *Appl. Opt.* **12**, 183 (1973).

¹⁴ A. J. Schwab and F. W. Hollinger, *IEEE J. Quantum Electron.* **QE-12**, 183 (1976).

¹⁵ C. S. Liu, D. W. Feldman, J. L. Pack, and L. A. Weaver, *J. Appl. Phys.* **48**, 194 (1977).

¹⁶ For example, commercial fluorescent lamps require alternating current to prevent the axial segregation of mercury.

APPENDIX D

A TECHNIQUE FOR DETERMINING GAS TEMPERATURE AND ATOMIC DENSITY

L. H. Taylor and R. B. Feldman*
Westinghouse R&D Center
Pittsburgh, Pennsylvania 15235

I. INTRODUCTION

The use of pulsed copper halide vapors to obtain laser emission from atomic copper lines at 510.6 nm and 578.2 nm has received considerable attention in recent years.¹⁻⁹ Similarly, laser action has been observed in other halide systems.¹⁰ Lasing is obtained by continuously applying electrical pulses at high repetition rates with each pulse acting as an excitation as well as a dissociation pulse for subsequent discharges. In other words, the initial copper halide molecules in the gas are first dissociated and then the resulting copper atoms are excited to higher electronic levels by direct electron impact. Stimulated or spontaneous emission relaxes these excited states to lower metastable states, which then relax slowly to the copper ground state. These ground state copper atoms are then available for subsequent re-excitation, or for recombination with halogen atoms to reconstitute the copper halide molecules.

Copper halide lasers are usually excited by a cylindrical longitudinal discharge within a high temperature oven, and are normally operated in a "burst" mode. A typical "burst" may consist of 100 pulses approximately 100 μ sec apart with an over-all burst duration of 10 msec. The discharge afterglow is that period of time immediately after the "burst" during which the excited gas slowly relaxes to thermodynamic equilibrium.

To understand the kinetics of these lasers it is imperative to know both the gas temperature and atomic level populations, but the

* Consultant

operating conditions make their determination very difficult. The gas temperature is primarily determined by electric discharge and molecular recombination heating, by thermal dissociation cooling, and by the fixed wall temperature. However, in a cylindrical longitudinal discharge the former three factors are strongly radially dependent, as well as time dependent. The situation for the atomic copper density is even worse: There are virtually no copper atoms at the wall whereas their density in the center of the tube may be as high as 10^{15} cm^{-3} .

Although gain measurements on vibrational-rotational transitions can be used to determine the gas temperature of molecules,¹¹⁻¹² there is only one direct and well-established technique for the determination of the gas temperature of atoms: the measurement of the thermal Doppler broadening of appropriate lines.¹³ This technique encounters difficulties both at high densities, where pressure broadening is significant, and at high temperatures, where the absorption is too high to measure.

The atomic level densities can be determined from interferometric optical refractivity measurements, or from line absorption measurements.¹³ The former method is difficult to execute, particularly in non-uniform plasmas or for uv wavelengths, whereas the latter method is only applicable at high densities where pressure broadening is dominant, unless the gas temperature is known by some other means.

To circumvent these problems we have developed a general technique for simultaneously determining in situ both gas temperature and atomic level densities. A narrow line dye laser is tuned through the atomic absorption line. A theoretical absorption line profile is then fitted to the measured profile by varying the theoretical atomic level density and gas temperature until the error sum of the squares is minimized. This approach extends the usefulness of conventional absorption measurements into regions where:

- Thermal and pressure broadening are both significant.
- Total absorption occurs at line center.
- Gas temperature is not known.

The following sections describe the absorption measurements, the technique for determining the atomic level density and gas temperature, and gives some sample results for the CuBr laser.

II. ABSORPTION MEASUREMENTS

When a radiation beam of intensity $I_d(\nu-\nu_d)$, centered about the wave number ν_d , passes through a length L of an absorbing medium, the transmitted radiation intensity is given by¹⁴

$$I_o = \int_0^{\infty} I_d(\nu-\nu_d) e^{-k(\nu-\nu_c)L} d\nu \quad (1)$$

where $k(\nu-\nu_c)$ is the absorption coefficient of the absorbing medium which is centered about the wave number ν_c . It is assumed that there is no transverse or longitudinal spatial variation, and no temporal variation of $k(\nu-\nu_c)$ within the physical volume and time increment sampled by the radiation beam. It is further assumed that emission from the upper level of the absorption line is negligible. The total input intensity is given by

$$I_i = \int_0^{\infty} I_d(\nu-\nu_d) d\nu \quad (2)$$

The transmission is the ratio of the output and input intensities:

$$T = I_o/I_i \quad (3)$$

and the absorption, A , is simply $1-T$.

The variation of $k(\nu-\nu_c)$ with ν is the line profile which is determined by the isotopic shift, hyperfine structure (hfs), and various broadening mechanisms. In the isotope shift, the center of the energy level of one isotope is displaced relative to the center of any other isotope. The effective line center lies between the centers of the individual isotopes at a position determined by the isotopic composition of the mixture.

The hyperfine structure of a line is a result of the interaction of the magnetic moment of the nucleus with the magnetic fields caused by the motion of the electrons. This interaction splits the upper and lower energy levels of each optical transition into a number of closely spaced levels.¹⁵⁻¹⁶ Transitions occur between individual pairs of these levels, and obey the usual selection rules. The relative intensities are given by the relative magnitude of each spectral line in a normal multiplet of Russell-Saunders coupling.¹⁷

The broadening of each component of the hfs is considered to be independent of all other components. The four broadenings mechanisms important in copper atoms are Doppler, natural, resonance, and van der Waals. Doppler broadening results from the thermal motion of the absorbing atoms and produces a Gaussian profile with a full-width half-maximum (FWHM) given by

$$\Delta\nu_D = 0.04572(T_g/273)^{1/2} \text{ cm}^{-1} \quad (4)$$

where T_g is the gas temperature, and the formulation is now restricted to the 324.8 nm transition from the Cu ground state.

Natural broadening results from the finite lifetimes of the energy states, resonance broadening results from collisions with ground state copper atoms, and van der Waals broadening results from collisions with foreign atoms, i.e., the predominant buffer gas. These three mechanisms produce a Lorentzian profile with a FWHM of

$$\Delta\nu_L = [0.5509 + 0.9882 (N_c/10^{15}) + 0.5319 P (273/T_g)^{0.7}] \times 10^{-3} \text{ cm}^{-1} \quad (5)$$

where the terms in the brackets are the natural, resonance, and van der Waals contributions, respectively.⁹ The density of ground-state copper atoms is denoted by N_c , and the buffer gas (Ne) pressure in Torr is denoted by P .

The combined effect of these broadening mechanisms, which are considered to be independent of each other, is to produce a Voigt profile:

$$k(\nu-\nu_c) = (1.435 \times 10^{-13}) N_c (a/\pi) \int_{-\infty}^{\infty} \frac{e^{-y^2}}{a^2 + (\omega-y)^2} dy \quad (6)$$

where

$$a = (\ln 2)^{1/2} \Delta \nu_L / \Delta \nu_D \quad (7)$$

$$\omega = (4 \ln 2)^{1/2} (\nu - \nu_c) / \Delta \nu_D \quad (8)$$

The upper state density is assumed to be negligible with respect to the ground state density. For practical operating conditions in the CuBr laser, $a < 0.2$, i.e., the absorption lines are primarily Doppler broadened. This situation is sufficiently prevalent that in many cases the absorption can be measured only in the wings of the Voigt profile where the Lorentzian broadening is dominant.

The total absorption profile is found by taking a Voigt profile for each hfs component, centering each component at the proper wave number, and multiplying by the appropriate relative intensity and isotope composition factors. At a given value of ν , the contributions from all of these components are added. A typical absorption profile is shown in Fig. 1. Included in this figure is the measured intensity profile, in arbitrary units, of the tunable dye probe laser.

The separation between the copper and dye line centers is given by

$$\delta = \nu_d - \nu_c \quad (9)$$

and is varied in the experiments by tuning the dye laser through the absorption profile. The effect of this tuning is quite large as shown in Fig. 2. This figure also demonstrates the large dependence of transmission on copper density. The dependence on gas temperature, shown in Fig. 3, is not nearly as great. These dependences of the transmission on the copper density and gas temperature form the basis of the technique described in the next section.

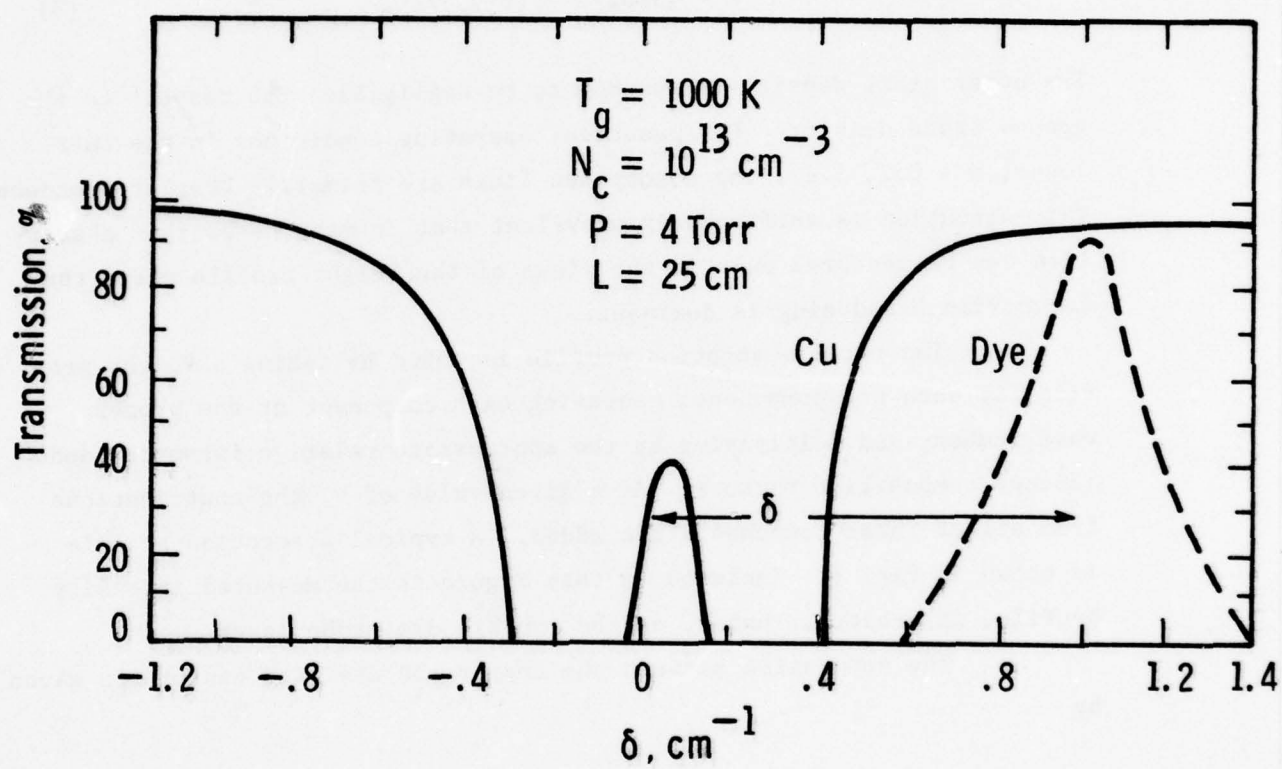


Fig. 1. Dye laser emission profile and copper absorption profile.

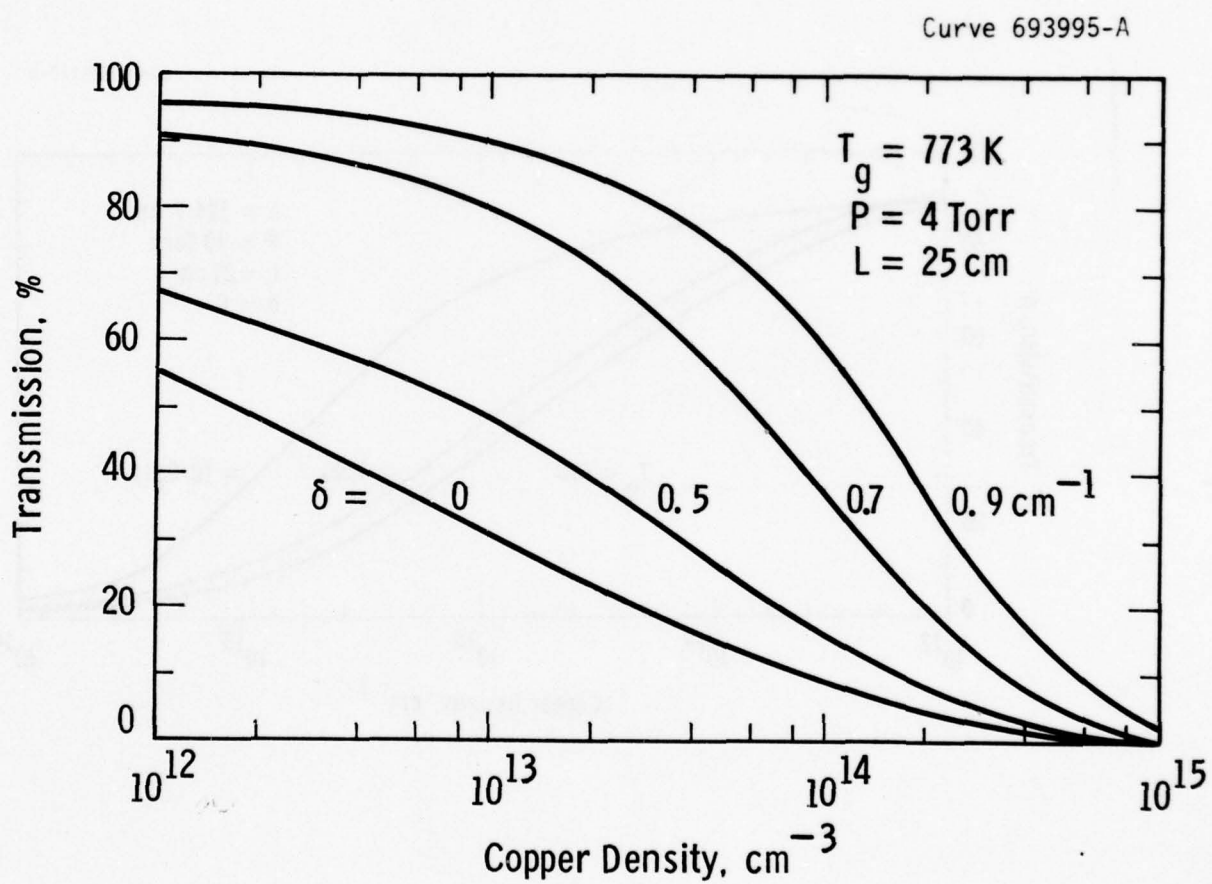


Fig. 2. Transmission as a function of copper density, and separation between absorption and probe line centers.

Curve 692124-A

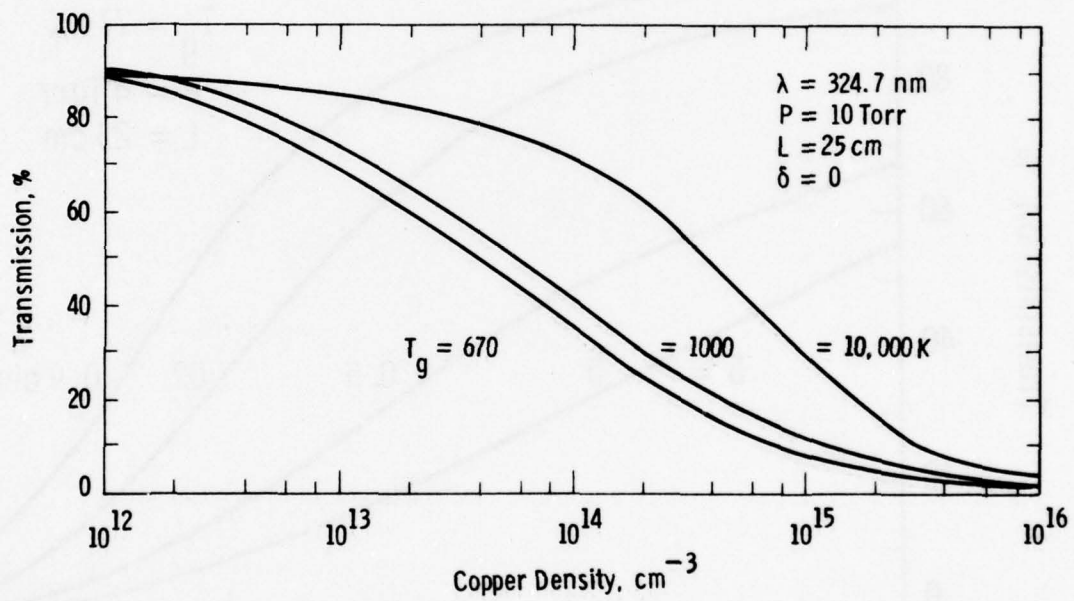


Fig. 3. Transmission as a function of copper density and gas temperature.

III. NEW TECHNIQUE

Based on the previous results it is a simple matter to conceptualize the basic approach to determining the atomic density and gas temperature from the absorption measurements. The dye probe laser is tuned through the copper absorption profile and absorption measurements are taken at several line separations, δ_i . The copper density and gas temperature are then adjusted in the theoretical absorption profile until the difference between the calculated and measured transmissions is minimized as measured by the error sum of the squares:

$$SS = \sum_i [T_i(\text{measured}) - T_i(\text{calculated})]^2 \quad (10)$$

where T_i is the transmission at the line separation δ_i , and the summation over i includes all of the measured transmissions.

The minimization of the error sum of the squares has proven to be a difficult problem fraught with many pitfalls. We first tried a regression analysis which seemed at the time like a reasonable approach.¹⁸ Complete failure was experienced, however, because, as we later determined, there is too much correlation between the density and temperature variables.

We then tried a gradient search technique.¹⁹ Although the Method of Steepest Descent²⁰ is commonly used in physics, we used a pattern search routine²¹ which we believe is faster. This routine is a trial-and-error iteration procedure which follows a decreasing slope to obtain a minimum. Failure was again the result.

Valuable insights into the problem were obtained by replacing the $T_i(\text{measured})$ values in Eq. 10 with theoretically computed values for $N_c = 10^{14} \text{ cm}^{-3}$ and $T_g = 1500 \text{ K}$, and then varying N_c and T_g in the computation of $T_i(\text{calculated})$. The results are shown in Fig. 4. As expected, the error sum of squares has a very sharp minimum at $N_c = 10^{14} \text{ cm}^{-3}$ and

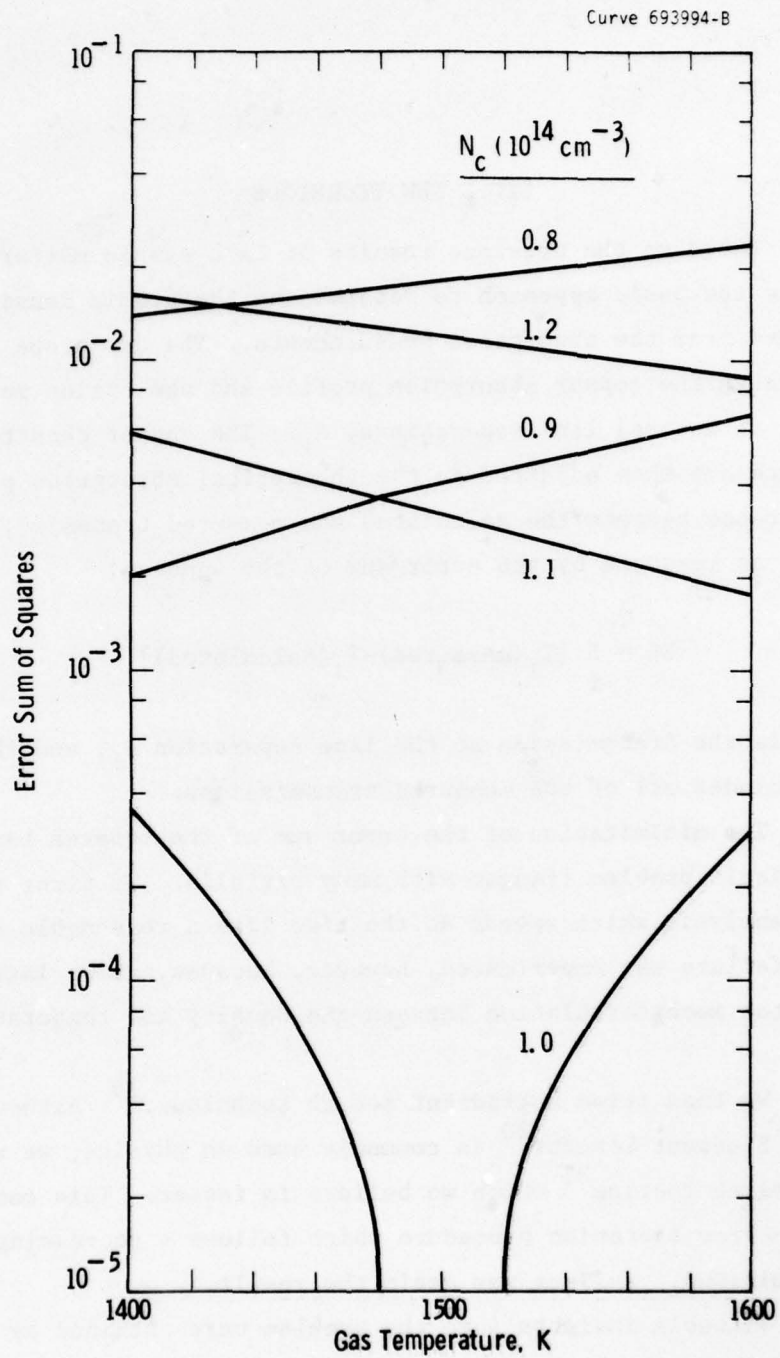


Fig. 4. Error sum of squares dependence on copper density and gas temperature.

$T_g = 1500$ K, and becomes worse as N_c either increases or decreases from 10^{14} cm^{-3} . However, if the density is too low, the error sum of squares increases monotonically with increasing temperature, whereas if the density is too high, the error sum of squares decreases monotonically with increasing temperature.

This monotonic behavior persisted when real measured data were used and, coupled with our previous difficulties with the minimization attempts, led us to believe that the sum of squares error surface must be of the form shown in Fig. 5. This surface is composed of three major areas:

- High Density: gentle hill sloping toward high temperatures and the correct density.
- Low Density: gentle hill sloping toward low temperatures and the correct density.
- Approximately Correct Density: a long (in the temperature direction), narrow (in the density direction) valley with many minima.

The extraneous minima arise from the errors in the measurements, and the correlation between the density and temperature variables. The general appearance of the surface agrees with the large density and small temperature dependencies shown in Fig. 3.

Given this error surface, a two-step procedure can be used to locate the lowest minimum. The steps, outlined in Fig. 6, are to apply the pattern search routine (or any other gradient search routine) to minimize the error sum of squares with respect to the density. This intermediate value of density, and the gas temperature are then varied by a shotgun search routine (a simple routine which we wrote) which systematically samples the valley to locate as many minima as reasonably possible. The density and temperature which yield the lowest minimum are taken to be the final values. The dashed arrow in Fig. 6 merely indicates that two separate computer programs are involved in this approach.

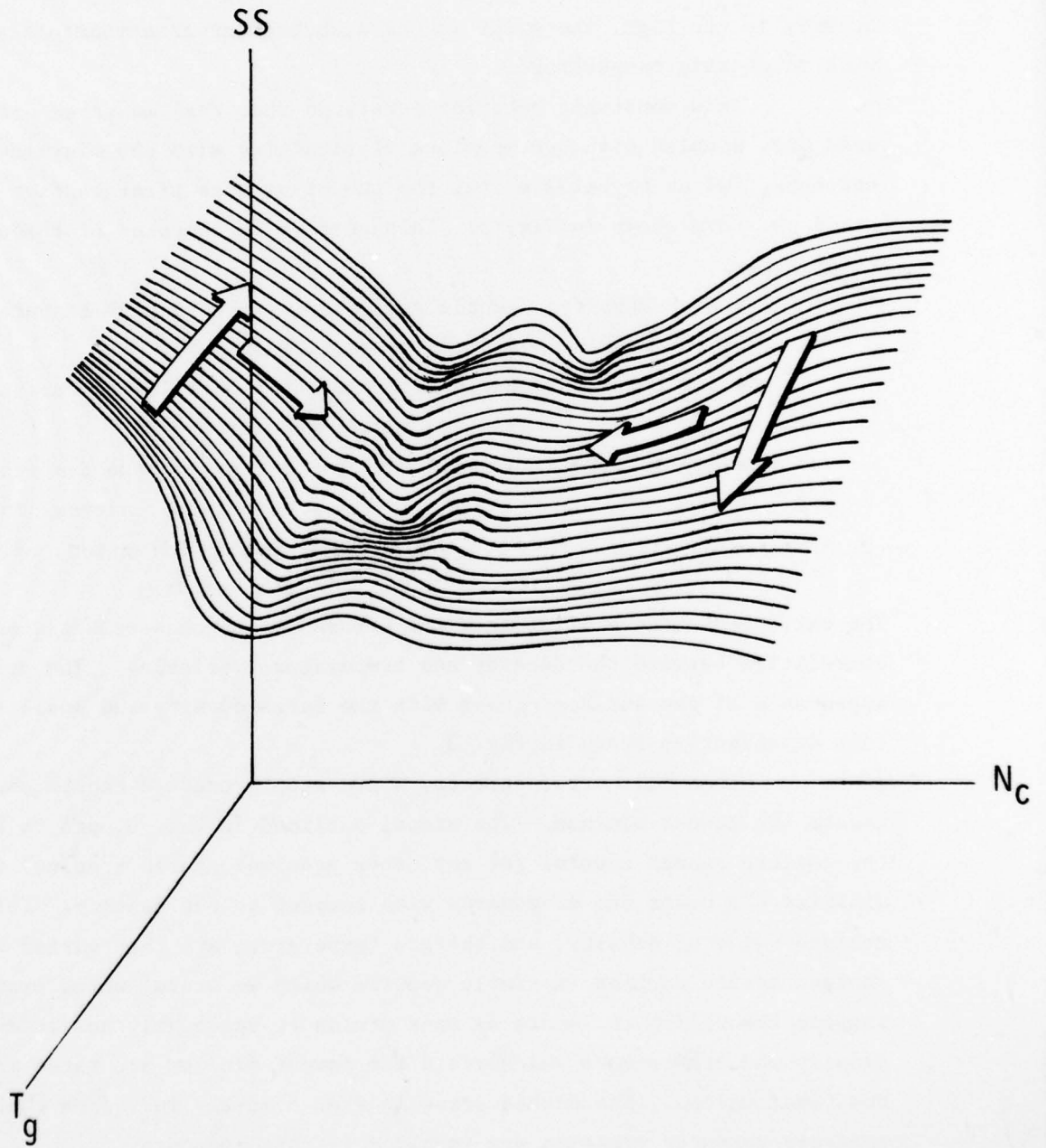


Fig. 5. Diagrammatic sketch of sum of squares (SS) error surface where arrows point downhill.

Dwg. 6427A04

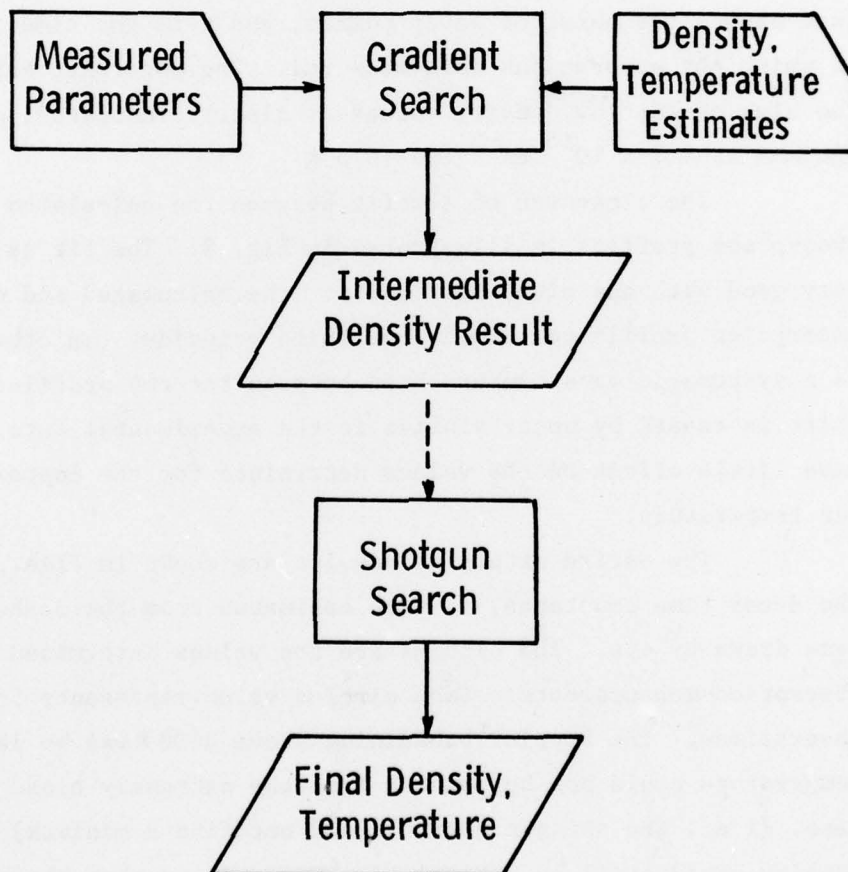


Fig. 6. Information flow for the determination of copper density and gas temperature.

IV. EXAMPLE APPLICATIONS

This new technique has been applied to absorption data taken along the axis of a cylindrical longitudinal discharge CuBr laser. A typical result is shown in Fig. 7 where T_0 is the initial gas temperature before the burst of laser pulses, and t is the time in the afterglow at which the absorptions were measured. The monotonic behavior of the too high or too low density values is clearly indicated, as well as the minimum at $1.2 \times 10^{15} \text{ cm}^{-3}$ and 1075 K.

The closeness of the fit between the calculated and measured absorption profiles is illustrated in Fig. 8. The fit is generally very good with one minor difficulty: the calculated and measured absorption profile centers do not quite coincide. In other words, there is a systematic wave number shift between the two profiles. This small shift is caused by uncertainties in the experimental data, but should have little effect on the values determined for the copper density and gas temperature.

The entire afterglow results are shown in Figs. 9 and 10 where the decay time constants, τ , were estimated from the dashed lines which were drawn by eye. The circles are the values determined from the absorption measurements. Each circled value represents 5-10 measured absorptions. The Doppler broadening above 3000 K was so large that the temperature could not be deduced from the extremely broad absorption line, (i.e., the shotgun search could not find a minimum) although the density could still be determined. We estimate that the copper density could be determined from 10^{11} to 10^{16} cm^{-3} with an accuracy of $\pm 20\%$, and that the temperature could be determined from 1000 to 3000 K with an accuracy of ± 200 K.

These results vividly demonstrate the utility of in situ, simultaneous determinations of density and temperature. The copper density along the axis of the tube decays exponentially, probably by recombination

Curve 692121-A

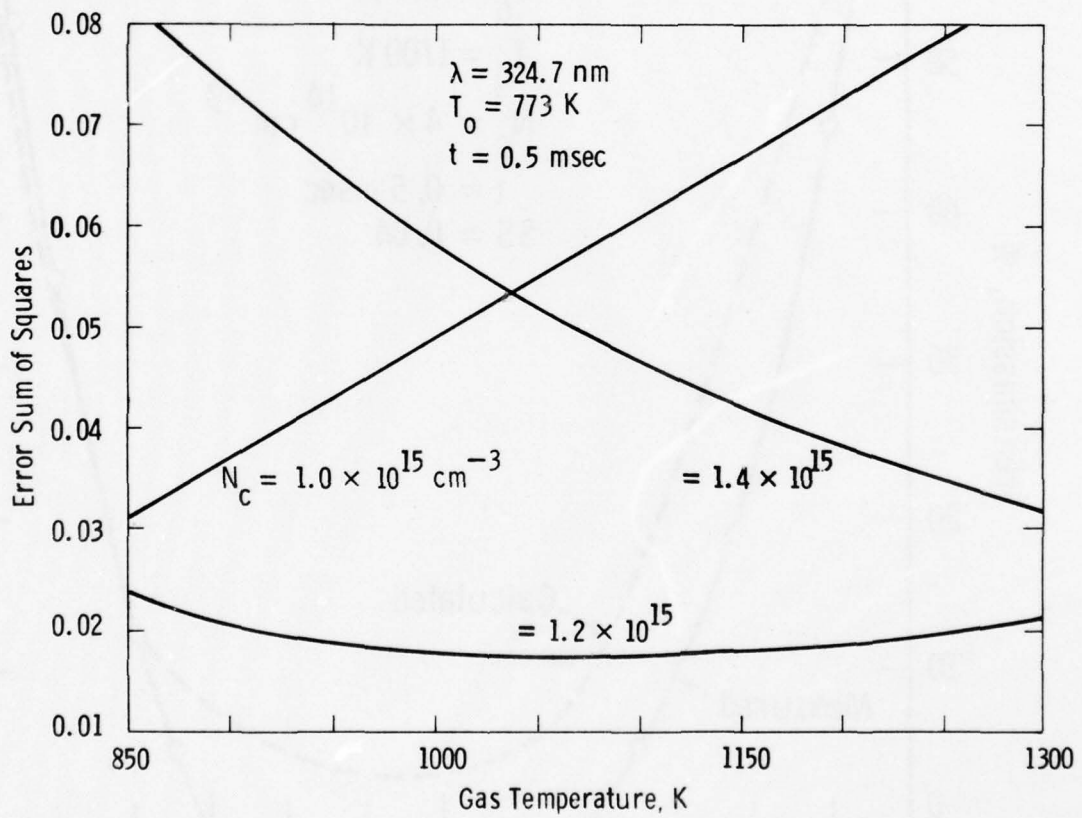


Fig. 7. Illustrative application of the minimization technique to the afterglow of a CuBr laser.

Curve 693996-A

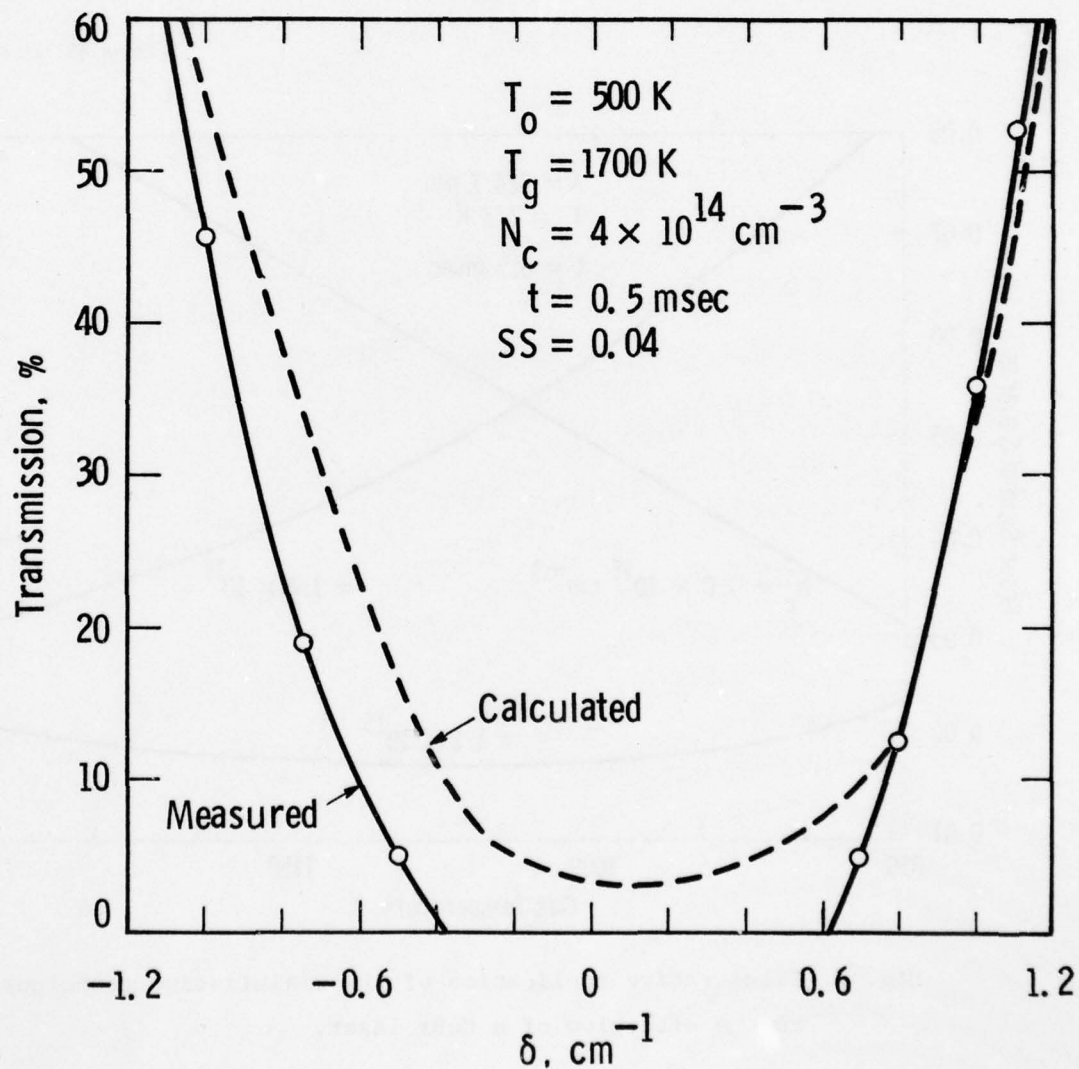


Fig. 8. Illustrative comparison of calculated and measured absorption profiles in the afterglow of a CuBr laser.

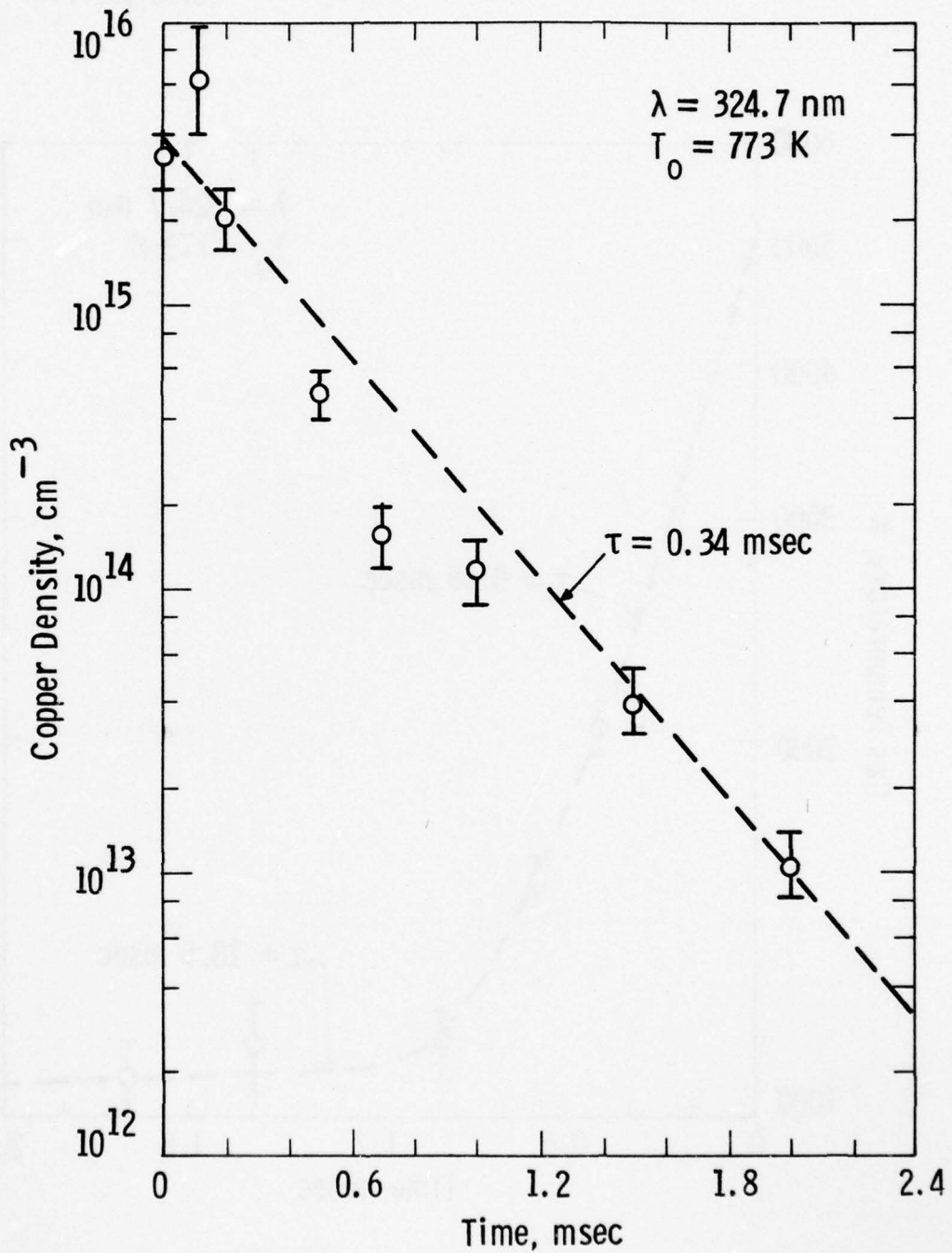


Fig. 9. Copper density decay in the afterglow of a CuBr laser.

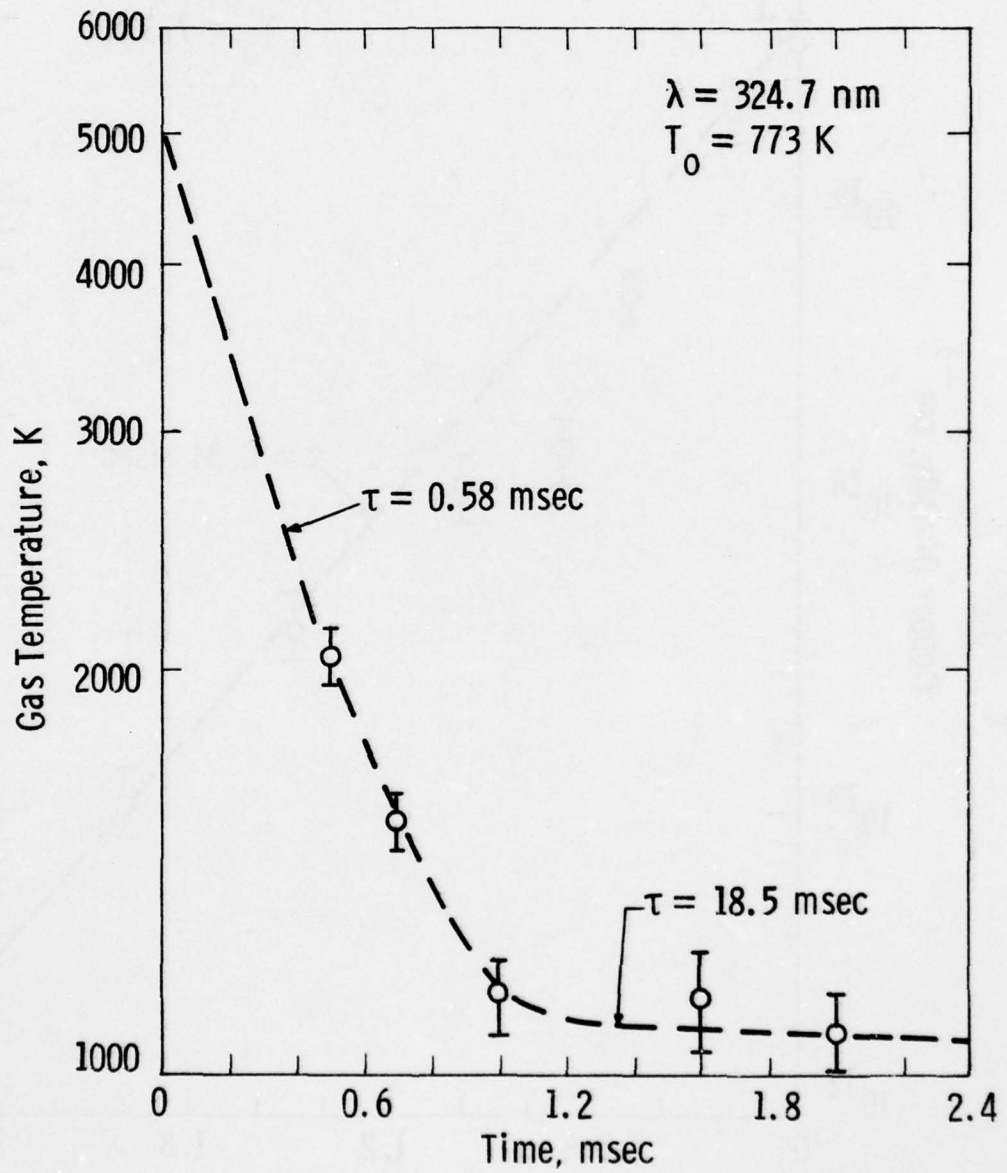


Fig. 10. Gas temperature decay in the afterglow of a CuBr laser.

with the bromine. On the other hand, the gas temperature decays rapidly at first, and slowly at later times. The initial decay may be caused by the rapid exchange of the hot buffer gas with the cooler gas surrounding the tube axis. This exchange would have little effect on the copper density because some of our other results indicate that the copper density increases slightly with radius up to half the distance to the wall. The slow thermal decay is probably ordinary thermal relaxation of the entire tube to thermodynamic equilibrium.

V. SUMMARY

We have developed a general technique for simultaneously determining in situ both gas temperature and atomic density of glow discharge constituents. A theoretical absorption line profile is fitted, by minimizing the error sum of squares, to the measured profile. This approach extends the usefulness of conventional absorption measurements beyond their normal range of validity.

The sum of the squares error surface was found to be complicated but amenable to a two step minimization search procedure. A gradient-following search routine was first used to locate a value of density quite close to the actual values. Because many extraneous minima existed in this region near the actual density, a shotgun search routine was then used to vary both density and temperature so as to map a long section of this region. The lowest minimum found in this manner was taken to be located at the actual values of density and temperature. This use of a gradient search with a shotgun search is an interesting combination of two old techniques and may be applicable to other problems with similar error surfaces.

The technique has already proven to be very useful. In applications to the cylindrical longitudinal discharge CuBr laser, the copper ground state density could be determined from 10^{11} to 10^{16} cm^{-3} with an estimated accuracy of $\pm 20\%$, while the gas temperature could be determined from 1000 to 3000 K with an estimated accuracy of ± 200 K. Furthermore, the results show that the thermal decay in the afterglow does not correlate with the density decay--thus indicating that the equilibration processes in the CuBr laser are more complicated than originally thought.

It should be emphasized that although the technique is applied herein to the ground state density of Cu in the CuBr laser, the technique can be easily extended to other systems such as excited state densities

in molecules. The only basic requirements are that the theoretical absorption line profile be well known, that a tunable probe be available, and that the absorption be in an easily measured range of values, say 5 to 99%.

VI. ACKNOWLEDGEMENTS

The experimentalists, D. W. Feldman, C. S. Liu and L. A. Weaver, have been very helpful in taking the measurements, discussing the physics, and lending continual moral support. The mathematicians, B. A. Powell and R. D. Fardo, were instrumental in developing the technique. This research has been partially supported by the Office of Naval Research under Contract N00014-74-C-0445.

REFERENCES

1. I. Liberman, R. V. Babcock, C. S. Liu, T. V. George and L. A. Weaver, *Appl. Phys. Lett.* 25, 334 (1974).
2. L. A. Weaver, C. S. Liu and E. W. Sucov, *IEEE J. Quantum Electron.* QE-10, 140 (1974).
3. C. J. Chen and G. R. Russell, *Appl. Phys. Lett.* 26, 504 (1975).
4. J. A. Piper, *Optics Commun.* 14, 296 (1975).
5. I. Smilanski, L. A. Levin and G. Erez, *IEEE J. Quantum Electron.* QE-11, 919 (1975).
6. C. S. Liu, D. W. Feldman, J. L. Pack and L. A. Weaver, *J. Appl. Phys.* 48, No. 1, January 1977.
7. C. S. Liu, D. W. Feldman, J. L. Pack and L. A. Weaver, *IEEE J. Quantum Electron.* QE-13, No. 9, September 1977.
8. A. A. Vetter and N. M. Nerheim, *Appl. Phys. Lett.* 30, 405 (1977).
9. N. M. Nerheim, *J. Appl. Phys.* 48, 3244 (1977).
10. C. J. Chen, *Appl. Phys. Lett.* 45, 4663 (1974).
11. W. T. Leland, M. J. Kircher, M. J. Nutter and G. T. Schappert, *J. Appl. Phys.* 46, 2174 (1975).
12. L. A. Weaver, L. H. Taylor and L. J. Denes, *J. Appl. Phys.* 46, 3951 (1975).
13. H. R. Griem, Plasma Spectroscopy, McGraw-Hill Book Co., New York (1964).
14. A.C.G. Mitchell and M. W. Zemanski, Resonance Radiation and Excited Atoms, Cambridge University Press, London (1961).
15. Landolt-Börnstein, Zahlenwerte und Funktionen, 6 Auflage, Band I, Atom and Molekularphysik, Teil 5, Atomkerne und Elementarteichen, Springer-Verlag, Berlin (1961).
16. W. Fisher, H. Huhnermann and K. J. Killath, *Z. Phys.* 194, 417 (1966); 200, 158 (1967).

17. C. H. Corliss and W. R. Bozman, Experimental Transition Probabilities for Spectral Lines of Seventy Elements, Natl. Bur. Stand. Monogr. 53, U.S. Government Printing Office, Washington, D.C. (1962).
18. H. O. Hartley, *Technometrics* 3, 269 (1961).
19. C. F. Wood, *IEEE Trans. Systems Science & Cybernetics* SSC-1, 14 (1965).
20. D. J. Wilde, Optimum Seeking Methods, Prentice-Hall, Englewood Cliffs, New Jersey (1964).
21. R. Hooke and T. A. Jeeves, *J. Assoc. Computing Machinery* 8, 212 (1961).